Production of a Diesel Fuel Cetane Enhancer from Canola Oil Using Supported Metallic Carbide and Nitride Catalysts

A Thesis

Submitted to the College of Graduate Studies and Research
In Partial Fulfillment of the Requirements for the Degree of
Masters of Science
In the Department of Chemical Engineering
University of Saskatchewan
Saskatoon, Saskatchewan

by

Hardi Sulimma

Copyright

Abstract

Six γ-Al_2O_3 supported metallic nitride and carbide catalysts were chosen for a scouting test for the production of a diesel fuel cetane enhancer from canola oil. The six catalysts chosen for study were γ-Al_2O_3 supported molybdenum (Mo) carbide and nitride, tungsten (W) carbide and nitride, and vanadium (V) nitride and carbide. All six catalysts were prepared by the impregnation method and characterized using various techniques. The six catalysts were screened for their affinity for oxygen removal, fatty acid conversion, alkane/olefin selectivity, hydrogen consumption, and gas-by product production from oleic acid. The scouting test was carried out at a reaction temperature of 390°C, a LHSV of 0.46 hr^{-1}, and elevated hydrogen partial pressures of greater than 7000 kPa, in a laboratory microreactor in an upflow configuration. The scouting test revealed that the two molybdenum catalysts performed the best with oxygen removal near 100% and alkane/olefin content of greater than 30%.

Next, the supported molybdenum carbide and nitride catalysts were compared against one another over a wider range of operating conditions. A temperature range of 380 – 390°C, a LHSV range of 0.64 – 1.28 hr^{-1}, and a hydrogen partial pressure of 7100 kPa were used. Both catalysts had the same metal loading of 7.4 wt% molybdenum. The two catalysts were compared on the basis of oxygen removal, alkane/olefin selectivity, diesel fuel selectivity, and hydrogen consumption, while using both triolein and canola oil as the feed. It was found that the supported molybdenum nitride was the superior choice for this process, specifically when using the more complex canola oil feed. The supported molybdenum nitride catalyst delivered oxygen removal of greater than 85%,

alkane/olefin selectivity of greater than 20%, and diesel fuel selectivity of greater than 40%, for all conditions studied.

Finally, a preliminary catalyst and process optimization was carried out on the chosen γ-Al_2O_3 supported molybdenum nitride catalyst. The catalyst optimization consisted of varying the metal loading of the catalyst from 7.4 wt% to 22.7 wt%. The catalysts were examined over a temperature range of 390 – 410°C, a LHSV range of 0.9 – 1.2 hr^{-1}, and a hydrogen partial pressure of 8300 kPa, with canola oil as the chosen feed. It was found that the increase in molybdenum loading on the catalyst delivered an average increase in the alkane/olefin selectivity of 43.2% and an average increase in the diesel fuel selectivity of 5.3 %. The process optimization studied a temperature range of 390 – 410°C, a LHSV range of 0.6 – 1.2 hr^{-1}, and a hydrogen partial pressure range of 7800 - 8900 kPa, with canola oil as the chosen feed. Within the limits of the design, it was found that the optimum operating conditions were 395°C, 1.05 hr^{-1}, and 8270 kPa. At these conditions the predicted yields of alkane/olefin products and diesel fuel are 47.3 and 50.5 g/100g liquid fed, respectively.

Acknowledgement

First and foremost, I would like offer sincere gratitude to my supervisors Dr. A. K. Dalai, University of Saskatchewan, and Dr. J. Monnier, Natural Resources Canada, for their invaluable guidance and time spent in helping me complete the magnitude of work that is contained within this thesis. I am grateful of their input and knowledge that was of great importance to the direction of this work. Finally, I am thankful for their patience and support throughout this entire process.

Secondly, I would like to thank the staff of the CANMET Energy Technology Centre, Natural Resources Canada that was essential to the successful implementation of my experimental work. I would like to sincerely thank Bruce Dyck, Luc Pelletier, Guy Tourigny, and Gianni Caravaggio, whom all provided me guidance and expertise in the lab.

I also would like to express my deep gratitude to the members of my advisory committee Dr. T. Pugsley and Dr. H. Wang for their contributions and guidance.

Financial support for this work is greatly acknowledged from NSERC and the University of Saskatchewan. In addition, I would like to thank Natural Resources Canada for their financial support by the means of laboratory facilities and supplies necessary to complete my work.

Finally, my endless gratitude goes to my fiancé Keryn. Her patience and support throughout this entire process have been motivating and unparalleled to no end. Thank you.

Table of Contents

Copyright	i
Abstract	ii
Acknowledgement	iv
Table of Contents	v
List of Tables	ix
List of Figures	xiv
Nomenclature	xvii
1. Introduction	1
1.1. Knowledge Gap	3
1.2. Hypothesis	4
1.3. Research Objectives	4
2. Literature Review	6
2.1. Diesel Fuel Cetane Enhancers	6
2.2. Renewable Sources for Biomass-Derived Oils	11
2.3. Hydrodeoxygenation	15
2.4. Metallic Nitride and Carbide Catalysts	21
2.5. Catalyst Characterization	29
3. Experimental Procedure	33
3.1. Catalyst Preparation	33
3.2. Catalyst Characterization	39
3.3. Experimental Setup	41
3.3.1. Experimental Setup – Design	42

3.3.2. Experimental Setup – Commissioning 46

3.4. Experimental Procedure 47

3.5. Product Characterization 53

3.5.1. Product Gas Characterization 53

3.5.2. Product Liquid Characterization 54

4. Scouting Tests 57

4.1. Catalyst Preparation and Characterization 57

4.1.1. Physical Properties 57

4.1.2. Chemical Properties 59

4.2. Reactor Loading 62

4.3. Process Parameters 66

4.4. Results and Discussion 68

4.4.1. Mass Transfer Limitations 68

4.4.2. Oxygen Content in the Organic Phase 75

4.4.3. Fatty Acid Content in the Organic Phase 77

4.4.4. Alkane and Olefin Content in the Organic Phase 78

4.4.5. Hydrogen Consumption 80

4.4.6. Gas By-Product Production 83

4.5. Conclusions 87

5. Comparison of Supported γ-Al_2O_3 Mo_2C and γ-Al_2O_3 Mo_2N for HYD and HDO of Canola Oil 88

5.1. Experimental Design 88

5.1.1. Statistical Design of Experiments 90

5.2. Catalyst Preparation and Characterization 94

5.3. Results and Discussion 94

5.3.1. Mass Transfer Limitations 96

5.3.2. Oxygen Content in the Organic Phase 96

5.3.3. Alkane/Olefin Content in the Organic Phase 101

5.3.4. Diesel Fuel Fraction in the Organic Phase 105

5.3.5. Hydrogen Consumption 109

5.4. Conclusions 113

6. Preliminary Process Optimization for HYD and HDO of Canola Oil Using Supported γ-Al_2O_3 Mo_2N 114

6.1. Experimental Design 114

6.1.1. Catalyst Optimization – Metal Loading 114

6.1.2. Process Optimization 115

6.2. Catalyst Preparation and Characterization 118

6.3. Results and Discussion 120

6.3.1. Catalyst Optimization – Metal Loading 120

6.3.2. Process Optimization 122

6.3.2.1.Oxygen Removal from the Organic Phase 122

6.3.2.2.Diesel Fuel Fraction in the Organic Phase 124

6.3.2.3.Alkane/Olefin Content in the Organic Phase 128

6.3.2.4.Hydrogen Consumption 130

6.3.2.5.Validation of Optimized Data from Experiments 132

6.4. Conclusions 135

7. Conclusions and Recommendations 137

7.1. Conclusions 137

7.2. Recommendations 141

8. List of References 142

Appendices

A: Liquid Product C/H/N Analytical Results 145

B: Liquid Product FAME GC/MS, GC/MS, and Simulated Distillation Analytical Results 148

C: Gas Product GC/MS Analytical Results 150

D: Conversion and Yield Sample Calculation 152

E: Internal and External Mass Transfer Sample Calculation 156

F: Analysis Procedures for FAME GC/MS and n-alkane/α-oleifn GC/MS (Carrivaggio, 2008) 167

List of Tables

Table 2.1	2004 Crop Production for Saskatchewan and Canada	14
Table 2.2	Fatty Acid Composition of a Typical Canola and Greenseed Oil	15
Table 2.3	Effect of Surface Area and Crystal Planes on Specific Conversion of HYD, HDS	23
Table 2.4	Values of Important Metallic Nitride and Carbide Catalyst Preparation Parameters	26
Table 3.1	Temperature Programmed Calcination Step Sequence	36
Table 3.2	Process parameters for Carburization / Nitriding of Metal Oxide Precursors	38
Table 3.3	Process parameters for Carburization / Nitriding of Metal Oxide Precursors	38
Table 4.1	Summary of BET Surface Area and Pore Volume / Size Characterization	58
Table 4.2	Chemical Compositions of the Phase I Scouting Test Catalysts (Oxide Precursor)	60
Table 4.3	Summary of Calculated Metal Loading	62
Table 4.4	Summary of Active Site Comparison Calculation	65
Table 4.5	Summary of Process Conditions for Phase I Scout Tests	67
Table 4.6	Summary of Internal Mass Transfer Estimations for the Phase I Scout Tests	72

Table 4.7	Summary of External Mass Transfer Estimations for the Phase I Scout Tests	74
Table 4.8	Scouting Test Conversion - % Removal of Oxygen in the Organic Phase (T = 380°C, LHSV = 0.45 hr^{-1}, P_{H2} = 7150 / 8350 kPa)	76
Table 4.9	Scouting Test Conversion – Residual Acids in the Organic Phase (T = 380°C, LHSV = 0.45 hr^{-1}, P_{H2} = 7150 / 8350 kPa)	77
Table 4.10	Scouting Test Selectivity – Alkane/Olefin Content of the Organic Phase (T = 380°C, LHSV = 0.45hr^{-1}, P_{H2} = 7150 / 8350 kPa)	78
Table 4.11	Gas By-Product Distribution – Phase I Scouting Tests (Reaction Temperature = 390°C)	86
Table 5.1	Summary of Hydrogen to Carbon Atomic Ratio in the Organic Phase	98
Table 5.2	Main and Interaction Effects of Temperature and LHSV on Hydrogen to Carbon Atomic Ratio in the Organic Phase	98
Table 5.3	Main and Interaction Effects of Catalyst and Feed Complexity on Hydrogen to Carbon Atomic Ratio in the Organic Phase	100
Table 5.4	Summary of the Alkane/Olefin Content of the Organic Phase	101

Table 5.5	Main and Interaction Effects of Temperature and LHSV on the Alkane/Olefin Content of the Organic Phase	101
Table 5.6	Main and Interaction Effects of Catalyst and Feed Complexity on the Alkane/Olefin Content of the Organic Phase	104
Table 5.7	Summary of the Diesel Fuel Fraction of the Organic Phase	106
Table 5.8	Main and Interaction Effects of Temperature and LHSV on the Diesel Fuel Fraction of the Organic Phase	106
Table 5.9	Main and Interaction Effects of Catalyst and Feed Complexity on the Diesel Fuel Fraction of the Organic Phase	108
Table 5.10	Summary of Hydrogen Consumption	109
Table 5.11	Main and Interaction Effects of Temperature and LHSV on Hydrogen Consumption	110
Table 5.12	Main and Interaction Effects of Catalyst and Feed Complexity on Hydrogen Consumption	111
Table 6.1	Summary of the Process Conditions for the Metal Loading Comparison	115
Table 6.2	Summary of the Process Conditions for the 3-Parameter Central Composite Design	118
Table 6.3	BET Results for the Catalyst/Process Optimization	119
Table 6.4	Chemical Compositions of the Phase III Metal Loading Study (Oxide Precursor)	119

Table 6.5	Design Expert 6 Simulation Results	132
Table A.1	C/H/N Analytical Results – Scouting Test	145
Table A.2	C/H/N Analytical Results – Comparison of Supported γ-Al_2O_3 Mo_2C and γ-Al_2O_3 Mo_2N for HYD and HDO of Canola Oil	146
Table A.3	C/H/N Analytical Results – Process Optimization for HYD and HDO of Canola Oil Using Supported γ-Al_2O_3 Mo_2N	147
Table B.1	FAME GC/MS / GC/MS / Simulated Distillation Analytical Results – Scouting Test	148
Table B.2	FAME GC/MS / GC/MS / Simulated Distillation Analytical Results – Comparison of Supported γ-Al_2O_3 Mo_2C and γ-Al_2O_3 Mo_2N for HYD and HDO of Canola Oil	148
Table B.3	FAME GC/MS / GC/MS / Simulated Distillation Analytical Results – Process Optimization for HYD and HDO of Canola Oil Using Supported γ-Al_2O_3 Mo_2N	149
Table C.1	Gas Product GC/MS Analytical Results – Scouting Test	150
Table C.2	Gas Product GC/MS Analytical Results – Comparison of Supported γ-Al_2O_3 Mo_2C and γ-Al_2O_3 Mo_2N for HYD and HDO of Canola Oil	150

Table C.3 Gas Product GC/MS Analytical Results – Process Optimization for HYD and HDO of Canola Oil Using Supported γ-Al_2O_3 Mo_2N 151

Table E.1 Summary of External Mass Transfer Estimations for the Molybdenum Carbide and Nitride Comparison Study 163

Table E.2 Summary of Internal Mass Transfer Estimations for the Molybdenum Carbide and Nitride Comparison Study 166

List of Figures

Figure 2.1	Process Flow Sheet for the SuperCetane Process at CANMET Energy Technology Centre – Ottawa	9
Figure 2.2	Typical Triglyceride Molecule	12
Figure 2.3	Molecular Structure of Di-Ethyl Sebascate	18
Figure 2.4	Oxygen Removal Reaction Mechanisms for (a) HDO and (b) Decarboxylation	19
Figure 2.5	Comparison of Steady-State HDO for an Industrial Catalyst and Various Metallic Nitride and Carbide Catalysts	28
Figure 3.1	Process Flow Sheet of the Carburization / Nitriding Apparatus	37
Figure 3.2	Process Flow Sheet of the Experimental Apparatus	43
Figure 3.3	Catalyst Bed Position in the Experimental Reactor (Furnace)	50
Figure 4.1	XRD Plot of 11.1 wt% Supported $MoO_3/\gamma\text{-}Al_2O_3$	60
Figure 4.2	XRD Plot of 12.6 wt% Supported $WO_3/\gamma\text{-}Al_2O_3$	61
Figure 4.3	XRD Plot of 5.6 wt% Supported $V_2O_5/\gamma\text{-}Al_2O_3$	61
Figure 4.4	Scouting Test Selectivity – Alkane/Olefine Distribution of the Organic Phase (T = 380°C, LHSV = 0.45hr^{-1}, P_{H2} = 7150 / 8350 kPa)	79
Figure 4.5	Hydrogen Consumption – Scouting Test (T = 380°C, LHSV = 0.45hr^{-1}, P_{H2} = 7150 / 8350 kPa)	82

Figure 4.6 Total Gas Production – Scouting Test (T = 380°C, LHSV = 0.45hr^{-1}, P_{H2} = 7150 / 8350 kPa) 85

Figure 5.1 'Lower' Tier 2^2 Factorial Experimental Design for the Evaluation of Mo_2C and Mo_2N 90

Figure 5.2 Hydrogen to Carbon Atomic Ratio in the Organic hase – Average Response Interaction for the Molybdenum Catalyst Comparison 100

Figure 5.3 Alkane/Olefin Content in the Organic Phase – Average Response Interaction for the Molybdenum Catalyst Comparison 104

Figure 5.4 Diesel Fuel Content in the Organic Phase – Average Response Interaction for the Molybdenum Catalyst Comparison 108

Figure 5.5 Hydrogen Consumption – Average Response Interaction for the Molybdenum Catalyst Comparison 112

Figure 6.1 Visual Representation of the 3-Parameter Central Composite Design 116

Figure 6.2 Metal Loading Comparisons – Diesel Fuel Yield 120

Figure 6.3 Metal Loading Comparisons – Alkane/Olefin Yield 121

Figure 6.4 Catalyst Deactivation - % Oxygen Removal from the Organic Phase 124

Figure 6.5 Surface Plot – Diesel Fuel Yield (P_{H2} = 8330 kPa) 125

Figure 6.6 Pressure Effect on Diesel Fuel Yield (T = 400°C, LHSV = 0.9hr^{-1}) 127

Figure 6.7 Surface Plot – Alkane/Olefin Yield (P_{H2} = 8330 kPa) 128

Figure 6.8 Pressure Effect on Alkane/Olefin Yield (T = 400°C, LHSV = 0.9hr^{-1}) 130

Figure 6.9 Effect of Time On Stream on Hydrogen Consumption (T = 400°C, LHSV = 0.9hr^{-1}, P_{H2} = 8330 kPa) 131

Figure 6.10(a) Boiling Point Distribution – Experiment # 11 (T = 395°C, LHSV = 1.05hr^{-1}, P_{H2} = 8067 kPa) 134

Figure 6.10(b) Organic Product Fractions – Experiment # 11 (T = 395°C, LHSV = 1.05hr^{-1}, P_{H2} = 8067 kPa) 134

Nomenclature

d	diameter *{m}*
k	reaction co-efficient *{m^3/g*s}*
k_La_i	liquid phase mass transfer coefficient *{s^{-1}}*
k_sa_c	liquid-solid mass transfer coefficient *{m/s}*
n	reaction order *{dimensionless}*
$-r_i$	rate of consumption of species i *{mol/g*s}*
r_i'(obs)	observed rate of reaction for species i *{mol/g*s}*
u_L	superficial liquid velocity *{m/s}*
v	volumetric liquid flow rate *{L/min}*
x_i	weight percent of species i *{%}*
y_i	volumetric fraction of species i
A	average of four measured responses, Y_j^k
ActiveSites	number of reaction sites available on the surface of the catalyst
AOY	alkane/olefin yield *{g/100g}*
C_i	concentration of species i *{mol/m^3}*
CN_i	co-ordination number of species i *{atoms/active site}*
C_{WP}	Weisz-Prater criterion *{dimensionless}*
$D_{eff,i}$	effective diffusion coefficient of species i *{m^2/s}*
DFY	diesel fuel yield *{g/100g}*
D_i	bulk diffusion coefficient of species i *{m^2/s}*
E_j	main effect of process input j
F	total volumetric gas flow rate *{ml/min}*

F_i	volumetric gas flow rate of species i *{ml/min}*
G_i	gas production of species i *{mol/min}*
G_i'	gas production of species i {*L of gas i at STP/L of liquid fed}*
GHSV	gas hourly space velocity *{hr^{-1}}*
HC	hydrogen consumption *{mol/min}*
HC'	hydrogen consumption *{L of H_2 at STP/L of liquid fed}*
HDO	hydrodeoxygenation
HYD	hydrogenation
J_D	mass transfer factor *{dimensionless}*
LHSV	liquid hourly space velocity *{hr^{-1}}*
LHSV'	modified liquid hourly space velocity *{dimensionless}*
M	total mass *{g}*
$\hat{M}_i$	molecular weight of species i *{g/mol}*
N_i	molar flow rate of species i {*mol/min}*
N_A	Avogadro's number – 6.022 x 10^{23} *{# atoms/mol}*
OLY	organic liquid yield *{g/100g}*
P	pressure *{kPa}*
R	ideal gas constant – 8.3145 *{J/mol*K}*
R	catalyst radius *{m}*
Re	Reynolds number *{dimensionless}*
R_{G-L}	gas-liquid external mass transfer resistance *{kg*s/m^3}*
R_{L-S}	liquid-solid external mass transfer resistance *{kg*s/m^3}*
RL	mass of catalyst loaded into the reactor *{g}*

Sh_M	Sherwood number *{dimensionless}*
SS_j	contribution of E_j to the total variation
SST	total variation
T	temperature *{°C}*
T'	modified temperature *{dimensionless}*
V_j	percent contribution to the total variation of E_j *{%}*
W	weight of catalyst charged to the reactor *{g}*
Y_j^k	measured response at process inputs j and k

Greek Letters

ε_b	catalyst bed porosity *{dimensionless}*
η	internal mass transfer efficiency *{dimensionless}*
μ	viscosity *{mPa*s}*
ρ_B	bulk catalyst density *{g/m^3}*
ρ_c	apparent catalyst density *{g/m^3}*
ρ_L	liquid density *{kg/m^3}*
τ	tortuosity *{dimensionless}*

Subscripts

b	bulk fluid
gc	conditions at the point of analysis (gas chromatography)
i	reacting species
metal	metal species

s	catalyst surface
Ar	argon
H_2	hydrogen
I	interaction
L	liquid hourly space velocity
IN	entering the reactor
N	normalized
OA	oleic acid
OUT	exiting the reactor
T	temperature

1.0 Introduction

In recent times, vegetable and plant oils have been studied for their use as a fuel product. The chemical structure of vegetable and plant oils, which are made up of triglycerides with long chained fatty acid groups 16 to 24 carbon atoms in length, makes them ideal sources for fuel products in the diesel fuel boiling point range (155 – 325°C). Traditionally, the process of converting vegetable and plant oils to diesel fuel products has been done through an acid-base catalytic reaction known as transesterification. However, an alternative method of converting vegetable and plant oils into diesel fuel products has been researched recently by using a straight-run hydrotreating process similar to what is found in the oil and gas industry.

By introducing a straight-run hydrotreating process to convert vegetable and plant oils into diesel fuel, the process may become more viable for commercial use as it can take advantage of the economy of scale. In addition to this, research by Monnier (1999) has shown that by hydrotreating vegetable and plant oils to produce diesel fuel, a product with high cetane values can be achieved. This product, called "SuperCetane", can not only be used directly as a diesel fuel, but has such superior properties to fossil fuel derived diesel fuels that it can also be mixed with the latter as a diesel fuel cetane enhancer. This increases the value of the product as there are ever increasing restrictions on the quality of diesel fuels used in Canada.

The research by Monnier (1999) has shown that using a standard oil and gas industry sulphided catalyst for hydrotreating yields an excellent diesel fuel cetane enhancer product. However, using this catalyst introduces sulphur into the process, which is not naturally occurring in vegetable and plant oils. The government of Canada

has mandated that the sulphur content of diesel fuel must be below 15 ppm for transportation use (Canadian Environmental Protection Act, 1999), and so it is desirable to find an alternative to the sulfided catalysts.

The use of non-sulphided catalysts for hydrotreating of fossil fuels has been extensively studied. It has been shown that non-sulphided catalysts can be successful in removing many impurities such as oxygen, sulphur, and nitrogen. Specifically, a review by Furimsky (2003) has shown that metallic carbide and nitride catalysts may have a high affinity for removing the impurities from fuel products via hydrotreating. However, a large gap in the literature exists when concerning the use of these catalysts for hydrotreating of vegetable and plant oils. Therefore, it is the objective of this thesis to investigate the suitability of metallic carbide and nitride catalysts for the hydrotreating of vegetable and plant oils (canola oil) to produce a diesel fuel cetane enhancer.

The following report discusses the experimental work that was carried out to show that metallic carbide and nitride catalysts are suitable for hydrotreating of vegetable and plant oils. The remainder of Chapter 1 discusses the knowledge gap, hypothesis, and research objectives. In Chapter 2, a literature search focusing on the SuperCetane process, metallic carbide and nitride catalysts, and renewable sources for biomass-derived oils is discussed. Following this, in Chapter 3, the experimental procedure and challenges are outlined. Chapters 4, 5, and 6 focus on the results of the experimental trials, specifically examining the three separate phases of work: Scouting Tests (Chapter 4), Comparison of Supported γ-Al_2O_3 Mo_2C and γ-Al_2O_3 Mo_2N (Chapter 5), and Process Optimization for HYD and HDO of Canola Oil Using Supported γ-Al_2O_3 Mo_2N (Chapter 6).

1.1 KNOWLEDGE GAP

The scope of this project can be differentiated into three general areas: production of a high-cetane diesel fuel product, hydrodeoxygenation, and metallic nitride and carbide catalysts. Within each of these topics the literature is lacking, or does not exist at all. These gaps in the literature are magnified when combining each of these areas with one or both of the others.

1. High-cetane diesel fuel products produced from biomass-derived oils have been produced previously only using conventional hydrotreating catalysts, such as a supported sulphided nickel-molybdenum catalysts. No work has been reported in the literature concerning the potential of using metallic nitride and carbide catalysts for the production of these diesel fuel products. Many different types of feed sources have been tested for their potential for producing diesel fuel, including tall oil, animal fats and vegetable oils. However, canola oil, Canada's number one produced oil seed, has received only limited attention.
2. Hydrodeoxygenation has been studied quite rigorously, however, dealing mainly with oxygenated compounds that are found in conventional fossil fuels. There has been limited work on HDO of oils that are derived from biomass, and those studies that have been reported deal almost exclusively with bio-oils derived from pyrolysis. There are very few studies that deal directly with the HDO of normal plant oils and their main constituent: long-chained fatty acids. As a result, there is also little information available about the reaction mechanism of HDO of fatty acids and essentially no information on kinetic parameters.

3. Metallic nitride and carbide catalysts have been studied in recent years as a potential replacement for conventional catalysts involved in hydrotreating processes. However, the application of these catalysts to HDO is not well represented in literature. Only one significant paper (Ramanathan et al., 1995) can be found in literature that gives significant results concerning HDO over metallic nitride and carbide catalysts. However, this study focused exclusively on the HDO of benzofuran. There has been no work reported on the HDO of normal plant oils (long-chained fatty acids) over metallic nitride and carbide catalysts.

1.2 HYPOTHESIS

1. Canola oil is an ideal feed source for the production of diesel fuel products, including high-cetane diesel fuel enhancers. Canola oil is capable of being hydrotreated, with high yields, into a high-cetane middle distillate fuel product that can be used as an additive to increase the overall cetane number of a conventional diesel fuel.
2. Metallic nitride and carbide catalysts have a high activity for the HDO and HYD of normal plant oils, specifically canola oil.

1.3 RESEARCH OBJECTIVES

The research objectives for this project are designed to test the hypotheses outlined above, as well as attempt to fill the gaps in the literature that have been identified in Section 1.1. The primary objective identifies the overall goal for this research.

Primary Objective

The primary objective of this project is to synthesize, characterize and test various metallic nitride and carbide catalysts for their activity for HDO and HYD of canola oil in order to produce diesel fuel products, specifically diesel fuel cetane enhancers.

In order to achieve the primary objective, three secondary objectives have been identified to direct the research ultimately towards the primary objective. The secondary objectives are:

1. Synthesize and characterize six different types of γ-Al_2O_3 supported metallic nitride and carbide catalysts to determine which one has the highest activity for HDO and HYD of oleic acid, the major fatty acid constituent of canola oil. The six catalysts to be tested are: Mo_2N, Mo_2C, WN, WC, VN, and VC supported on γ-Al_2O_3.
2. After determining the most active catalyst(s), perform further activity tests for this catalyst(s) using triolein (model compound triglyceride) and real canola oil to confirm the potential of using this catalyst on a naturally occurring feedstock.
3. Optimize the most active catalyst for its activity for HDO and HYD of canola oil with respect to important catalyst parameters, such as metal loading, and important operating parameters, such as temperature, hydrogen partial pressure, and residence time (LHSV).

2.0 Literature Review

A literature review was carried out with the objective to study the various areas of interest that are influential to the production of diesel fuel products from biomass-derived oils. This review began by studying a technology named SuperCetane developed and patented by Natural Resources Canada (Monnier, 1998). The SuperCetane process uses hydro processing technologies to produce a diesel fuel product from renewable feedstocks containing triglycerides. The review of this technology outlines the motivation behind developing a process to produce a diesel fuel product high in cetane value from biomass-derived oils. Following this, the potential biomass-derived oil sources that are significant to Canada, specifically Saskatchewan, were examined in an effort to understand the resources available that can make this process viable. Next, a review of previous work done on the topic of hydrodeoxygenation, as well as the synthesis of metallic carbide and nitride catalysts was considered. Following this, common characterization methods for traditional hydrotreating catalysts, as well as metallic carbide and nitride catalysts, were examined. Included in the study of characterization methods, the issue of completing a justifiable comparison amongst different types of catalysts was addressed.

2.1 DIESEL FUEL CETANE ENHANCERS

The potential of using biomass-derived oils to produce usable fuel products has attracted much attention in recent decades. Recently, the interest in this area has increased dramatically with decreasing reserves of conventional hydrocarbon resources, increasing gas prices, and growing concerns of what effect emissions from burning

conventional fuel products has on the environment. Biomass-derived oils can be prepared from various sources by different methods, such as wood or peat by pyrolysis and normal plant oils by crushing and solvent extraction (Furimsky, 2000). The product that is obtained from these processes may differ significantly, especially with respect to the oxygen-containing species.

In each case described above, it is either necessary or advantageous to further process these oils in order to upgrade them into useable fuel products. This upgrade of the fuel has been traditionally carried out by employing the transesterification process, which yields a mixture of fatty acid alkyl esters as the primary fuel by reacting the triglycerides with an alcohol in either an acid or base catalyst. The resultant fuel product from the transesterification process, biodiesel, has many current applications, but has limitation surrounding its use. The most significant limitation of biodiesel is its high oxygen content that leads to:

- Increased NOx emissions
- Physical property limitations – cloud point (cold weather climates)
- Oxidative stability and gum formation

However, an alternative approach to transesterification for upgrading biomass-derived oils exists: hydrotreating. Hydrotreating of biomass-derived oils is the process of reacting triglyceride molecules with hydrogen under high pressure and temperature in the presence of a catalyst. Unlike the transesterification process, catalytic hydrotreating is capable of selectivity removing the oxygen molecules by means of hydrodeoxygenation (Section 2.1.3). This yields a product that has very low or zero oxygen content and is similar in structure to traditional fossil fuel derived products (diesel fuel).

After hydrotreating biomass-derived oils, restrictions of its direct use may still arise because of important physical properties such as viscosity and cloud point (Dmytryshyn, 2004). In addition to this, higher production costs may be associated with the hydrotreating process of biomass-derived oils as compared with conventional diesel fuels and/or the transesterification process. For these reasons, it is desired to develop a product that has high quality fuel characteristics so that it can be used not only as a pure product, but could also provide value when blended with conventional fuels. Based on the structural make up of biomass-derived oils, the most attractive fuel characteristic in this sense is cetane number, which is an important quality measure of diesel fuel.

Biomass-derived oils are dominated in composition by triglycerides that contain long-chained fatty acids ($C_{16} - C_{22}$) (Dmytryshyn, 2004). During the hydrotreating of biomass-derived oils, the long-chained fatty acids are detached from one another due to C-O bond breaking, treated to remove oxygen, and saturated. This yields long-chained hydrocarbons that are high in cetane number. Cetane number is a measure of the quality of ignition of a diesel fuel (Monnier, 1999). It is based on the relative ignition qualities of the test fuel (product) as compared to a mixture of two standard fuels: n-hexadecane (C_{18}), which has a cetane number of 100, and heptamethyl nonane (HMN), which has a cetane number of 15 (ASTM D 613-05). The cetane value of the test fuel is calculated by the following formula:

$$CETANE\# = (\%\_n-hexadecane) + 0.15 * (\%\_HMN) \tag{1.2}$$

It can be seen from this formula that a fuel with a cetane number of 50 will have the same ignition properties as a mixture of approximately 41.2% n-hexadecane and 58.8% HMN. A low cetane value means that the diesel fuel may suffer from poor cold

weather starting, long ignition delays, increased combustion noise, and possible misfiring (Monnier, 1999).

Natural Resources Canada (NRCan) has developed a process that attempts to maximize the cetane value from biomass-derived oils. The process has been termed the "SuperCetane Process" because of its ability to produce high quality diesel fuel with extremely high cetane values (Monnier, 1998). . A great advantage of the SuperCetane process is that it has been successful, to different degrees, with many different feedstocks. Various sources of biomass-derived oils have been used in this process, such as tall oil (a by-product of the Kraft pulping process), wood oils (from the pulping of hardwood species), animal fats (tallow grease), waste-restaurant (yellow) grease, and vegetable oils (soybean oil, canola oil) (Monnier, 1998). NRCan's SuperCetane process is carried out using a standard hydrotreating process, as shown below in Figure 2.1:

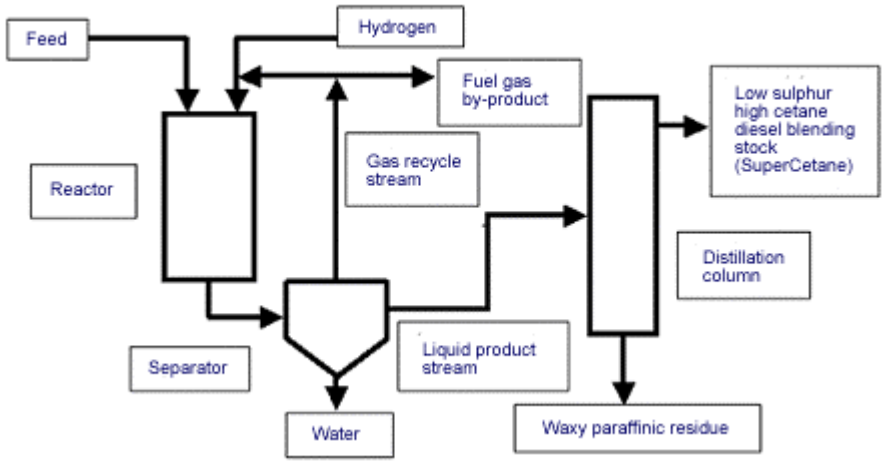

Figure 2.1: Process Flow Sheet for the SuperCetane Process at CANMET Energy Technology Centre – Ottawa (Website 1, Accessed 2008)

During the SuperCetane process, the various feedstocks are contacted with hydrogen gas, at typical hydroprocessing conditions, over a conventional hydrotreating catalyst in a trickle-bed reactor. The various catalysts that have been studied in the SuperCetane process include γ-alumina supported cobalt-molybdenum (Co-Mo), γ-alumina nickel-molybdenum (Ni-Mo) and other supported transition metal catalysts (Monnier, 1998). It has been found that the optimum operating conditions, depending on the feed chosen, range from temperatures of 370 – 450°C, system pressures of 4 – 15 MPa, and liquid hourly space velocities of 0.5 – 5 hr^{-1} (Monnier, 1998).

When exiting the reactor, the product stream produced by the SuperCetane process is a hydrocarbon fuel with a broad boiling point range (~60 – 400°C). This product stream is then further processed through distillation and separated into three fractions: naphtha, middle distillate, and waxy residues. The middle distillate product, named SuperCetane, is the desired product with high cetane values. The final cetane values of SuperCetane were found to be as high as 100, depending on the feedstock and process conditions. It was found that the highest cetane values were obtained when using yellow grease and animal tallow as the feedstock (Website 1, Accessed 2008). SuperCetane product yields were approximately 70-80% after the waxy residues are removed (Website 1, Accessed 2005). The naphtha fraction was usually found to be very small, and combined with the high cetane value of the middle distillate, did not need to be removed from the SuperCetane.

It has been noted that SuperCetane is more attractive to be used as a fuel additive as opposed to a straight run fuel (Monnier, 1998). This is because the cetane value of SuperCetane is much greater than the minimum requirement of 40. Therefore, it takes

only a small volume of SuperCetane to significantly enhance the quality of the oil sands derived middle distillates that normally have cetane values in the range of 30-35. Furthermore, it has been shown that SuperCetane has a linear additive effect on cetane number. That is, the increase in cetane number of the overall mixture will be directly proportional to the amount of cetane enhancer added. This makes SuperCetane a more effective cetane additive than traditional alkyl-nitrate cetane enhancers, which have a non-linear additive effect (that is, only minimal increases in cetane number are realized, even with an excess amount of additive used).

2.2 RENEWABLE SOURCES FOR BIOMASS-DERIVED OILS

Biomass-derived oils originate from many different sources, often requiring a number of processing steps to convert them to useable fuels. Biomass-derived oils can be formed by various means, such as pyrolysis, crushing, and solvent extraction. However, each process produces a different type of product, which can significantly affect its potential use as a fuel. The oxygen content of the final oil is one characteristic that can limit the potential use of biomass-derived oils as fuels and has been found to vary significantly depending on the formation process from which it was made. Pyrolysis oils, for example, typically contain up to 50% oxygen (Furimsky, 2000). It has been found that oils, such as these, with high oxygen contents are less attractive for use as fuels because they require a large amount of processing to reduce the oxygen levels.

However, crushing and solvent extraction can also be used to produce biomass-derived oils and is the primary method for producing normal plant oils. Most plant oils made from this process have been found to typically contain oxygen levels of

approximately 10%. The low oxygen content makes these oils more attractive for use as fuel products. Common oilseed products that are often used to produce plant oils include soybean, sunflower, rapeseed, palm, and coconut (Sirvastava, 2000).

Normal plant oils are especially ideal candidates for the production of a diesel fuel, and specifically a cetane enhancer, because they are made up primarily of triglycerides (+90%). Triglycerides are complex molecules that contain a glycerol group that has three fatty acid chains attached to it (Figure 2.2).

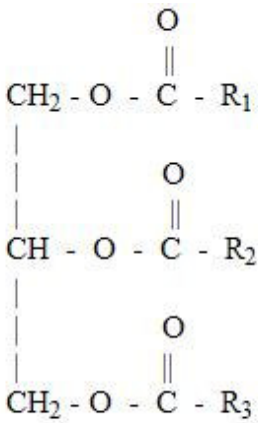

Figure 2.2: Typical Triglyceride Molecule (Website 2, Accessed 2008)

The remainder (~10%) of normal plant oils is made up of mono- and di-glycerides, as well as free fatty acids (Sirvastava, 2000). The length and saturation of the hydrocarbon chain that makes up the fatty acid component ($R_{1,2,3}$) may vary from triglyceride to triglyceride, and may also vary within a single triglyceride. These carbon chains commonly contain between 16 and 22 carbon atoms and can vary in degrees of saturation from completely saturated to three degrees of saturation (three carbon-carbon double bonds). The length of the fatty acids is what makes normal plant oils an attractive source for diesel fuel products because they have similar chemical properties such as molecular formula, molecular weight, etc. In addition to this, the fatty acids can lead to a

final product with high cetane values by removing the oxygen and producing long-chained hydrocarbons.

As described in Section 2.1.1, the process of converting biomass-derived oils to a usable fuel product is a long and expensive one. Purchasing feedstock and transporting it to the processing site account for a significant portion of these costs. Due to the large selection of normal plant oils that can be used to produce diesel fuel products, the choice of feedstock may depend significantly on the grain growing patterns of the local region to reduce tariffs and transportation costs. For example, in the United States, because of the climate and soil conditions, soybean oil is produced in a higher quantity than many other plant oils (Sirvastava, 2000). This makes soybean oil the most logical choice of feedstock in this region. Likewise, in Europe, the production of rapeseed and sunflower oils dominates many other plant oils (Sirvastava, 2000). As a result, Europe would be best served by focusing primarily on these two plant oils as feedstocks.

The same regional consideration should be made when considering the production of diesel fuel from biomass-derived oils in Canada, and in particular, Saskatchewan. Shown below in Table 2.1 is the crop production for 2004 of various grains in both Saskatchewan and Canada (Website 3, Accessed 2005). It can be seen from Table 2.1 that canola oil is a major contributor to the total crop production of both Saskatchewan (~11%) and Canada (~13.5%). This contribution substantially outweighs any of the other oil seeds that are produced in Saskatchewan, or Canada. These statistics show that using canola oil as a feedstock for producing diesel fuel products from normal plant oils in Saskatchewan and Canada would provide the greatest opportunity for a successful process.

Table 2.1: 2004 Crop Productions for Saskatchewan and Canada (Website 3, Accessed 2005)

Grain/Oilseed	Production (*1000 tonnes)	
	Saskatchewan	Canada
Winter Wheat	171.5	2447.4
Spring Wheat	8143.4	18451.0
Durum	3946.3	4962.0
Oats	1434.3	3683.1
Barley	5007.7	13186.4
Fall rye	160.0	403.9
Spring rye	5.1	14.0
Flax	355.6	516.9
Canola	2903.0	7728.1
Mixed Grains	5.1	318.0
Dry Peas	2476.7	3338.2
Triticale	44.5	n.a
Sub Total	**24653.2**	**55049.0**
Mustard Seed	250.4	305.5
Sunflower Seed	8.6	54.4
Lentils	948.9	961.0
Canary Seed	284.4	300.5
Chickpeas	42.6	51.2
Total	**26188.1**	**56721.6**

Characterization of canola oil shows that it contains a large number of different fatty acid components. In addition to this, greenseed oil, an inedible grade of canola oil, has a similar chemical makeup and could be used for the production of diesel fuel products. A study by Dmytryshyn et al. (2004) investigated the chemical composition of both canola and greenseed oil and presented the fatty acid composition of both oils (Table 2.2).

Table 2.2: Fatty Acid Composition of a Typical Canola and Greenseed Oil (Dmytryshyn, 2004)

Fatty Acid	% of total Fatty Acid composition	
	Canola Oil	Greenseed Oil
Palmitic	4.21	4.38
Stearic	2.03	1.98
Oleic	62.33	62.74
Linoleic	19.13	19.99
Linolenic	9.18	9.60
Eicosenoic	1.26	0.00
Erucic	1.87	1.31
Total	**100.01**	**100.00**

It can be seen from Table 2.2 that Oleic acid is the primary constituent of both canola and greenseed oils. Oleic acid is the common name for a straight-chained carboxylic acid containing eighteen carbon atoms and one carbon-carbon double bond. The next two abundant fatty acids are linoleic acid and linolenic acid, respectively. Both linoleic and linolenic acids are also straight-chained carboxylic acids containing eighteen carbon atoms, but with two and three carbon-carbon double bonds, respectively. From the study by Dmytryshyn et al. (2004), it can be seen that the hydrodeoxygenation and hydrogenation of oleic, linoleic and linolenic acids will be the key steps in producing a high-cetane diesel fuel product from canola (greenseed) oil.

2.3 HYDRODEOXYGENATION

The previous sections have shown that there are two important chemical steps that occur during the conversion of biomass-derived oils into a high-cetane diesel fuel product: removal of oxygen (hydrodeoxygenation (HDO) and other direct mechanisms such as hydrodecarbonylation and hydrodecarboxylation) and hydrogenation (HYD). Both of these chemical processes are included in a larger group of processes generally referred to as hydrotreating. Hydrotreating also includes hydrodesulphurization (HDS),

hydrodenitrogenation (HDN) and hydrodemetallization (HDM). All of these reactions can occur simultaneously during a catalytic hydrotreating process. However, the extent of each of these chemical reactions depends greatly on the type of feedstock, chemicals, catalysts, and operating conditions that are involved.

HYD is often included in the studies of the more difficult HDS, HDN, or HDO. From these studies, general trends have been established for HYD. Of particular interest is the effect of metal promoters on HYD with traditional supported molybdenum-sulphide catalysts. It has been found that when certain metal atoms are incorporated within the supported molybdenum-sulfide catalysts, the result is an increase in HYD activity. Specifically, nickel, cobalt, and iron have been shown to improve HYD activity of supported molybdenum-sulfide catalysts. Nickel has the largest effect on HYD activity, cobalt has the next largest effect, and iron has the least effect of the three metals, but still improves the HYD activity of the catalysts (Satterfield, 1991).

As mentioned above, HYD is often the easiest hydrotreating mechanism to carry out. As a result, any catalyst that is found to carry out the more difficult mechanisms, such as HDO, is often found to be capable of carrying out the required HYD. For this reason, the primary focus of the experimental work found in this project focuses on the HDO of fatty acids contained in canola oil.

A comprehensive review of catalytic HDO was completed by Furimsky (2000). In this review, many aspects of catalytic HDO were discussed including oxygen-containing compounds in fuels, the mechanisms of HDO, the kinetics of HDO, relative reactivity of HDO to other hydrotreating processes, HDO of real feeds, and other topics.

Many of the conclusions about HDO made by Furimsky are relevant to the processing of biomass-derived oils and are discussed here.

The review by Furimsky (2000) identifies many different compounds that have been studied for HDO. These compounds are categorized into four general groups: furans, phenols, ethers and compounds from bio-oils. The first three groups are all oxygenated compounds that are commonly found in conventional fossil fuels. The final group, compounds from bio-oils, includes a wide variety of oxygenated compounds, including phenols, ketones, aldehydes, carboxylic acids, esters, alcohols and ethers (Furimsky, 2000).

The distribution of the oxygenated compounds found in bio-oils depends greatly on the method of processing. In the case of pyrolysis, cyclic oxygenated hydrocarbons are formed (phenols), which cause great instability in the fuel. The majority of studies that have examined the HDO of these groups of oxygenated hydrocarbons were done using conventional hydrotreating catalysts, such as supported Co-Mo or Ni-Mo catalysts. The remainder of the studies examined the potential of using novel catalysts, including metallic nitrides and carbides.

Biomass-derived oils formed by crushing and solvent extraction, such as normal plant oils, form more stable, linear oxygenated hydrocarbons. Canola oil is an example of this, which contains primarily tri-glyceride molecules with long-chained fatty acids groups. However, very little work has been done to study the HDO of these compounds, including any studies employing metallic nitride or carbide catalysts.

As stated previously, most of the studies on the HDO of oxygenated hydrocarbons have been focused on compounds derived from pyrolysis. The reason for this is the

demand to remove these unstable compounds from conventional fossil fuels. However, within the studies on pyrolysis bio-oils, important information can be found that is useful in the study of HDO of canola oil with metallic nitrides and carbides.

Laurent et al. (1994) carried out a model compound study on the HDO of bio-oils derived from pyrolysis. The model oxygenated hydrocarbons that were used as feedstock included a ketonic group, a carboxylic ester group, and a methoxy group. The model compound that is most similar to canola oil is the carboxylic ester group or specifically, di-ethyl decanedioate (di-ethyl sebascate or DES) (Figure 2.3).

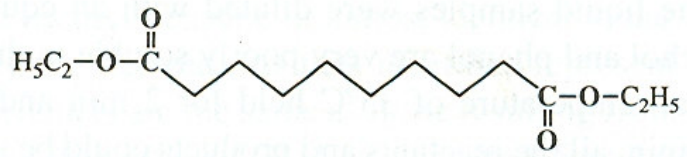

Figure 2.3: Molecular Structure of Di-Ethyl Sebascate (Laurent, 1994)

The exact molecule DES would not be found in canola oil, but the results of this study give important information about the removal of oxygen of carboxylic acid type molecules. Most importantly, this study showed that two types of reaction mechanisms simultaneously occur during the removal of oxygen from a carboxylic acid: partial HDO of the COOH to a methyl group or direct decarboxylation (removal of CO_2) (Figure 2.4). In the case of HDO, the C=O double bond is attacked first, resulting in the transformation of the carboxylic acid into an alcohol. After this, the attack on the remaining C-O bond continues and the alcohol is further transformed to an alkane. In the case of direct decarboxylation, the C-C single bond is attacked first and the oxygen atoms are removed directly in the form of CO_2.

$$[CH_3-(CH_2)_m-COOH] \xrightarrow{2H_2} [CH_3-(CH_2)_m-CH_2OH] + H_2O \xrightarrow{H_2} [CH_3-(CH_2)_m-CH_3] + 2H_2O \quad \text{(a)}$$

$$[CH_3-(CH_2)_m-COOH] \longrightarrow [CH_3-(CH_2)_{m-1}-CH_3] + CO_2 \quad \text{(b)}$$

Figure 2.4: Oxygen Removal Reaction Mechanisms for (a) HDO and (b) Decarboxylation.

The experiments carried out by Laurent et al. (1994) were performed with either sulphided Co-Mo or Ni-Mo catalysts supported on γ-alumina. Nearly all of the DES was converted to hydrocarbons not containing oxygen. Two major differences in the performance of the catalysts were found. The Ni promoted catalyst had a higher overall activity, but also had a higher decarboxylation rate than the Co promoted catalyst. One explanation for this may be that the Ni promoted catalyst was more acidic than the Co promoted catalyst. Higher acidity levels promote cracking reactions, and therefore the nickel promoted catalyst would be more likely to favour the breaking of the C-C bond (Furimsky, 2000). In addition to this, Ni also has a higher hydrogenation activity than Co, which leads to higher HDO rates. Both of these characteristics of nickel promoted catalysts, acidity and HDO activity, contribute to the higher overall activity for the Ni promoted catalyst. Also reported by Laurent et al. (1994) was an increase in the decarboxylation rate with an increase in temperature for both the nickel and cobalt promoted catalysts. This is a result of an increase in thermal cracking due to the elevated temperatures, which leads to more C-C bond breaking and the formation of CO_2.

Gusmao et al. (1989) carried out another study that examined the two types of reaction mechanisms, HDO and decarboxylation, described above. This study is of particular interest because it did use normal plant oils as a feedstock, specifically babacu oil and soybean oil. It is reasonable to assume that the conclusions made about soybean oil will be transferable to canola oil to a certain degree because of the similar chemical

structure between the two biomass-derived oils. Gusmao et al. (1989) noted the presence of the competing reactions, HDO and decarboxylation, during the removal of oxygen from the soybean oil (carboxylic acid molecules). Two types of catalysts were studied: reduced Ni/SiO_2 and an industrially prepared sulphided $Ni\text{-}Mo/\gamma\text{-}Al_2O_3$. As in the case of the previous study, the HDO activity was attributed to the Ni content of the catalyst, and the decarboxylation mechanism was linked to the acidity of the catalyst.

The study by Gusmao et al. (1989) was carried out in a batch reactor at temperatures ranging from 623 – 673 K and pressures of up to 20 MPa. It was found that the HDO of the carboxylic acid molecules was restricted by a thermodynamic equilibrium. However, further study experimental work showed that the equilibrium restrictions could be overcome by increasing the partial pressure of hydrogen, up to 20 MPa. Gusmao et al. (1989) found that under increased hydrogen pressure, 97% of the carboxylic acids in the soybean oil were converted to normal alkanes, primarily in the C_{15} – C_{18} range. It was also found that the excess hydrogen pressure favoured the HDO reaction mechanism over the decarboxylation mechanism.

Finally, Afonso et al. (1992) examined the removal of oxygen from carboxylic acids from the pyrolysis of Irati Shale oil. The experiments were carried out in a three-phased fluidized-bed reactor with an industrial sulfided $Ni\text{-}Mo/Al_2O_3$ catalyst. Similarly to the previous studies, the presence of two reaction mechanisms was noted: HDO and decarboxylation. In this case, the reactions were carried out under strong reducing conditions (high hydrogen pressure of ~12.6 MPa), which significantly favoured the HDO mechanism. Total oxygen removal of the shale oil was found to be approximately 87% and the product contained primarily normal alkanes. After manipulating

temperature and pressure, it was found that the overall rate of oxygen removal was increased with an increase in temperature over the range of 350 – 430°C and an increase in pressure from 5 – 12.6 MPa.

The most important conclusion to be drawn from these studies is that the removal of oxygen from carboxylic acids involves two key mechanisms: hydrodeoxygenation and decarboxylation. With the objective of producing a high-cetane diesel fuel product, it is desirable to produce normal alkanes with chain lengths in the range of C16 – C20. The probability of producing these chain lengths is increased when maximizing the HDO mechanism, and minimizing the cracking (decarboxylation). These studies have shown that HDO can be increased by significantly increasing the partial pressure of hydrogen. Also, these studies indicate that using nickel as a metal promoter may also have a positive effect on maximizing HDO mechanism.

2.4 METALLIC NITRIDE AND CARBIDE CATALYSTS

The study of metallic nitride and carbide catalysts has been driven by the increasing restrictions that are being applied to today's fuels. With more strict limitations on fuels, such as lower allowable limits for toxic elements such as sulphur and nitrogen, modifications to the way these fuels are produced are necessary. The most common changes that have been implemented to meet these restrictions include an increase in the amount of catalyst used, decrease of daily throughputs or an increase in hydrogen consumption (Furimsky, 2003). These are costly measures, and as the restrictions increase, the costs will also increase to a level where a new, novel catalyst may become more economically favourable than the increasing processing demands. One such group

of catalysts that have been identified as potential candidates for this scenario with respect to hydroprocessing are metallic nitrides and carbides.

An extensive review by Furimsky (2003) of metallic carbide and nitride catalysts covered many important topics about these catalysts such as structure, preparation techniques, hydrogen adsorption and catalyst activity and stability. It can be seen from this review that the majority of work that has been done with metal nitride and carbide catalysts for hydrotreating has focused on HDS, HDN and HYD. Many of theses studies showed that numerous forms of metallic nitride and carbide catalysts possess the ability to adsorb and transfer hydrogen in order to carry out these reactions. The most common and most successful transition metal used in these catalysts was molybdenum. Tungsten also showed potential to be a good transition metal in metallic nitride and carbide catalysts, as did vanadium, iron and nickel when used in specific applications.

In the review by Furimsky (2003), the adsorption of hydrogen on metallic nitrides is discussed. Due to the crystal structure of metallic nitrides (body-centered cubic), there are two crystal planes within the structure on which the reactants can access the catalyst: {1 1 1} and {2 0 0}. It has been observed that when a large ratio of {1 1 1}/{2 0 0} planes exists, a substantial increase in hydrogen adsorption occurs. Consequently, when this is the case, the specific conversion (conversion per active site) increases (Table 2.3).

Table 2.3: Effect of Surface Area and Crystal Planes on Specific Conversion of HYD, HDS (Zhang, 1999)

Catalyst Code	Surface Area (m^2/g)	I(1 1 1)/I(2 0 0)	Specific Conversion	
			HYD	HDS
Mo_2N-1	13	1.39	1.92	1.62
Mo_2N-2	23	1.37	1.52	1.39
Mo_2N-3	33	1.36	1.12	1.15
Mo_2N-4	77	0.79	0.68	0.71
Mo_2N-5	100	0.53	0.55	0.60
Mo_2N-6	120	0.50	0.46	0.53
Mo_2N-7	140	0.41	0.40	0.42

This phenomenon is attributed to the difference in the molecular structure between the {1 1 1} planes and the {2 0 0} planes, where the former have a higher affinity for hydrogen adsorption than the latter. Through various studies of unsupported metallic nitrides, it has been found that the ratio of these two types of planes increases when the particle size increases. However, when the particle size is increased, the surface area is decreased. This means, that if the catalyst is designed for large particle size, which gives low surface area, the ratio of planes is high and the result is high specific conversion (Zhang, 1999). Conversely, when the catalyst is designed for high surface area, which means small particle size, the ratio of planes is low and the result is low specific conversion. The conclusion from this is that when considering the overall conversion, an optimum point will exist between large particle size (high specific conversion) and large surface area (high number of active sites).

The review by Furimsky (2003) also points out the low number of studies on the promotion of a metallic nitride or carbide to a bi-metallic nitride or carbide. However, by studying what results have been generated, it can be seen that bi-metallic promotion leads to an increase in the activity of the catalyst. Another deficiency in the study of metallic

nitrides and carbides identified by Furimsky (2003) is the variation in the type of support used with metallic nitride and carbide catalysts. However, it was shown that the role of the support with respect to metal nitride and carbide catalysts will be similar to its role in the use of conventional catalysts (ie: increased surface area, acidity, etc.) (Furimsky, 2003).

As mentioned above, the study of metallic nitride and carbide catalysts has been primarily focused on HDS, HDN, and HYD. Furimsky (2003) reports in his review that metallic nitride and carbide catalysts are active for all three of these reactions. This is especially true when considering HDN, for which catalyst activity has been reported to even be higher for some metallic nitride and carbide catalysts than the activity observed with conventional hydrotreating catalysts. However, only a small number of studies have been done specifically focusing on HDO using metallic nitride and carbide catalysts. Furthermore, no studies have been carried out focusing on the HDO of biomass-derived oils using metallic nitride and carbide catalysts.

Ramanathan et al. (1995) carried out one of the few studies on HDO using unsupported metallic nitride and carbides. This study considered the hydrotreating of aromatics by many different hydrotreating mechanisms simultaneously, including HDO, HDS, HDN, and HYD. The aromatic feed was a mixture of model compounds intended to represent a realistic fossil-fuel derived feed. The feed contained 3000 ppm sulphur (dibenzothiophene), 2000 ppm nitrogen (quinoline), 500 ppm oxygen (benzofuran), 20 wt% aromatics (tetralin), and the balance aliphatics (tetradecane). The catalysts under investigation were unsupported metallic nitride and carbide catalysts containing molybdenum, tungsten, vanadium, niobium or titanium.

Metallic nitride and carbide catalysts are commonly prepared by either impregnation of the metal onto a support, such as alumina, to produce a supported catalyst, or by chemical precipitation to produce an unsupported catalyst. In both cases, the catalyst is then dried and calcined, similar to the procedure for traditional hydrotreating catalysts, to produce the metal oxide precursor.

Up to this point in the catalyst preparation, the procedure does not differ depending on whether the catalyst is to be a metallic nitride or carbide. The next step in the procedure is a temperature programmed reaction (TPR) that is dependent on the final catalyst desired. In the case of the nitride catalyst, the TPR is carried out by passing a pure stream of ammonia over the metal oxide. This is a critical step in the catalyst preparation that has a significant impact on how well the catalyst is dispersed and how high the catalyst activity will be. Ramanathan et al. (1995) identified heating rate, final temperature, the time of hold at the final temperature and the space velocity of the ammonia as the key parameters for this step. These parameters were empirically optimized by trial and error by Ramanathan et al. (1995) as shown in Table 2.4.

Table 2.4: Values of Important Metallic Nitride and Carbide Catalyst Preparation Parameters (Ramanathan, 1995)

Catalyst (precursor)	Heating Rate (β_2/K s^{-1})	Final Temp (T_{max}/K)	Time of Hold (t_{hold}/h)	Space Velocity (Sv_{molar}/h^{-1})
VC (V_2O_5)	0.033	1253	0.20	310
NbC (Nb_2O_5)	0.166	1173	3.00	1640
Mo_2C (MoO_3)	0.033	1003	0.33	220
WC (WO_3)	0.025	1124	1.00	400
TiN (TiO_2)	0.083	1223	1.50	230
VN (V_2O_5)	0.083	1148	0.00	1300
Mo_2N (MoO_3)	0.025	973	0.50	250

When preparing metallic carbides, the procedure is the same with the exception of the reactant used in the TPR, which is a carbon-containing gas rather than ammonia. Ramanathan et al. (1995) employed a mixture of 20% CH_4/H_2; however, other concentrations and gases have been used successfully in this step, such as an ethane/hydrogen mixture. The key operating parameters for this step, as described above, were also empirically optimized by Ramanathan et al. (1995) and are shown in Table 2.4. An alternative method of preparing metallic carbide catalysts has also been studied, in which the metallic nitride catalyst, as described above, is used as the precursor to the metallic carbide, rather than the metal oxide. TPR is then carried out on the nitride catalyst using the carbon containing gas.

In the case of both the nitride and carbide catalysts, after the TPR step is complete the catalyst is quenched under helium flow. The catalyst is then exposed to a low oxygen concentration gas (0.5% O_2/He) in order to create a passivated layer on the catalyst to protect it during handling. Due to the passivated layer, the final step in the catalyst preparation is a reduction, which is done in situ with pure hydrogen, prior to the start of the reaction.

The experiments executed by Ramanathan et al. (1995) were carried out in a three-phase trickle-bed reactor. Operating parameters were 3.1 MPa, 643 K and a liquid-hourly space velocity of 5 hr^{-1}. The catalysts were in the form of coarse powders or pellets (16/20 mesh) and were loaded along with inert quartz chips into the reactor to maintain a constant catalyst bed volume of 1 cm^3. The amount of catalyst used in each case was calculated such that a constant surface area of 30 m^2 was maintained for each catalyst loading. The experiments were allowed to reach steady state and the percentage of overall heteroatom removal (HDS, HDN, and HDO) was reported for each catalyst studied.

The discussion by Ramanathan et al. (1995) focused primarily on the HDN results, however, there were interesting conclusions made about the removal of oxygen when using metallic nitride and carbide catalysts. As stated above, the oxygenated hydrocarbon present in the feed was benzofuran. During the hydrotreating over the metallic nitride and carbide catalysts, benzofuran was found to be transformed into two compounds: ethylcyclohexane and ethylbenzene. The total percentages of oxygen removal were determined for each catalyst and are shown in Figure 2.5.

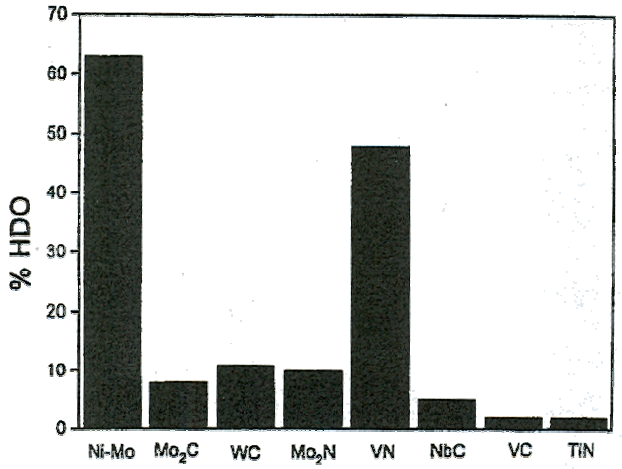

Figure 2.5: Comparison of Steady-State HDO for an Industrial Catalyst and Various Metallic Nitride and Carbide Catalysts (Ramanathan, 1995)

It can be seen from examining Figure 2.5 that when normalizing for the amount of catalyst loaded, the industrial, sulphided catalyst outperforms all of the nitride or carbide catalysts. It can also be seen that of the nitride and carbide catalysts, the vanadium-nitride (VN) catalyst has the highest HDO activity. It is proposed by Ramanathan et al. (1995) that the reason why the VN catalyst has the highest activity is that it possesses an optimal binding energy for HDO (K1s = 5465 eV). Also, it was found that when using the VN catalyst, the primary product of the HDO was ethylbenzene. This result was found to be significantly different than the results found when using the industrial catalyst, which produced mostly ethylcyclohexane. This suggests that there may be a completely different HDO mechanism for the nitride catalysts, which may indicate that this catalyst may be able to provide different selectivity than the traditional hydrotreating catalysts.

It was also noted by Ramanathan et al. (1995) that comparing the catalysts based on surface area might show misleading results. As stated previously, the basis of comparison for Figure 2.5 was a catalyst loading corresponding to a total surface area of

30 m^2. However, the characterization results obtained by Ramanathan et al. (1995) showed that the percentage of the total surface area that was catalytically active during the reaction was significantly greater for the industrial catalyst. The active surface area was measured in terms of active sites per gram of catalyst by CO uptake for the VN catalyst (62 μmol/g) and by O atoms from O_2 uptake for the industrial catalyst (718 μmol/g). The active surface areas of the catalysts were found to be 60 m^2/g for the VN catalyst and 160 m^2/g for the industrial catalyst. From Figure 2.5, it can be taken that the HDO activity was 63% for the industrial catalyst and 48% for the VN catalyst. With this information, the HDO activities can be related to one another by normalizing for active surface area (based on CO (O_2) uptake) rather than total surface area by carrying out the following transformation:

$$\frac{VN}{Ni-Mo} = \frac{(48\%/30m^2)*(60m^2g^{-1}/62\mu mol.g^{-1})}{(63\%/30m^2)*(160m^2g^{-1}/718\mu mol.g^{-1})} = 3.31 \qquad (2.1)$$

This normalization suggests that the VN catalyst is over three times as active as the industrial catalyst. Ramanathan et al. (1995) suggest that these results show great potential for metallic nitride and carbide catalysts as further improvements in the catalyst preparation techniques to optimize the active surface area may lead to higher overall activities.

2.5 CATALYST CHARACTERIZATION

Catalyst characterization is an important part of any study that is carried out on hydroprocessing reactions in order to understand what exactly is present on the catalyst surface at the time of reaction. Proper catalyst characterization can also lead to a better understanding of the reaction mechanisms present. In addition to this, it is often possible

to correlate catalytic activity to specific properties of the catalyst, which can lead to improved preparation procedures that optimize those properties.

In a study by Ferdous et al. (2004), the characterization methods commonly used on conventional hydrotreating catalysts are outlined. Eight different characterization methods that are discussed are related to the production of diesel fuel cetane enhancers from canola oil: elemental analysis, BET analysis, temperature programmed reduction (TPR), temperature programmed desorption (TPD), X-ray diffraction (XRD), scanning electron microscopy, nuclear magnetic resonance and fourier transform infrared spectroscopy (FTIR).

Elemental analysis is very important in characterizing what is present in the catalyst. This technique gives an elemental weight distribution. This is especially useful in determining the metal loadings on the catalyst and comparing the actual loadings to the targeted ones. Elemental analysis will also be an important characterization technique used on the reactants and products.

A BET analysis is also a necessity when characterizing a catalyst. BET studies give information on the surface area of the catalyst, pore volume, pore size and pore size distribution. These parameters are important in establishing a basis of comparison among different catalysts. As well, properties like pore size distribution can be used to help understand reaction mechanisms and factors such as diffusion limitations.

TPR/TPD studies are also important in the characterization of a catalyst. These studies give information on the reducibility of the catalyst, which can play a major role in the hydrogen adsorption steps of the overall reaction mechanism. These studies can also give information on the acidity properties of the catalyst. Also useful for gaining

information on acidic strength and acidic site distribution is FTIR. Studies of the acidity of metallic nitride and carbide catalysts may not be extremely crucial for the study of HDO; however, it may be useful in understanding the reaction mechanisms occurring. For example, knowing the acidity of the catalytic sites during the HDO of carboxylic acids may help explain the presence of products from decarboxylation.

Another characterization technique that is necessary when examining hydrotreating catalysts is XRD. XRD gives information on the composition and nature of the crystal structure of the bulk catalyst. This is even more important for metallic nitride and carbide catalysts as there is a great dependence of catalytic activity on the nature of the crystal planes present in the catalyst. The study by Ramanathan et al. (1995) supports the importance of XRD for the characterization of metallic nitride and carbide catalysts. In addition to this, Ramanathan et al. (1995) discuss the usefulness of using X-ray photoelectron spectroscopy (XPS) to better understand the surface composition and structure of the surface, before and after the reactions.

As discussed in Section 2.1.4, the issue of finding a basis of comparison for the different types of catalysts being studied is important in reporting meaningful results. In the study by Ramanathan et al. (1995), the experiment was designed to maintain the total catalytic surface area in the reactor at 30 m^2. However, because of the extensive work that has been done to optimize the preparation procedure of the industrial catalyst, it had a much more active surface area than the nitride or carbide catalysts. As a result, a comparison using constant catalytic surface area has less value. To overcome this, Ramanathan et al. (1995) considered the total amount of active surface area, based on chemisorption techniques, that was present on the specified surface area (30 m^2).

In order to determine the total amount of active surface area Ramanathan et al. (1995) used another common characterization technique, chemisorption. Chemisorption is similar to TPR; however, chemisorption often uses a gas other than hydrogen. Chemisorption measures the number of moles of a gas that are chemisorbed to the surface of the catalyst. The number of moles that are adsorbed can then be correlated to the number of active reaction sites that can be related to the amount of surface area that is actually active and involved in the reaction. By using this technique, Ramanathan et al. (1995) were able to make a more meaningful comparison and show that the specific activity of the metallic nitride and carbide catalysts is comparable, or in some cases better than the specific activity of the industrial catalyst.

3.0 Experimental Procedure

3.1 CATALYST PREPARATION

As defined in the primary objective of this project, the focus of this study was to examine various metallic nitride and carbide catalysts. An important component of achieving this objective, in addition to characterizing and testing the catalysts, was the task of synthesizing the catalysts in the laboratory. The need for synthesizing these catalysts was derived from two limitations. Primarily, it was of great importance to have control and flexibility over the physical properties of the catalysts, as these properties were the parameters upon which the different catalysts were evaluated. Secondly, the catalysts that were to be studied were not readily available to be purchased and as such were made in the laboratory. As a result, all of the catalysts studied in this project were synthesized in the Processing and Environmental Catalysis (PEC) laboratory of CANMET Energy Technology Centre-Ottawa (CETC-Ottawa), Natural Resources Canada.

In order to obtain similar end products for each of the catalysts prepared, a specific procedure was developed for the catalyst preparation and applied to all of the synthesized catalysts. This procedure was developed based on information found in the literature in conjunction with expertise at the laboratories at the CETC-Ottawa. Prior to developing this procedure, an evaluation of two common techniques for preparing supported metallic nitride and carbide catalysts was carried out. These common techniques are referred to as the impregnation method and the co-precipitation method. The impregnation method for catalyst preparation was chosen for this study as it is seen

as a better preparation method for catalysts with low metal loadings (<20 wt%). A detailed description of the procedure that was developed for this study is found below.

The catalyst preparation began with the preparation of the catalyst support. The catalyst support acts to facilitate the dispersion of metal active sites on the surface of the catalyst. The catalyst support chosen for this project were γ-Al_2O_3 extrudates (#43855, Alfa Aesar). The γ-Al_2O_3 extrudates had an original surface area of 220 m^2/g, an original average pore diameter of 7 nm, and an original pore volume of 0.62 cm^3/g. The γ-Al_2O_3 extrudates were first crushed into small particles ranging in size from 40 – 20 mesh (0.425 – 0.850 mm in diameter). It was important to crush the catalyst support into small particles due to the small size of the reactor bed. By reducing the diameter of the particles with respect to the diameter of the catalyst bed, channeling and void space effects were minimized.

After preparing the catalyst support, the required metal for each catalyst (Mo, W, or V), was then impregnated onto the surface of the support. This was done using an aqueous solution containing the appropriate metal salt and deionized water. The following metal salts were used to provide the required metals:

- Molybdenum – Ammonium Molybdate Tetrahydrate (#93-0245, Strem Chemicals)
- Tungsten – Ammonium Tungstate Pentahydrate (#93-0250, Strem Chemicals)
- Vanadium – Ammonium Metavanadate (#AC-0657, Anachemia)

Each of these salts was mixed with deionized water. The volume of water used was calculated based on the incipient wetness of the catalyst; that is, the volume of water was equal to the total pore volume of the catalyst support used. The purpose of this was to

avoid uneven metal impregnation due to excess water. In the event that the metal salt would not completely dissolve at room temperature, low heat (<50°C) and light mixing was applied to aid in the dissolution.

Once the metal salt was completely dissolved in the deionized water, the solution was immediately poured over the prepared catalyst support in a round bottom flask. The solution was poured over the catalyst support evenly and agitated slightly if necessary to ensure that the entire catalyst support was covered with solution. Following this, the round bottom flask containing the catalyst support and the metal salt solution was placed in a constant temperature bath (50°C) and left stationary for 6-12 hours to allow the water to evaporate.

The impregnated catalyst support was then transferred from the round bottom flask to a crucible and placed in a programmable high-temperature oven. The catalyst was then dried in air for an additional two hours at a temperature of 110°C to remove water that may have been trapped in the pores of the catalyst. This was followed by the calcination of the catalyst, which was carried out at 500°C for six hours.

During calcination, the metallic salts impregnated on the catalyst support are oxidized and the impurities from the metal salt solution (ammonia, water) are driven off the catalyst. In addition to this, research has also shown that during the calcination step, the metal oxide particles are able to migrate across the catalyst support surface. As a result, the product of the calcination step is a highly dispersed supported metal oxide with low impurities – an ideal catalyst precursor. The temperature programmed calcination schedule is outlined below in Table 3.1.

Table 3.1: Temperature Programmed Calcination Step Sequence

Description (Step)	Initial Temperature (°C)	Final Temperature (°C)	Rate (°C/min)	Duration (min)
Drying Period	110	110	0	120
Ramp Up	110	500	1	490
Calcination	500	500	0	360
Ramp Down	500	25	-2	238

At the end of the calcination step, the impregnated metals are in a stable oxide form. These stable catalyst precursors were then removed from the temperature programmed oven and stored for later use. Characterization of the metal oxides was carried out at this time and is discussed in detail for each phase of this project in Chapters 4, 5, and 6.

The final step in the procedure that was developed to synthesize the metallic nitride and carbide catalysts was the carburization or nitriding of the metal oxide precursor to yield the final active catalyst. This step was carried out at atmospheric pressure conditions in a tubular quartz reactor. The metal oxide precursor (mass equal to 3 grams) was loaded into the quartz reactor and placed in a temperature-controlled heater. The inlet of the reactor was preceded by mass flow controllers that delivered continuous, measured volumes of gas to the reactor to carry out the carburization / nitriding (Figure 3.1).

The inlet gases were specified depending on the desired final catalyst. In the case of the metal carbide catalysts, a carbon containing mixture of gases was used; a mixture of 10% Ethane, 85% Hydrogen and 5% Nitrogen. The carbon containing gas mixture was delivered at a total volumetric flow rate of 200 ml/min (GHSV = ~2750 hr^{-1}). In the case of the metal nitride catalysts, 100% ammonia was used to provide the nitrogen

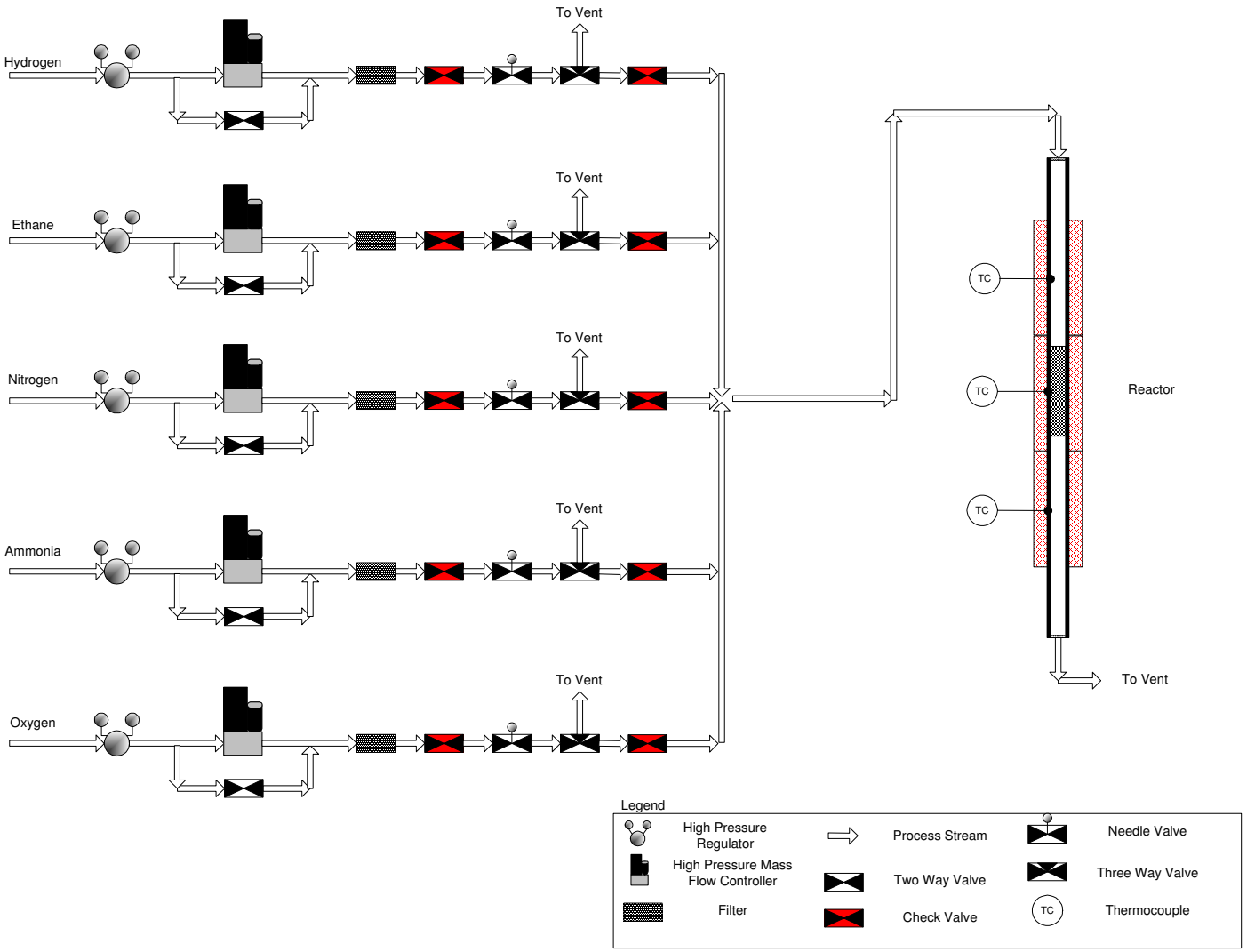

Figure 3.1: Process Flow Sheet of the Carburization / Nitriding Apparatus

required for the reaction. The ammonia was delivered at a total volumetric flow rate of 100 ml/min (GHSV = ~1375 hr^{-1}).

The temperature was electronically controlled to provide uniform temperature and heating rates for the carburization / nitriding. A final temperature of 700°C and a heating / cooling rate of 1°C/min were used. The final process parameters that were used for the carburization / nitriding were based on previous work in literature (Ramanathan et al., 1995) and expertise from the laboratory at the CETC-Ottawa. The final process parameters are summarized below in Table 3.2 and Table 3.3.

Table 3.2: Process Parameters for Carburization / Nitriding of Metal Oxide Precursors

Description (Step)	Initial Temperature (°C)	Final Temperature (°C)	Rate (°C/min)	Duration (min)
Ramp Up - Stage 1	25	200	1	175
Temperature Hold #1	200	200	0	120
Ramp Up - Stage 2	200	700	1	500
Temperature Hold #2	700	700	0	300
Ramp Down - Stage 1	700	500	-1	200
Ramp Down - Stage 2	500	25	-1	475
Passivation	25	25	0	240

Table 3.3: Process Parameters for Carburization / Nitriding of Metal Oxide Precursors

Description (Step)	Carburization		Nitriding	
	Flowing Gas (vol %)	Volumetric Gas Rate (ml/min)	Flowing Gas (vol %)	Volumetric Gas Rate (ml/min)
Ramp Up - Stage 1	10 (C_2H_6), 85 (H_2), 5 (N_2)	200	100 (N_2)	100
Temperature Hold #1	10 (C_2H_6), 85 (H_2), 5 (N_2)	200	100 (N_2)	100
Ramp Up - Stage 2	10 (C_2H_6), 85 (H_2), 5 (N_2)	200	100 (NH_3)	100
Temperature Hold #2	10 (C_2H_6), 85 (H_2), 5 (N_2)	200	100 (NH_3)	100
Ramp Down - Stage 1	10 (C_2H_6), 85 (H_2), 5 (N_2)	200	100 (NH_3)	100
Ramp Down - Stage 2	90 (H_2), 10 (N_2)	100	100 (N_2)	100
Passivation	1 (O_2), 99 (N_2)	40	1 (O_2), 99 (N_2)	40

The end products of the carburization / nitriding step are the desired final metallic carbide and nitride catalysts that are to be tested in the experimental reactor. However, it is necessary to handle the catalysts in air while transferring them from the quartz reactor to the experimental reactor. In order to prevent damage to the catalysts, they are passivated by exposing the catalyst to a low concentration of oxygen (1 vol %) to form a metal oxide layer on the outside surface of the catalyst (Table 3.3). This metal oxide layer then protects the active catalyst beneath it when the sample comes in contact with the air. This passivated layer is then removed immediately before the laboratory tests by flowing hydrogen through the catalyst bed after it is loaded into the experimental reactor.

3.2 CATALYST CHARACTERIZATION

Catalyst characterization played an important role in this study as it was important to understand the physical characteristics of each of the catalysts. Since the catalysts were synthesized in the laboratory at CETC-Ottawa, it was important that a complete understanding of the physical and chemical properties or "signature" be established for each of the catalysts. Using this unique signature for each catalyst, a fare comparison of the catalysts could then be carried out. The catalysts were characterized at different stages of the preparation procedure with different techniques in order to generate these unique signatures. A summary of the different techniques and equipment used for analysis is found below. The results of the characterizations are found in each chapter to which the results are related.

The first sets of characterization were done on the metal oxide precursors that were used to synthesize the various active catalysts. X-ray Fluorescence (XRF) analysis was carried out on all of the metal oxide precursors to determine the metal loading of each catalyst. During the XRF analysis, the sample is exposed to a high energy x-ray (primary) that has enough energy to knock electrons out of the inner most orbitals of the atoms in the sample. This renders the atoms unstable ions, and in order to return to a stable state, an electron from an outer orbital moves into the inner orbital. This electron movement then emits a secondary x-ray at an energy that is different for each atom, allowing the content of the sample to be identified. The intensity of this secondary x-ray is then used to determine the quantity of each atom in the sample. The XRF analysis was carried out on a Rigaku RIX 3000 WD-XRF incorporating a 3kW generator. The analysis was performed in the Characterization Laboratory located at CETC-Ottawa.

Also at this time, an X-ray Diffraction (XRD) analysis was carried out on all of the metal oxide precursors. XRD analysis is used to identify the different molecular structures that are present on the surface of the catalyst. This is done by exposing the sample to a constant energy x-ray light source. As the light passes through the sample, the crystal structure of the different molecules diffracts the single light into a series of beams leaving the sample at varying angles relative to the original beam. The intensity and position of each of these light beams is plotted to generate a diffraction pattern that is unique for each molecule. The diffraction patterns are then compared to a library of known patterns to identify the different molecules that may be present in the sample. The XRD analysis was carried out on BRUKER D500TT and D5000 automated diffractometers using Cu(Kα) radiation, 1.54 Å. These instruments are each equipped

with a diffracted-beam graphite monochromator and a scintillation detector. The generator voltage and current settings were 40 kV and 30 mA, respectively. The analysis was performed in the Characterization Laboratory located at CETC-Ottawa.

After the metal oxide precursors had been carburized / nitrided, further characterization was carried out in order to determine the physical characteristics of the catalysts. This was done to ensure that the physical properties of the catalysts (surface area, pore size, pore diameter) were the same to provide an equal comparison between the different catalysts. This information was also required to examine the external and internal mass transfer limitations of the system. To determine these physical characteristics, a BET (Brunauer – Emmett - Teller) analysis was carried out on all of the catalysts that were tested. The BET analysis begins by evacuating the catalyst sample to remove any foreign molecules adsorbed on the surface. Following this, the sample is exposed to low temperature nitrogen at varying pressures and the amount of gas adsorbed to the surface is measured and plotted to generate an adsorption isotherm. This isotherm can then be used to determine the surface area (using the known area occupied by one nitrogen molecule), pore size and distribution, and pore volume. The BET analysis was carried out on a Micromeritics ASAP 2000 Accelerated Surface Area and Porosity System. The analysis was performed in the PEC Laboratory at CETC-Ottawa.

3.3 EXPERIMENTAL SETUP

The experimental apparatus used in this study was a high-pressure micro-reactor system that was designed to model a high-pressure hydrotreating process. The experimental apparatus consisted of a high-pressure tubular reactor, an electronically

controlled furnace, gas and liquid delivery systems, and automated data collection. The experimental apparatus was located in one of PEC's laboratories at CETC-Ottawa. Both the design of the system and the commissioning stages of the setup played an important role in this project as the experimental apparatus was constructed specifically for this process.

3.3.1 Experimental Setup – Design

The objective of this experimental apparatus was to generate experimental data on conversion, yields, and selectivity. While doing this, it was also desirable to model a high pressure, high temperature tubular reactor, similar to what would be found in a real world hydrotreating environment. The key components of a typical hydrotreating process were all included in the experimental design: a high pressure tubular reactor (micro-reactor), a gas and liquid delivery system, liquid collection system, online gas characterization, and automatic continuous data acquisition. The completed experimental apparatus is depicted below in Figure 3.2.

The experimental micro-reactor was a stainless steel tubular reactor. The micro reactor had an inner diameter of 6.0 mm, an outer diameter of 9.1 mm, and a total length of 395 mm. The micro-reactor also contained a thermowell through the centre of the reactor during experimental trials that had an outside diameter of 1.7 mm. These dimensions resulted in a total available reactor volume of approximately 10 mL. The reactor was heated using an electric furnace that completely encircled the micro reactor. The electric furnace was comprised of two heating zones, each 150 mm in length, which was controlled with electric thermocouples. The placement of the catalyst bed in the

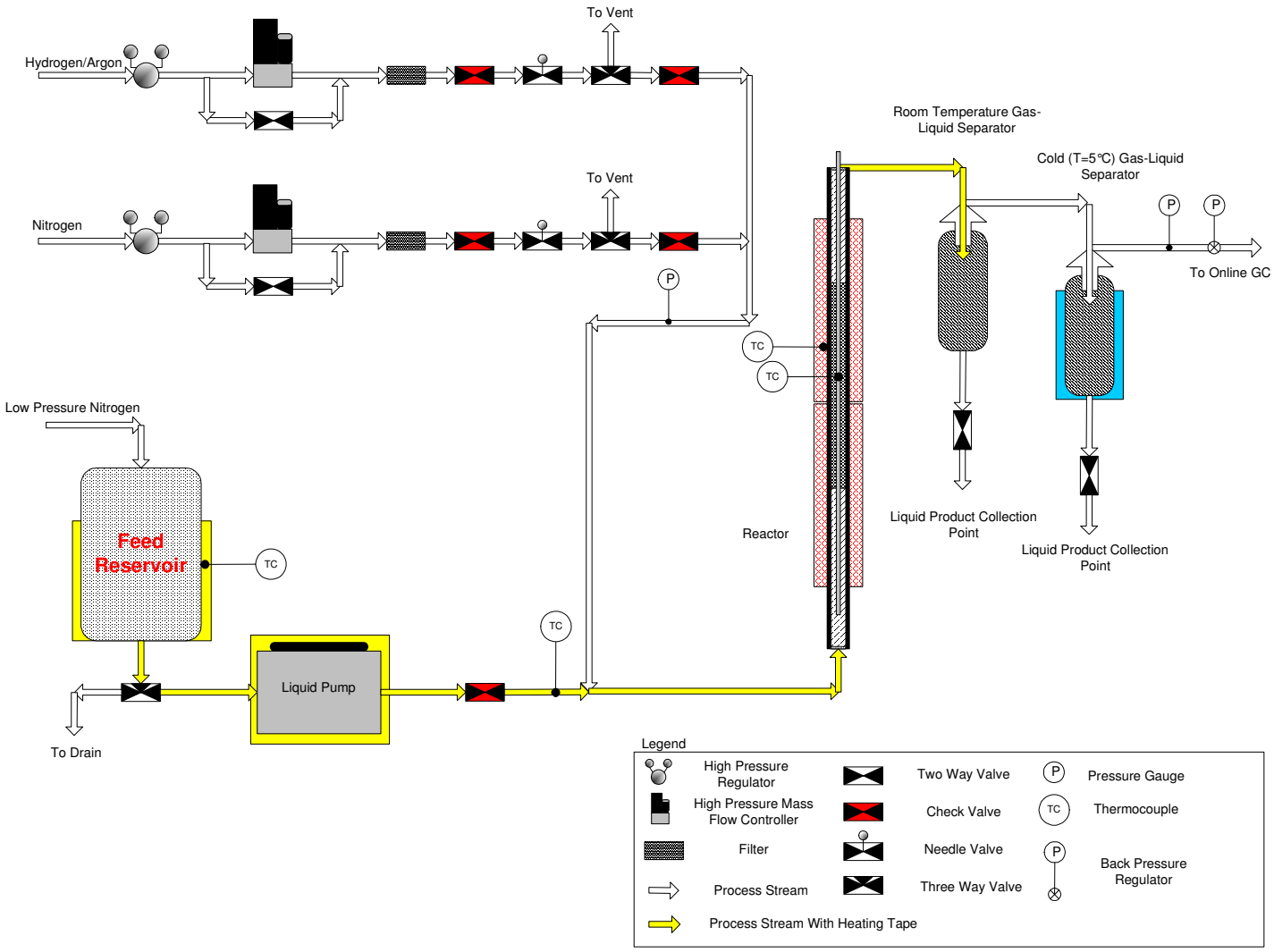

Figure 3.2: Process Flow Sheet of Experimental Apparatus

reactor was carefully calculated to ensure that the bed was centered in the furnaces for all experimental trials.

The gas delivery system consisted of Brooks Smart (5850S) Mass Flow Controllers that were calibrated for high-pressure operation. The mass flow controllers delivered both the reactant gas and nitrogen for purging and pressure testing. The reactant gas that was used throughout the experimental trials was a certified mixture of hydrogen (90%) and argon (10%) provided by BOC Gases. Argon was included in the mixture as an inert tracer gas in order to monitor, and correct for, any discrepancies in the outlet gas flow measurements.

The liquid delivery system that was used consisted of a high-pressure liquid pump that delivered liquid feed from a reservoir tank to the micro-reactor. A small positive pressure, maintained with nitrogen, was supplied to the reservoir tank to ensure that continuous liquid was supplied to the pump inlet and no air entered the system. The entire liquid delivery system was maintained at an elevated temperature (>50°C) to prevent any solidifying of the reactants. The elevated temperatures were provided with heat tapes controlled by manual rheostats.

Over the course of the experimental trials, two different liquid pumps were used. The first liquid pump that was used was a Harvard Apparatus Pump 44 high-pressure syringe pump. After successfully using this pump for several months, the syringe pump began to have difficulty delivering enough pressure to maintain constant volume delivery. At this time, the pump was replaced with a Beckman-Coulter high-pressure liquid chromatography pump (System Gold Model 118 Solvent Module). This pump was used

throughout the rest of the experimental trials without problem. All of the experimental trials that were affected by the syringe pump failing were omitted from the results.

From the gas and liquid delivery systems, the reactants flowed through high-pressure stainless steel lines to the micro reactor. Prior to entering the reactor, the lines were connected to one another and followed by sufficient tubing to allow the gas and liquid to mix. The lines remained heated with heating tapes to above 50°C from the point of mixing to the inlet of the reactor. Check valves were installed in both the gas and liquid lines to prevent back flow into the gas and liquid delivery systems. The mixture of gas and liquid were then fed to the bottom of the micro-reactor and flowed upward through the packed catalyst bed. The upward flow direction was chosen to create a uniform flow distribution and minimize the flow effects that are often seen when using a small reactor diameter.

After the gas and liquid had reacted and flown through the reactor, the products were fed into a room temperature gas-liquid separator. The lines were heated with heating tapes, controlled by manual rheostats, to maintain the temperature of the outlet lines above 100°C to prevent rapid cooling that may lead to solidifying of the heavier products in the lines. The gas-liquid separator, which was maintained at room temperature, collected the majority of the liquid product at the end of each experimental trial. The gases were then fed into a second gas-liquid separator at a temperature of 5°C. This separator was used to remove any condensable products and water (vapour) that may be entrained in the gases prior to sending them to the gas chromatograph. Any liquid samples that were found in the low temperature gas-liquid separator were then

added to the sample taken from the room temperature separator to form the final liquid sample.

During each experimental trial, after the gases had passed through the low temperature separator, they were fed to an online gas chromatograph. The gases were analyzed with an HP5890 gas chromatograph that was equipped with both a thermal conductivity detector (TCD) and flame ionization detector (FID). In addition to this, on some experimental trials, an Agilent micro gas chromatograph model 3000A was used to analyze the light end gases. In these cases, the HP5890 gas chromatograph continued to analyze the hydrocarbon gases. Samples were injected on a continuous basis throughout each experimental trial to give a complete time dependent picture of the extent of the reaction (equilibrium).

The process parameters such as pressure, temperature, and delivered flow rates were continuously monitored and recorded by an automated data acquisition system. The data acquisition was performed by National Instruments Field Point (version 3.01), which communicates between the process equipment and the computer software. National Instruments Lookout software (version 5.0) was used to organize, display and log the data.

3.3.2 Experimental Setup – Commissioning

Commissioning the experimental apparatus was important because the apparatus was reconstructed for this project. It was important to ensure that the data, both inputs and results, were reliable and consistent. In order to obtain the desired reliability, the following measures were taken to prepare the apparatus for experimental trials:

- Pressure testing of all high-pressure lines and vessels.
- Calibration of the mass flow controllers.
    - A series of set points were applied to the mass flow controllers and the volumetric flow rate (determined by a wet test meter) and various gas compositions of the outlet of the controllers (gas chromatography) were analyzed.
- Calibration of the liquid delivery system.
    - A series of set points were applied to the liquid pumps and the total liquid recovery of the (inert) system was analyzed.
    - This quality control issue was monitored closely when the type of pump had to be changed.
- Volumetric displacement study. It was important that the gas and liquid samples were taken once the system had equilibrated. To confirm this, the effective system volume at the required pressures was determined in order to specify the appropriate time until samples could be taken.
- Gas chromatography calibrations. Calibrations of the gas chromatography equipment were done on a regular basis to ensure that the results were reliable.

3.4 EXPERIMENTAL PROCEDURE

In order to ensure a consistent and reliable evaluation between the results of the experimental trials, it was important to strictly follow an experimental procedure that did not vary from trial to trial. This procedure was developed along with the help of the resident expertise at CETC-Ottawa. The same procedure was followed for each trial.

Changes in inputs such as pressure, temperature, catalyst loading in the reactor, etc., were only implemented as a part of the experimental design.

The first step in the experimental trial was to load the catalyst bed into the micro reactor. This process began by determining the catalyst loading for each different trial. The catalyst loading for each experimental trial was a function of the experimental design for each step of the study. Further details on how these loadings were determined are discussed in Chapters 4, 5, and 6. Once the catalyst loading was determined, the appropriate loading of inert silicon carbide was determined. The silicon carbide was added to the catalyst to lengthen the catalyst bed and reduce the effects of the reactor walls on heat and mass transfer due to the small inner diameter of the reactor. The silicon carbide used was the same size as the catalyst support: 40-20 mesh (0.425 mm – 0.850 mm). The ratio of silicon carbon to active catalyst was held constant over all trials at one part silicon carbide (by volume) to every two parts active catalyst (by volume).

The active catalyst was then loaded into the reactor (actual loadings discussed in Chapters 4, 5, and 6). The reactor was loaded top to bottom (upside down on the bench). The internal thermowell was installed prior to loading the catalyst bed and was held in the centre of the reactor to ensure that the bed was loaded evenly around the thermowell and prevented it from touching the walls of the reactor.

First, a bed of inert quartz chips was loaded into the reactor. The height of this bed was calculated in order to place the active catalyst bed in the centre of the furnace. Next, the active catalyst, diluted with silicon carbide, was loaded into the reactor. The catalyst and silicon carbide were mixed together prior to loading the catalyst bed into the reactor using a sample vial. The diluted active catalyst bed was then slowly added to the

reactor on top of the quartz bed. While loading the catalyst, light tapping on the side of the reactor was used to ensure that the bed was packed tightly.

Following this, a second bed of inert quartz chips was loaded into the reactor. The quartz chips were added until the reactor was full and was aided by light tapping on the reactor walls to ensure that the entire bed was packed and would not shift after the reactor was closed. This quartz bed served a second purpose in that it acted as a preheating zone in the furnace prior to the active catalyst bed. This zone then provided the reactants time to reach reaction temperatures prior to entering the active catalyst bed. A typical reactor loading is shown below in Figure 3.3. After the catalyst bed had been loaded into the reactor, the reactor was sealed and installed into the furnace. Following this, the inlet and outlet of the reactor were tied back into the appropriate inlet and outlet process lines.

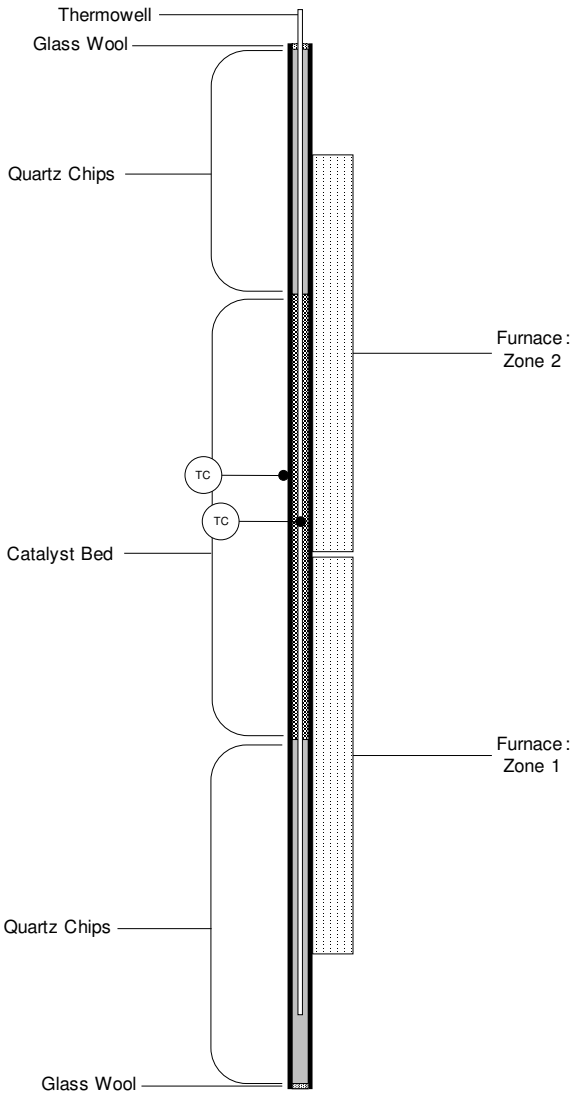

Figure 3.3: Catalyst Bed Position in the Experimental Reactor (Furnace)

The next step in the experimental procedure was to reduce the passivated layer of metal oxides on the surface of the catalyst. It is necessary to remove this layer prior to beginning the experimental trial. To carry out the reduction, the reactant gas (90% H_2, 10% Ar) was delivered to the catalyst bed. Initially, the flow rate of gas was brought up to 90 mL/min (GHSV = ~1850 hr^{-1}) flowing against slightly higher than atmospheric pressure (200 kPa). A backpressure regulator was used to set the desired pressure. The

temperature of the catalyst bed at this time was room temperature. The temperature was then raised manually from room temperature to 300°C in 50°C increments every 30 minutes. Following this, the temperature was increased from 300°C to the maximum reaction temperature in 20°C increments every 20 minutes. After reaching the maximum reaction temperature, the temperature, pressure, and gas flow rate were held constant for 2-3 hours to complete the reduction. During the entire reduction, no liquid was delivered to the reactor.

After the reduction was complete, the temperature and gas flow set points were changed to the value required for the first experimental trial. In addition to this, the backpressure regulator was adjusted to increase the system pressure to the desired pressure for the first experimental trial. These conditions were allowed to reach steady state while only delivering gas to the reactor. Finally, after all of the other process parameters were stable, the liquid delivery system was put online to pump at the specified rate of the first experimental trial.

Each experimental trial was made up of two distinct stages. The first was the transient stage; the time immediately after a set-point change in which the system was still responding to the change. During this time the products from the system were also changing (monitored online by gas chromatography). The samples taken during this stage were considered non applicable and were discarded. The gas chromatography results were monitored throughout this stage for an indication that the system had reached equilibrium. This was indicated by the gas compositions becoming constant and marked the end of the transient stage and the beginning of the experimental (steady-state) stage. At this time, the liquid samples were removed from the gas-liquid separators, so that new

samples (at steady-state conditions) could be collected. Also, mass balances were started at this time in order to evaluate the experimental trial.

The experimental stage was allowed to run for various lengths of time generally between 8 and 24 hours depending on the time that was required to obtain a sizable liquid sample. Throughout the experimental stage, the gas composition was measured online by gas chromatography at regular intervals. The average gas compositions were then taken and used in the mass balance calculations. At the end of the experimental stage the mass balance was closed and the liquid sample was collected from the gas-liquid separators. In order to complete the mass balance calculations, the following information was collected for each experimental trial:

- Start and end times of experimental trial.
- Initial and final weights of liquid feed reservoir.
- Average volumetric gas rates.
- Average temperatures.
- Final weights of liquid products (aqueous phase and organic phase).

Following the experimental stage, process parameters were changed to the required set points of the next experimental trial. The two-stage process was then repeated by allowing the system to reach equilibrium then starting the experimental stage. This process was repeated for all of the desired experimental trials for each catalyst based on the experimental design.

At the end of all of the experimental trials for one catalyst, the reactor was slowly decommissioned. First, the liquid flow was turned off and the gas flow was maintained in order to prevent damage to the catalyst by exposing it to air while at high temperatures.

Next, the temperature set points were dropped to room temperature and the catalyst bed was allowed to cool. Once at room temperature, the gas flows were shut off and the reactor was disconnected from the process lines. The catalyst bed was then removed from the reactor and the catalyst was sealed in a sample vial for storage. This entire procedure was then repeated for the next catalyst to be studied.

3.5 PRODUCT CHARACTERIZATION

3.5.1 Product Gas Characterization

The product gases from each experimental test were analyzed by online gas chromatography. As discussed previously, the primary gas chromatograph that was used was an HP5890 gas chromatograph; however some trials were analyzed using an Agilent micro gas chromatograph model 3000A. The gases were sent directly to the gas chromatograph from the experimental apparatus and regular samples were taken every three hours during each experimental trial.

The reactant gas that was used was a mixture of approximately 90% hydrogen gas and 10% argon. Prior to using each new cylinder of reactant gas, the exact compositions of the inlet gas were determined using the same gas chromatographs as were used in those experimental trials. The purpose of the argon was to provide an inert tracer gas that could be used to back calculate the product gas rate. Raw data (area) was taken from the output of the gas chromatograph and using the calibration data for the gas chromatograph, volume percents of the product gas were determined. The volume percents of the product gas were then summed and normalized to 100%. Typically, the sum of the raw volume percents was in the 96-98 % range.

The molar flows (in and out) of each gas were calculated using the ideal gas law and the conditions at the time of analysis (Equation 3.1). The molar flows of argon were then balanced (Equation 3.2) in order to back calculate the total product gas flow (Equation 3.3). Following this, the molar flows of the remaining product gases were determined using the calculated product gas volumetric flow (Equation 3.4).

$$N_{i,IN} = F_{IN} * v_{i,IN} * \left(\frac{P_{gc}}{R * T_{gc}} \right) \tag{3.1}$$

$$N_{Ar,IN} = N_{Ar,OUT} \tag{3.2}$$

$$F_{Ar,OUT} = F_{Ar,IN} * \left(\frac{v_{Ar,IN}}{v_{Ar,OUT}} \right) \tag{3.3}$$

$$N_{i,OUT} = F_{OUT} * v_{i,OUT} * \left(\frac{P_{gc}}{R * T_{gc}} \right) \tag{3.4}$$

where $N_{i,IN/OUT}$ is the molar flow rate of species i entering or leaving the reactor, $F_{IN/OUT}$ is the total volumetric gas rate entering or leaving the reactor, $F_{i,IN/OUT}$ is the volumetric gas rate of species i entering or leaving the reactor, $v_{i,IN/OUT}$ is the volumetric fraction of species i entering or leaving the reactor, P_{gc} is the pressure at the point of measurement, T_{gc} is the temperature at the point of measurement, and R is the ideal gas constant.

3.5.2 Product Liquid Characterization

The liquid products from each experimental trial were collected in two gas-liquid separators placed in series. The first separator was maintained at room temperature and was where the majority of the liquid products were collected. A second separator, maintained at 5°C, was placed in series after the room temperature separator. The

primary purpose of the second separator was to protect the online gas chromatography equipment, but it also collected some liquid samples. The total liquid product was determined by collecting the entire product from both separators.

After collecting the samples, the weight of the total sample was determined. Following this, the sample was transferred into a separatory funnel and allowed time for the two product phases to separate. Both an aqueous and an organic phase were found in the liquid product. The two phases were then separated and the weights of both were determined. The aqueous phase was discarded at this time. The organic phase was sealed in a sample vial and sent for further analysis.

A variety of analysis was carried out on the liquid products, as well as the liquid feedstock. The alkane and olefin content of the final product was an important parameter that was determined for the liquid product. It was desirable to obtain a final product with high levels of long chained alkanes and olefins as they are primary indicators of a product with high cetane levels. A detailed procedure of this analysis is found in Appendix F. This analysis was carried out by gas chromatography / mass spectrum (GC/MS) in the Characterization Laboratory at CETC-Ottawa.

Similar to the alkane and olefin content of the product, it was also desirable to get a boiling point distribution of the final product. This is also a key indicator of the yield of diesel fuel produced in a particular test. In order to do this, the liquid products were characterized by simulated distillation in order to obtain boiling point distribution. This analysis was also carried out in the Characterization Laboratory at CETC-Ottawa.

It was also desired to characterize the liquid product in terms of conversion. This was done in two ways. The first was to characterize the liquid product in terms of

conversion of fatty acids. The liquid products were analyzed for fatty acid content by using BF_3/MeOH to convert the fatty acids to fatty acid methyl esters (FAME) and then analyzing the methyl esters using GC/MS. A detailed procedure for this method is found in Appendix F. This analysis was carried out on a GC/MS in the Characterization Laboratory at CETC-Ottawa.

The second measure of conversion was oxygen content of the liquid product. The change in oxygen content of the liquid product demonstrated not only the extent of which the fatty acids were broken down, but the complete removal of oxygen from the liquid product. This is an important parameter in characterizing diesel fuel products because it gives the extent of hydrodeoxygenation. The oxygen content of the liquid samples was determined by difference from a C/H/N elemental analysis. This analysis was carried out on a LECO LE-CHN-2000 in the Characterization Laboratory at CETC-Ottawa.

4.0 Scouting Tests

The experimental work carried out in this project was divided into three distinct phases, which are described in Chapters 4, 5, and 6. The first phase, discussed in this Chapter, is a series of scouting tests that are designed to quickly identify a small number of catalyst candidates to be further studied in phases two and three. Section 4.1 describes the catalyst preparation and characterization of the six catalysts chosen for the scouting test. The results of these characterizations are compared with one another to show that the six catalysts were all similar with respect to both physical and chemical properties. Sections 4.2 and 4.3 discuss the reactor loading and process parameters that were used to carry out the scouting test. Finally, in Section 4.4, the performance of the catalysts is discussed with respect to five key performance indicators: oxygen content in the organic product (conversion), fatty acid content in the organic product (conversion), alkane/olefin content of the organic product (selectivity), hydrogen consumption, and gas by-product production.

4.1 CATALYST PREPARATION AND CHARACTERIZATION

4.1.1 Physical Properties

To ensure an unbiased comparison, it was important that all of the process parameters were held constant with the exception of catalyst type. A major part of achieving this was ensuring the physical properties of the catalyst were the same. To do this, an identical catalyst preparation procedure was used for all six catalysts. Details of this procedure are outlined in Chapter 3. A BET surface area and pore volume/size analysis was carried out on each of the prepared catalysts to confirm that the physical

characteristics of the catalysts were similar. It was found from this analysis that there were only very small differences between the catalysts with respect to both surface area and pore volume/size. The surface area of each catalyst ranged from 185 – 200 m^2/g, the pore volume of each catalyst ranged from 0.475 – 0.575 cm^3/g, and the average pore diameter of each catalyst ranged from 10 – 11.2 nm. A summary of these results is shown below in Table 4.1.

Table 4.1: Summary of BET Surface Area and Pore Volume/Size Characterization

Catalyst*	BET Surface Area (m^2/g)	Pore Volume (cm^3/g)	Average Pore Diameter (nm)
7.4 wt% Mo / γ-Al_2O_3	191	0.478	10.0
10 wt% W / γ-Al_2O_3	194	0.491	10.1
3.1 wt % V / γ-Al_2O_3	197	0.538	10.9
7.4 wt% Mo / γ-Al_2O_3	187	0.486	10.4
10 wt% W / γ-Al_2O_3	186	0.504	10.8
3.1 wt % V / γ-Al_2O_3	198	0.555	11.2

*Catalyst compositions to be discussed in Section 4.1.2

After confirming that the physical properties of the catalysts were similar, it was equally important to confirm that these physical properties do not contribute to large mass transfer resistances that may result in a mass transfer limited catalyst. However, this confirmation could not be made until after the results from the phase I scouting test was obtained. A full discussion on the mass transfer limitations is found later in this chapter in Section 4.4.1.

4.1.2 Chemical Properties

Equally important in performing an unbiased comparison was the consideration of the chemical properties of each of the six catalysts that were studied in the phase I scouting tests. As stated previously, the objective of these tests was to compare the chemical structure of the catalysts. To do this, it was important to control the other chemical properties that could have had an impact on the final results, such as metal dispersion and catalyst loading.

The objective in preparing the catalysts for these tests was to have a highly dispersed active metal on the support of the catalyst. Furthermore, it was important that all of the catalysts were equally dispersed to ensure a fair comparison. The metal dispersion was determined by carrying out two tests on the catalyst. First, X-ray fluorescence (XRF) was carried out on the three metal oxide precursors (molybdenum-oxide supported on γ-Al_2O_3, tungsten-oxide supported on γ-Al_2O_3, and vanadium-oxide supported on γ-Al_2O_3) as described in Chapter 3. These results were used to confirm the presence of the metallic components and measure their quantity. Second, the catalysts were analyzed by X-ray diffraction (XRD) to determine if a signature for the metallic components could be seen. It was then concluded that the catalyst was highly dispersed if the XRF confirmed the presence of the metallic components, but they were undetectable by XRD.

The XRF analysis was carried out on the metal oxide precursors and the results are shown below in Table 4.2.

Table 4.2: Chemical Compositions of the Phase I Scouting Test Catalysts (Oxide Precursor)

Catalyst Precursor	Al_2O_3 (wt%)	MoO_3 (wt%)	WO_3 (wt%)	V_2O_5 (wt%)	SiO_2 (wt%)	P_2O_5 (wt%)	Cl (wt%)
Mo	88.5	11.1	--	--	0.1	0.2	0.1
W	87.2	--	12.6	--	0.1	--	--
V	94.2	--	--	5.6	0.1	--	--

It can be seen in Table 4.2 that the desired metals molybdenum, tungsten, and vanadium are present in each of their respective samples with the other primary component being the γ-Al_2O_3 support. The XRD analysis was also carried out on the three metal oxide precursors and the XRD plots of these are shown in Figures 4.1, 4.2, and 4.3.

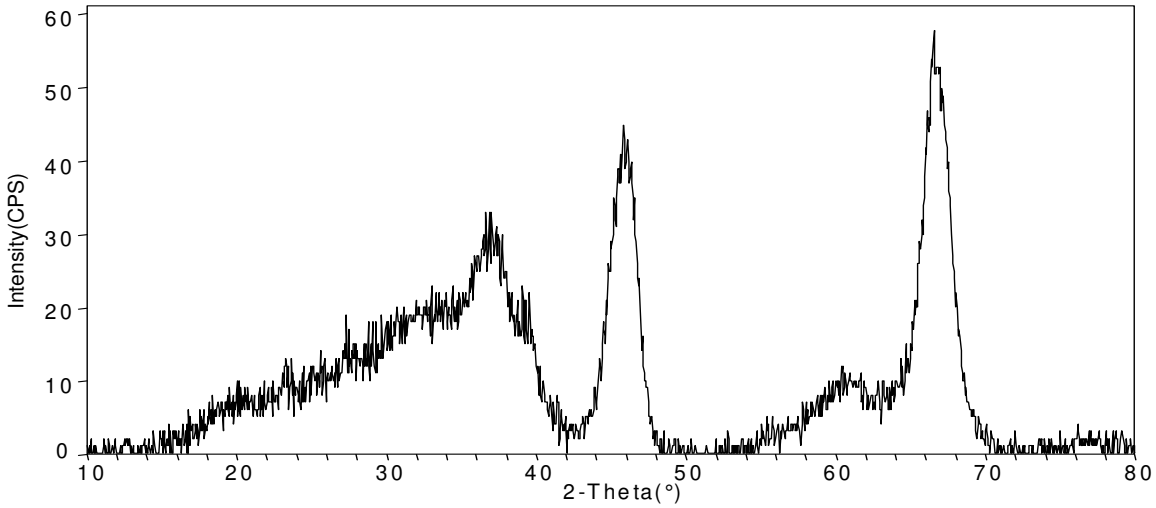

Figure 4.1: XRD Plot of 11.1 wt% Supported MoO_3/γ-Al_2O_3

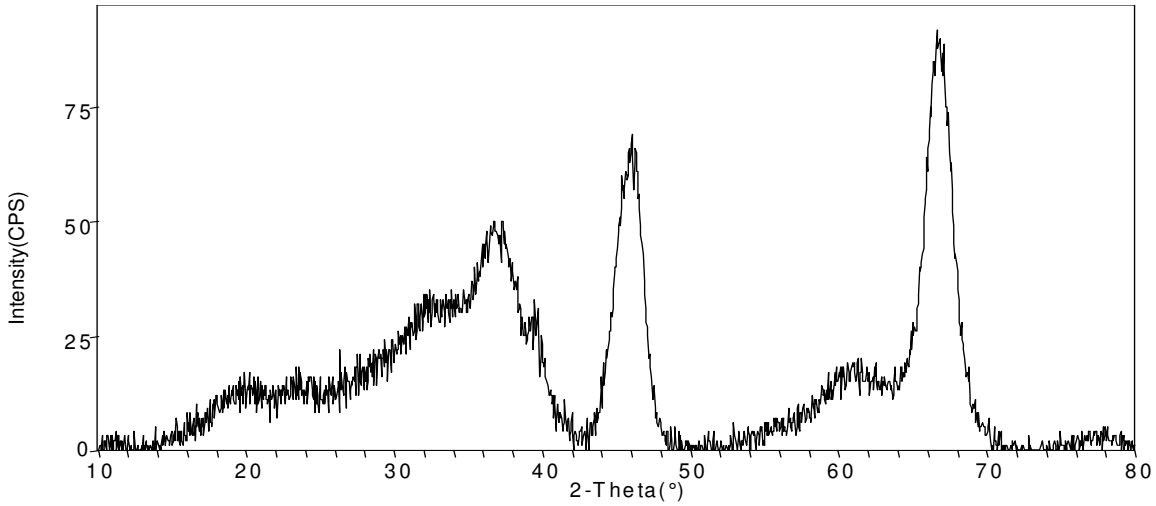

Figure 4.2: XRD Plot of 12.6 wt% Supported $WO_3/\gamma\text{-}Al_2O_3$

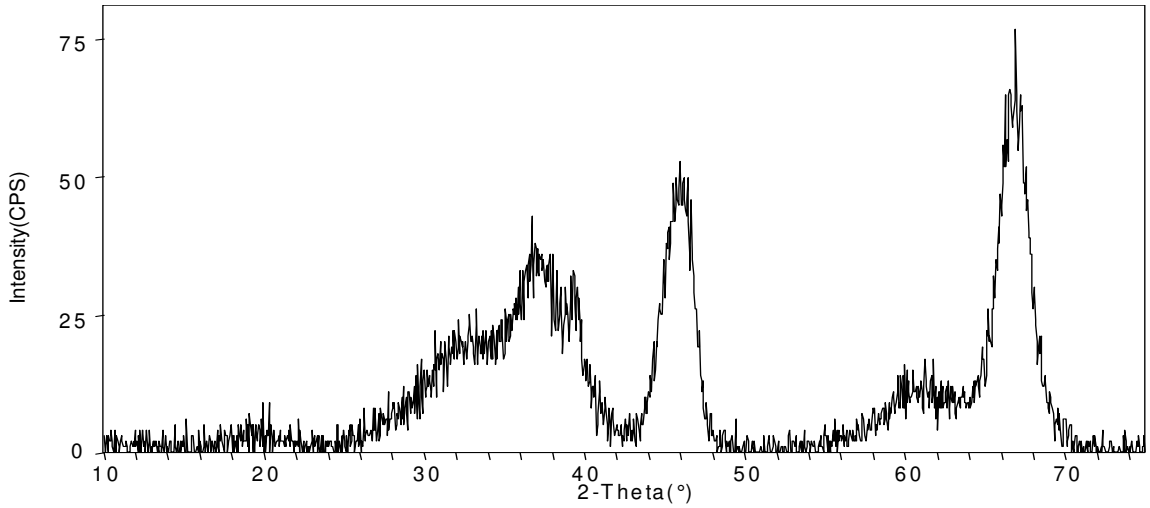

Figure 4.3: XRD Plot of 5.6 wt% Supported $V_2O_5/\gamma\text{-}Al_2O_3$

It was difficult to identify the peaks of the three oxides from the XRD data given in Figures 4.1, 4.2, and 4.3. When searching for molybdenum oxide, it would be expected to see peaks on Figure 4.1 at 2θ values of approximately 23° and 27°. Similarly, peaks for tungsten oxide should appear on Figure 4.2 at 2θ values of approximately 23° and 33° and peaks for vanadium oxide should be present on Figure 4.3 at 2θ values of 20° and 26°. These peaks cannot be identified however in any of the

cases, as there is only a large broad shoulder with intensity less than 40 at these 2θ values, which is characteristic of the γ-Al_2O_3 support. However, the XRF results confirm the presence of the transition metals and this leads to two possible conclusions. First, the transition metals are in amorphous rather than crystalline phases and therefore may not appear in the XRD pattern. Second, the expected high dispersion of the transition metals on the alumina surface can result in weak peaks for the metal species or no peak at all. Table 4.3 shows the calculated metal loading. Already confirmed from XRD studies, the catalysts are highly dispersed.

Table 4.3: Summary of Calculated Metal Loading

Catalyst	Metal Loading x 10^6 (moles/m^2)
7.4 wt% Mo / γ-Al_2O_3	4.04
10 wt% W / γ-Al_2O_3	2.80
3.1 wt % V / γ-Al_2O_3	3.12
7.4 wt% Mo / γ-Al_2O_3	4.13
10 wt% W / γ-Al_2O_3	2.92
3.1 wt % V / γ-Al_2O_3	3.10

4.2 REACTOR LOADING

After ensuring that both the physical and chemical properties of the catalysts were controlled such that a fair comparison could be made, the next task was to choose a basis of comparison. Since the phase I scout tests were designed to examine these different catalysts on their chemical structure, it was important that an equal amount of catalytic reaction sites were charged to the reactor in each experimental trial. Often when studying catalysts, this can be simply done by considering the total mass of catalyst contained

within the reactor during the experiment. However, as discussed by Ramanathan et al. (1995) in their comparison of chemically different catalysts, this cannot be applied in the same way when the catalysts have different active metals (Mo, W, and V) and different active phases (carbide vs. nitride).

When Ramanathan et al. (1995) compared the results of HDN, HDS, and HDO using their synthesized catalysts (i.e: molybdenum-carbide, tungsten-carbide, etc.) to that of a commercial Ni-Mo catalyst, they found that the synthesized catalysts had lower absolute activities. However, upon further examination using chemisorptions, they found that due to many years of optimization, the commercial catalysts had a much more active surface area. The basis chosen by Ramanathan et al. (1995) had been equivalent surface area, meaning that prior to beginning the experiment the commercial catalyst had an advantage due to its highly active surface area. After making a correction using the results from the chemisorptions, they found that with an equally active surface area, the synthesized catalysts could be in some cases greater than two times more active than the commercial catalysts.

A proactive approach was taken for the phase I scouting tests in order to remove this variable when selecting the basis, or catalyst loading, for each of the experimental trials. Rather than choosing the total mass of the catalyst or the total surface area, it was desired to define an 'active surface area' that took into consideration the molecular weights of the active metals and their co-ordination number in the active phase. That is, the total mass of catalyst charged to the reactor in each case was selected such that the total number of active sites (reaction centre) for each catalyst was the same.

In order to quantify the number of active sites for each catalyst, Equation 4.1 was derived.

$$ActiveSites = \left(\frac{x_i}{\hat{M}_i * CN_i} * N_A \right) * RL \qquad (4.1)$$

where x_i is the weight percent of the active metal, i, of the catalyst, $\hat{M}_i$ is the molecular weight of the metal i (g/mol), CN_i is the co-ordination number or number of metal atoms of metal i required for each active site of the catalyst (# of metal atoms/Active Site), N_A is Avogadro's number (# atoms/mol), and RL is the mass of catalyst loaded in the reactor (g).

A basis was needed, so the molybdenum weight percent was selected to be 10 wt% and using Equation 4.1, target metal loadings of tungsten and vanadium were determined to be 9.62 and 2.87 wt% respectively. If all target metal loadings were obtained precisely, then the mass of catalyst charged to the reactor in each case would be the same in order to obtain an equal number of active sites within the system.

However, as shown previously by the XRF results (Table 4.2), the actual metal loadings were not the same as the targeted values. The XRF results found that the actual metal loadings were 7.4 wt% for molybdenum, 10.0 wt% for tungsten, and 3.1 wt% for vanadium. There are various explanations for why these values are different than the targeted metal loadings. In the case of the MoO_3, the weight percent of the active metal is much lower than expected. This may be a result of excess metallic salt being left on the walls of the preparation flask as a larger volume of deionized water, as compared to the volume defined by the insipient wetness, was used to dissolve the salt. This deficiency in the catalyst preparation procedure was identified and quickly resolved, as is

shown by the metal loadings that were found to be much closer to the targeted values for the subsequent catalysts. In the case of the tungsten and vanadium, these values are both only slightly higher than what was targeted. It is possible that this error occurred due to a loss of the support material during catalyst preparation (physical transferring, calcining, etc) that would have slightly driven up the final weight percent of the metal.

Due to the discrepancy between the targeted and actual metal loadings found with the XRF analysis, the reactor loading had to be adjusted to equate the number of active sites present in each experimental trial. This was done by once again using Equation 4.1 to calculate the reactor loading. A basis of 2.00 g was chosen for the mass of molybdenum carbide/nitride charged to the reactor. It was then calculated that the other reactor loadings should be 1.42 g for the tungsten carbide/nitride catalysts and 1.26 g for the vanadium carbide/nitride catalysts. A summary of this calculation is shown below in Table 4.4.

Table 4.4: Summary of Active Site Comparison Calculation

Catalyst	Metal Molecular Wt (g/mol)	Active Site Co-ordination (# molecules/Active Site)*	Metal Loading (wt%)	Reactor Loading (g)	Active Sites
7.4 wt% Mo / γ-Al_2O_3	95.94	2	7.4	2.00	4.64E+20
10 wt% W / γ-Al_2O_3	183.85	1	10.0	1.42	4.64E+20
3.1 wt % V / γ-Al_2O_3	50.94	1	3.1	1.26	4.65E+20
7.4 wt% Mo / γ-Al_2O_3	95.94	2	7.4	2.00	4.64E+20
10 wt% W / γ-Al_2O_3	183.85	1	10.0	1.42	4.64E+20
3.1 wt % V / γ-Al_2O_3	50.94	1	3.1	1.26	4.65E+20

* Co-ordination number based on the molecular form of the metal expected on the catalyst surface (Furimsky, 2003)

4.3 PROCESS PARAMETERS

After preparing the catalysts as outlined in Chapter 3, the process parameters had to be selected. The objective in the selection of these parameters was to provide results that were visible, but at the same time provide clear and definitive evidence of differences between the six different catalysts. Prior to beginning this test, the effectiveness of these six catalysts with respect to HYD and HDO of canola oil was essentially unknown. As a result, the choice of the initial feed to be studied was made with the objective of maximizing the HDO activity of the catalysts in order to evaluate the catalysts. Consequently, oleic acid was chosen as the feedstock for the phase I scouting tests. Oleic acid is a long-chained fatty acid with one unsaturated double bond at the C8 position (C18:1). Oleic acid was chosen because it is by far the most abundant fatty acid component of canola oil (over 60 wt %).

The other process parameters were chosen based on previous results obtained by Monnier et al. (1998, 1999) when carrying out the same process with an industrial catalyst. The feed gas was chosen to be a 90/10 volume percent ratio of hydrogen to argon. The argon was added as an inert tracer gas. For each experimental trial, a molar balance on the inert argon was closed and used to normalize the remaining gas by-products. The absolute pressure was chosen to be approximately 7900 kPa, which provided a hydrogen partial pressure of approximately 7100 kPa. The liquid hourly space velocity (LHSV) of oleic acid was chosen to be 0.457 hr^{-1}. The absolute flow rate of liquid delivered to the reactor was varied for each catalyst to obtain this value of LHSV based on the specific reactor loading for each catalyst as given in Section 4.2.

After determining the absolute liquid flow rate, the gas flow rate was calculated using a ratio of 900:1 gas to liquid by volume. The high gas to liquid ratio was chosen based on previous work by Monnier et al. (1998, 1999) and serves two purposes: (1) provide the high levels of hydrogen required by the reaction and (2) approximate constant hydrogen partial pressure in the reactor even with the high rates of hydrogen consumption.

Finally, the reaction temperature range was chosen from 380 – 410°C. A range of temperatures was chosen because the temperature was believed to have the greatest individual effect on the overall activity of the catalyst. Due to the large number of trials that were run for each catalyst, only one sample was sent for a full liquid product analysis (GC/MS, FAME GC/MS, and C/H/N). This sample was taken with a reaction temperature of 390°C. The process conditions used during the phase I scouting tests are summarized below in Table 4.5. It is noteworthy that there were mechanical difficulties with the syringe pump and liquid delivery that restricted the total system pressure after the first two tests were completed. This resulted in a slightly lower hydrogen partial pressure for the final four scouting tests.

Table 4.5: Summary of Process Conditions for Phase I Scout Tests

Catalyst	Feed	H2/Ar	H2 Partial Pressure (kPa)	LHSV (hr-1)	Liquid Flowrate (ml/hr)	Gas Flowrate (ml/min)	Temperature (°C)
$Mo_2C/\gamma\text{-}Al_2O_3$	Oleic Acid	90/10	8350	0.457	1.333	20.0	390
$WC/\gamma\text{-}Al_2O_3$	Oleic Acid	90/10	8350	0.457	0.917	13.8	390
$VC/\gamma\text{-}Al_2O_3$	Oleic Acid	90/10	7150	0.457	0.893	13.4	390
$Mo_2N/\gamma\text{-}Al_2O_3$	Oleic Acid	90/10	7150	0.457	1.333	20.0	390
$WN/\gamma\text{-}Al_2O_3$	Oleic Acid	90/10	7150	0.457	0.917	13.8	390
$VN/\gamma\text{-}Al_2O_3$	Oleic Acid	90/10	7150	0.457	0.893	13.4	390

4.4 RESULTS AND DISCUSSION

The objective of the phase I scouting tests was to determine which of the six catalysts selected for study had the highest activity for HYD and HDO of canola oil and showed the greatest potential for the production of a diesel fuel cetane enhancer. In order to do this, key performance indicators were identified and their results were evaluated to make this selection. Those key parameters included: 1. Hydrogen Consumption; 2. Gas By-Product Production; 3. Oxygen Content in the Organic Product (Conversion - % HDO); 4. Fatty Acid Content in the Organic Product (Conversion); 5. Alkane/Olefin Content in the Organic Product (Selectivity).

4.4.1 Mass Transfer Limitations

As mentioned previously, when carrying out a screening test such as this one, it is important that an unbiased comparison of the catalysts be done to ensure that the catalyst with the superior performance is shown to be the best. In Section 4.1 it was shown that each of the catalysts has similar physical and chemical properties, such as surface area, pore volume, and metal dispersion. Furthermore, in Section 4.2 it was shown how each of the reactor loadings was controlled so each catalyst had an equal amount of active surface area in the reactor. In addition to these controls, it is still necessary to examine the mass transfer limitations on the system to show that the reactor and catalyst design has ensured an unbiased comparison of the chemical nature of the catalysts.

Prior to beginning the discussion on mass transfer, it should be noted that to fully evaluate these limitations information about the intrinsic reaction rates and mechanisms

must be known. Since this information was not gathered, the following assumptions have been made:

- The reaction is first order with respect to both oleic acid and hydrogen (Veldsink, 1997).
- Reactions are irreversible.
- The catalyst pellets are spherical.
- Steady-state conditions are achieved.

Applying these assumptions, as discussed by Fogler (1999), the mass transfer of hydrogen from the bulk gas phase to the reaction site can be described in five stages:

1. Transport from the bulk gas phase to the gas-liquid interface.
2. Equilibrium at the gas-liquid interface.
3. Transport from the gas-liquid interface to bulk liquid.
4. Transport from the bulk liquid to the external catalyst surface.
5. Diffusion from the external catalyst surface to the reaction site.

Stage 1 has been assumed negligible for this system due to the high partial pressures of hydrogen and the up-flow configuration of the reactor. That is, as hydrogen is transferred away from the gas-liquid interface, it will be readily replaced by hydrogen from the gas phase due to the high hydrogen partial pressure. Considering the remaining four stages, the following relationship can be derived to describe the mass transfer of hydrogen in this system (Fogler, 1999):

$$-r_{H_2} = \frac{1/H_{H_2}}{\left[\underbrace{\frac{(1-\varepsilon_b)\rho_c}{k_L a_i} + \frac{1}{k_S a_C}}_{\text{External Resistance}} + \underbrace{\frac{1}{\eta k C_{OA,S}}}_{\text{Internal Resistance}}\right]} * p_{H_2(g)} \qquad (4.2)$$

where, $-r_{H2}$ is the actual rate of consumption of hydrogen {mol/s*g_{cat}}, H_{H2} is the Henry's constant for hydrogen in oleic acid for the given pressure and temperature {Pa*m^3/mol}, p_{H2} is the hydrogen partial pressure {Pa}, ε_b is the catalyst bed porosity, ρ_c is the catalyst density {g_{cat}/m^3}, $k_L a_i$ is the mass transfer coefficient for hydrogen in oleic acid from the gas-liquid interface to the bulk liquid {s^{-1}}, k_s is the mass transfer coefficient for hydrogen in oleic acid from the bulk liquid to the surface of the catalyst {m/s}, a_c is the external catalyst surface area per gram of catalyst {m^2/g_{cat}}, η is the internal mass transfer efficiency, k is the rate constant {m^6/mol*s*g_{cat}}, and $C_{OA,S}$ is the concentration of oleic acid at the surface of the catalyst {mol/m^3}.

Within equation 4.2, the Henry's constant represents the hydrogen equilibrium across the gas-liquid interface. The first two terms of the denominator represent the external resistance or the resistance to hydrogen mass transfer from the gas-liquid interface to the external surface of the catalyst. The final term in the denominator represents the internal resistance or the resistance to hydrogen mass transfer from the external surface of the catalyst to the reaction site.

Considering the mass transfer of oleic acid, from the bulk liquid phase to the reaction site, the assumption that the entire catalyst surface is wetted with liquid is applied based on the co-current up-flow configuration of the reactor. Applying this assumption, the mass transfer of oleic acid can be described in two stages:

1. Transport from the bulk liquid to the external catalyst surface.
2. Diffusion from the external catalyst surface to the reaction site.

An equation similar to Equation 4.2 can then be derived to describe the mass transfer of oleic acid in this system (Fogler, 1999):

$$-r_{OA} = \frac{C_{OA,b}}{\left[\underbrace{\frac{1}{k_S a_C}}_{\text{External Resistance}} + \underbrace{\frac{1}{\eta k C_{H_2,S}}}_{\text{Internal Resistance}}\right]} \tag{4.3}$$

where, $-r_{OA}$ is the actual rate of consumption of oleic acid {mol/s*g_{cat}}, $C_{OA,b}$ is the concentration of oleic acid in the bulk liquid {mol/m^3}, k_s is the mass transfer coefficient for oleic acid from the bulk liquid to the surface of the catalyst {m/s}, and $C_{H2,S}$ is the concentration of hydrogen at the surface of the catalyst {mol/m^3}.

Since the intrinsic rates are not known, equations 4.2 and 4.3 cannot be fully solved. As a result, two well known dimensionless criteria that employ the observed reaction rates were used to estimate the impact of mass transfer on the system. For the internal resistance the Weisz-Prater criterion was used and for the external resistance the Mears criterion was used (Folger, 1999).

To determine if the internal resistance to mass transfer was significant, the Weisz-Prater criterion (C_{WP}) was used:

$$C_{WP} = \frac{-r_i'(obs)\rho_C R^2}{D_{eff,i} C_{i,S}} \tag{4.4}$$

where $-r_i'$(obs) is the observed reaction rate of species i, ρ_C is the catalyst pellet density, R is the catalyst pellet radius, $D_{eff,i}$ is the effective diffusion of species i, and $C_{i,S}$ is the concentration of species i at the external surface of the catalyst. If C_{WP} is found to be much (one order of magnitude) less than one, it is concluded that there are no mass transfer limitations inside of the catalyst pellet and that no concentration gradient exists.

If C_{WP} is found to be much greater than one, it is concluded that internal diffusion limits the reaction severely.

The C_{WP} was considered for both hydrogen and oleic acid at both the reactor inlet (highest concentration) and reactor outlet (lowest concentration). The results are shown below in Table 4.6. A sample calculation of the Weisz-Prater criterion is found in Appendix E.

Table 4.6: Summary of Internal Mass Transfer Estimations for the Phase I Scout Tests

Catalyst	Weisz - Prater Criterion			
	Oleic Acid		Hydrogen	
	Inlet	Outlet	Inlet	Outlet
$Mo_2C/\gamma\text{-}Al_2O_3$	0.019	1.449	0.078	0.082
$WC/\gamma\text{-}Al_2O_3$	0.017	0.323	0.011	0.011
$VC/\gamma\text{-}Al_2O_3$	0.017	N/A	0.005	0.005
$Mo_2N/\gamma\text{-}Al_2O_3$	0.018	N/A	0.059	0.062
$WN/\gamma\text{-}Al_2O_3$	0.016	0.438	0.024	0.025
$VN/\gamma\text{-}Al_2O_3$	0.016	0.414	0.012	0.013

It can be seen from the results shown in Table 4.6 that internal diffusion played only a small role in the evaluation of the phase I scouting tests. For all scenarios considering the hydrogen concentration gradient, the C_{WP} was well below one indicating that there were no mass transfer limitations on hydrogen. Considering the C_{WP} values for oleic acid, entering the reactor all values were well below one indicating that the mass transfer limitations were negligible. However, it can be seen that for all of the catalysts, the value of C_{WP} exiting the reactor has risen substantially and is either approaching one or has exceed one. In the case of the VC and Mo_2N catalysts, the bulk concentration of oleic acid became so small that given the assumptions to calculate the external mass transfer coefficients, a zero concentration was predicted at the catalyst surface. As a result, the C_{WP} criteria could not be calculated in these cases.

The rising values of C_{WP} for oleic acid at the reactor outlet are due to the high conversion of oleic acid for these experimental tests. It will be shown that for all catalysts the oleic acid conversion was greater than 95%. This means that the concentration of oleic acid was very small at the reactor exit and the onset of mass transfer limitations through the catalyst pellet could not be avoided. This result was not further investigated as it was interpreted as an indication that all of the original feed was readily available for reaction. For example, in the case of molybdenum nitride the C_{WP} value is above 50. However, it will be shown that the conversion of oleic acid for this trial greater than 99%, leaving essentially no oleic acid to be transferred through the pellet at the reactor outlet. It can be concluded from these results that internal mass transfer limitations had no impact on the evaluation of these catalysts.

The determination of external mass transfer limitations was considered in two steps. First, the two external resistances in series for hydrogen were considered. From Equation 4.2, the external mass transfer resistances for hydrogen are:

$$R_{G-L} = \frac{(1-\varepsilon_b)\rho_c}{k_L a_i} \tag{4.5a}$$

$$R_{L-S} = \frac{1}{k_S a_C} \tag{4.5b}$$

where $R_{G\text{-}L}$ is the resistance to transfer from the gas-liquid interface to the bulk liquid, ε_b is the void fraction of the catalyst bed, $k_L a_i$ is the liquid phase mass transfer coefficient, $R_{L\text{-}S}$ is the resistance to transfer from the liquid to the catalyst surface, k_S is the liquid-solid mass transfer coefficient, and a_C is the external surface area of the catalyst per unit mass of catalyst. A sample calculation of the mass transfer resistances is found in Appendix E. The values for the two resistances to hydrogen mass transfer are found

below in Table 4.6. It can be seen from these results that the resistance to flow of hydrogen is approximately ten times as big for $R_{L\text{-}S}$ as it is for $R_{G\text{-}L}$. This means that that limiting step in the external mass transfer of hydrogen is the transfer from the bulk liquid to the catalyst surface.

The second step in assessing the external mass transfer is to employ the Mears criterion. The Mears criterion compares the external mass transfer resistance to the observed reaction rate. The Mears criterion can be expressed as:

$$\frac{-r_i^{'}(obs)n}{C_{j,i}/R_j} < 0.15 \qquad (4.6)$$

where n is the reaction order, $C_{j,i}$ is the bulk concentration of species j at the gas-liquid interface, and R_j is the total external resistance to mass transfer for species j. If the Mears criteria are met (<0.15) it can be concluded that the external mass transfer limitations are not significant. The values of the Mears criterion for both hydrogen and oleic acid at the reactor inlet and outlet are given in Table 4.7. A sample calculation for the Mears criterion is found in Appendix E.

Table 4.7: Summary of External Mass Transfer Estimations for the Phase I Scout Tests

Catalyst	Oleic Acid			Hydrogen			
	$R_{L\text{-}S}$	Mears Criteria		$R_{G\text{-}L}$	$R_{L\text{-}S}$	Mears Criteria	
	kg*s/m3	Inlet	Outlet	kg*s/m3	kg*s/m3	Inlet	Outlet
$Mo_2C/\gamma\text{-}Al_2O_3$	17137	0.003	0.197	73	795	0.007	0.007
$WC/\gamma\text{-}Al_2O_3$	20219	0.003	0.061	91	938	0.001	0.001
$VC/\gamma\text{-}Al_2O_3$	19578	0.004	1.992	89	909	0.001	0.001
$Mo_2N/\gamma\text{-}Al_2O_3$	16725	0.003	9.905	77	776	0.006	0.006
$WN/\gamma\text{-}Al_2O_3$	18458	0.003	0.079	94	857	0.003	0.003
$VN/\gamma\text{-}Al_2O_3$	18547	0.003	0.082	88	861	0.002	0.002

It can be seen in Table 4.7 that the oleic acid showed little mass transfer limitations. At the reactor inlet, the Mears criterion was met for all catalysts. At the

reactor outlet, as was the case with the Weisz-Prater criterion, in some cases the Mears criterion was approached or exceeded. This again can be contributed to the very small concentrations of oleic acid due to the high conversions. It can be concluded that the external mass transfer of oleic acid was not significant and no impact on the results of the comparison.

With respect to hydrogen, it can be seen that the Mears criterion was also met for all catalysts at both the reactor inlet and outlet. This confirms that the external mass transfer was not significant in comparison to the rate of reaction of hydrogen. It is interesting to note that the trends in the Mears criteria for hydrogen are consistent for both carbide and nitride catalysts, with molybdenum showing the most significant external mass transfer limitations. It will be shown in the upcoming discussion that molybdenum had much higher rates of reaction for hydrogen, and this is likely the explanation for this.

4.4.2 Oxygen Content in the Organic Phase

Each liquid sample that was collected had two phases: an aqueous phase and an organic phase. The organic phase, which made up the majority (>90%) of the total liquid product, was the desired product. The remainder of the liquid product was an aqueous phase that is a by-product of the direct hydrogenation mechanism (Figure 2.4a). These two phases were separated manually in a separatory funnel. The organic phase was collected and further analyzed and the aqueous phase was measured and then discarded.

The first analysis carried out on the organic phase was a C/H/N elemental analysis to determine the elemental distribution of the sample. The objective of this test was to

determine the elemental oxygen content of the sample by difference using the sum of the carbon and hydrogen present in the sample. Before the test samples were analyzed, the oleic acid feed was also analyzed by this method and it was found to contain 77.19% carbon, 12.14% hydrogen and 10.67% oxygen (by difference). The elemental values of oxygen in each of the six samples collected during the phase I scouting tests were then used to calculate the conversion of oxygen as follows:

$$\%HDO = \frac{\left(x_0^{IN} - x_O^{OUT}\right)}{x_O^{IN}} * 100 \qquad (4.9)$$

where $\%HDO$ equals the percentage of oxygen removed from the organic phase, x_O^{IN} is the liquid weight percent of oxygen in the organic feedstock fed to the reactor, and x_O^{OUT} is the liquid weight percent of oxygen in the organic product (see Appendix A). The %HDO results from the phase I scouting tests are shown below in Table 4.8.

Table 4.8: Scouting Test Conversion - % Removal of Oxygen in the Organic Phase (T = 380°C, LHSV = 0.45 hr^{-1}, P_{H2} = 7150 / 8350 kPa)

Catalyst	**Mo_2C / γ-Al_2O_3**	**WC / γ-Al_2O_3**	**VC / γ-Al_2O_3**	**Mo_2N / γ-Al_2O_3**	**WN / γ-Al_2O_3**	**VN / γ-Al_2O_3**
% HDO	100	86	69	100	100	72

It can be seen in Table 4.8 that this process has successfully removed the majority of the oxygen from the organic phase in the case of all six catalysts. The lowest conversion of oxygen was found to be approximately 70 %HDO in the case of both vanadium catalysts. As mentioned in previous sections, it can be seen that the molybdenum catalysts performed the best amongst the six tested. Both the molybdenum carbide and nitride removed 100% of the oxygen from the organic phase. It may be noted that experimental error in the results of the C/H/N analysis exists for all

experimental trials. However, since the oxygen content of the organic phase was calculated by difference, in the case where the %HDO was nearing 100%, the relative error in the result increased dramatically (see Section 5.3.2). This means that the results that are reported as 100% HDO are likely nearing 100% HDO, but are not exactly 100%.

4.4.3 Fatty Acid Content in the Organic Phase

The liquid samples collected were also analyzed for their fatty acid content. This is another measure of conversion, similar to %HDO discussed in the previous section. The method used for this analysis was Fatty-Acid-Methyl-Ester (FAME) gas chromatography. This analysis provided much more accurate results as compared with %HDO as it was a direct measurement and not calculated by difference. The fatty acid content remaining in each of the organic phases is summarized below in Table 4.9 expressed in terms of total weight percent of fatty acids in the organic product.

Table 4.9: Scouting Test Conversion – Residual Acids in the Organic Phase (T = 380°C, LHSV = 0.45hr^{-1}, P_{H2} = 7150 / 8350 kPa)

Catalyst	Mo_2C / γ-Al_2O_3	WC / γ-Al_2O_3	VC / γ-Al_2O_3	Mo_2N / γ-Al_2O_3	WN / γ-Al_2O_3	VN / γ-Al_2O_3
Residual Acids (wt%)	1.81	4.43	0.16	0.03	3.47	3.56

The results shown in Table 4.9 immediately reflect the higher level of accuracy from the FAME test as there measurable differences between all of the catalysts, even at very low fatty acid content (high conversion). Staying consistent with previous results, the two molybdenum catalysts continue to perform amongst the best catalysts and both show a fatty acid content in the organic product of less than 2 wt%. Comparing these results to the %HDO results discussed in the previous section, on average the conversion

of fatty acids (over 95wt% acids removed in all cases) are higher than the %HDO. This suggests that various oxygen-containing intermediates are being created when converting the fatty acids to straight-chained alkanes. Possible oxygen containing species such as alcohols and esters may be included in this group of intermediates.

4.4.4 Alkane and Olefin Content in the Organic Phase

Reiterating the objective of this project, the desired final product is a diesel fuel cetane enhancer. While the removal of oxygen from the organic product is very important, it is not the only key performance indicator for the production of a diesel fuel cetane enhancer. To produce an effective diesel fuel cetane enhancer, the product selectivity should be maximized for long-chained alkanes that have high diesel fuel properties (specifically cetane number). As a result, the liquid samples collected were analyzed for their alkane and olefin content by means of GC/MS. The total alkane plus olefin content for each of the six samples is summarized below in Table 4.10.

Table 4.10: Scouting Test Selectivity – Alkane/Olefin Content of the Organic Phase (T = 380°C, LHSV = 0.45hr^{-1}, P_{H2} = 7150 / 8350 kPa)

Catalyst	Mo_2C / γ-Al_2O_3	WC / γ-Al_2O_3	VC / γ-Al_2O_3	Mo_2N / γ-Al_2O_3	WN / γ-Al_2O_3	VN / γ-Al_2O_3
Alkane + Olefin Content (wt%)	34.77	10.58	14.02	33.55	12.97	10.00

Table 4.10 shows that the molybdenum catalysts, both carbide and nitride, significantly outperformed the other active metals in terms of alkane/olefin selectivity of the organic product. The molybdenum catalysts were found to be producing more than two times as many alkanes/olefins than the other catalysts tested. However, these catalysts still only produced approximately 34 wt% alkanes/olefins in the organic

product. It is suspected that the remaining organic product (~66%) is primarily other hydrocarbon products such as highly branched isomers or cyclic compounds, due to the high oxygen removal reported in Section 4.4.2. The GC/MS analysis that was carried out on these samples also provided an alkane/olefin product distribution, which is shown below in Figure 4.4.

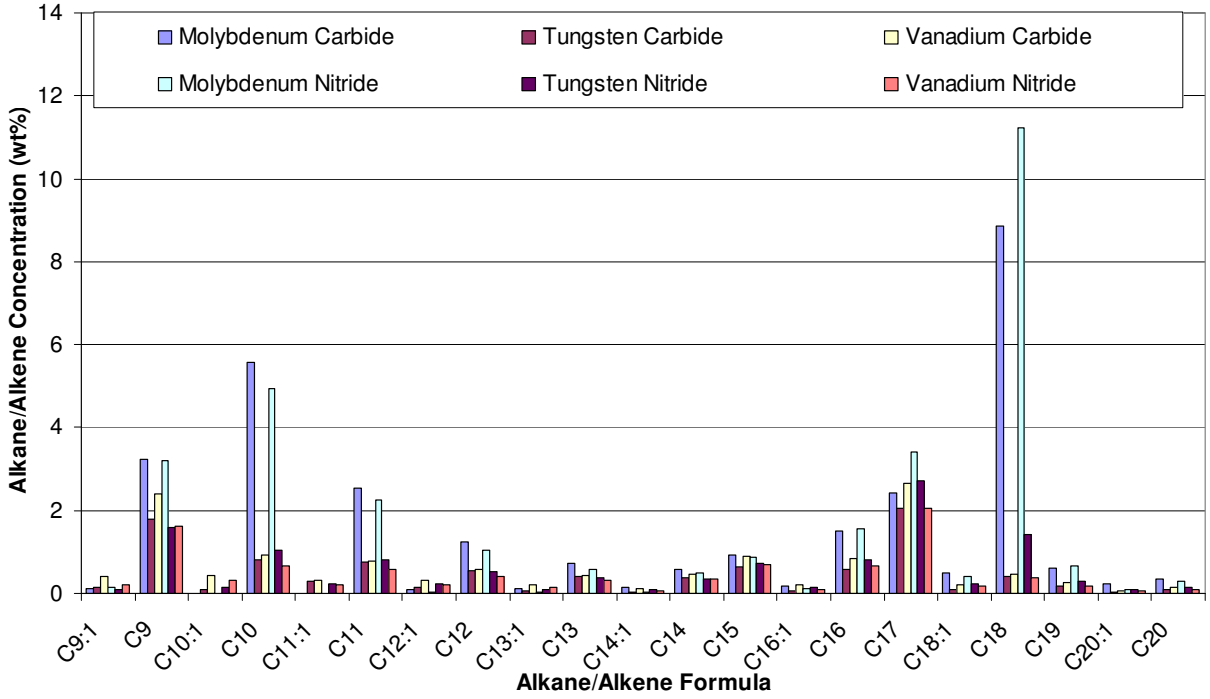

Figure 4.4: Scouting Test Selectivity – Alkane/Olefin Distribution of the Organic Phase (T = 380°C, LHSV = 0.45hr^{-1}, P_{H2} = 7150 / 8350 kPa)

The product distribution of alkanes and olefins shown in Figure 4.4 reveals three interesting characteristics about the final product. First, it can be seen that the amount of alkanes significantly dominates the amount of olefins at all molecular weights. This shows that the degree of saturation is nearly complete and that most of the olefins that are produced are easily converted to alkanes, which are better for increased diesel fuel properties such as cetane number. Secondly, a peak of alkanes can be seen centering on C10. This shows that some level of catalytic cracking occurred at the double bond of

oleic acid. Figure 4.7 shows that this occurs most significantly when the molybdenum catalysts are being used, suggesting that this is related to the high hydrogenation capability of these catalysts. Thirdly, the two peaks centering on C10 and C18 appear for the molybdenum catalysts only. These two peaks are critical to the diesel fuel like properties that are desired, especially the peak centering on octadecane.

4.4.5 Hydrogen Consumption

Hydrogen consumption is an important parameter for all hydrotreating processes because hydrogen is a very costly feedstock that is consumed in large quantities during hydrotreating operations. Generally, it is desired to keep hydrogen consumption as low as possible to make the process more economic. Conversely, high hydrogen consumption can be an indicator that the reaction is proceeding and that the desired end products are being produced. This creates a situation where an optimum is desired where hydrogen consumption is minimized without compromising the end products of the process.

As discussed previously, the hydrogen consumption was determined by using an online gas chromatograph (GC) and the tracer argon present in the gas feed. The change in gas volume was calculated by setting the moles of argon entering the reactor equal to the moles of argon leaving the reactor. Using this value, plus the volume percent of hydrogen in the outlet gas, the hydrogen consumption was calculated using the following equation:

$$HC = F_{IN}\left[y_{H2}^{IN} - y_{H2}^{OUT} * \frac{y_{Ar}^{IN}}{y_{Ar}^{OUT}} \right] \frac{P_{gc}}{RT_{gc}} \tag{4.7}$$

where HC is hydrogen consumption in mol/min, F_{IN} is the volumetric flow rate of gas entering the reactor, y_x^{IN} is the volumetric fraction of component x entering the reactor, and y_x^{OUT} is the volumetric fraction of component x leaving the reactor. As mentioned in section 4.2, each catalyst had a different catalyst loading, which led to different absolute gas and liquid flow rates. This meant that the rate of hydrogen consumption for each catalyst had to be normalized so they could be compared amongst one another. The volume of liquid fed to the reactor was chosen as the basis of comparison and the hydrogen consumption was adjusted to standard temperature and pressure (assuming the ideal gas law) as follows:

$$HC' = HC * \frac{1}{v} * \frac{RT_{ST}}{P_{ST}} \tag{4.8}$$

Where HC' is hydrogen consumption in L of H_2 at STP/ L of liquid fed, v is the liquid flow rate in L/min, R is the ideal gas constant, and T_{ST} and P_{ST} are standard temperature (0°C) and pressure (0.1 MPa). Figure 4.5 shows HC' plotted as a function of temperature for each of the six catalysts.

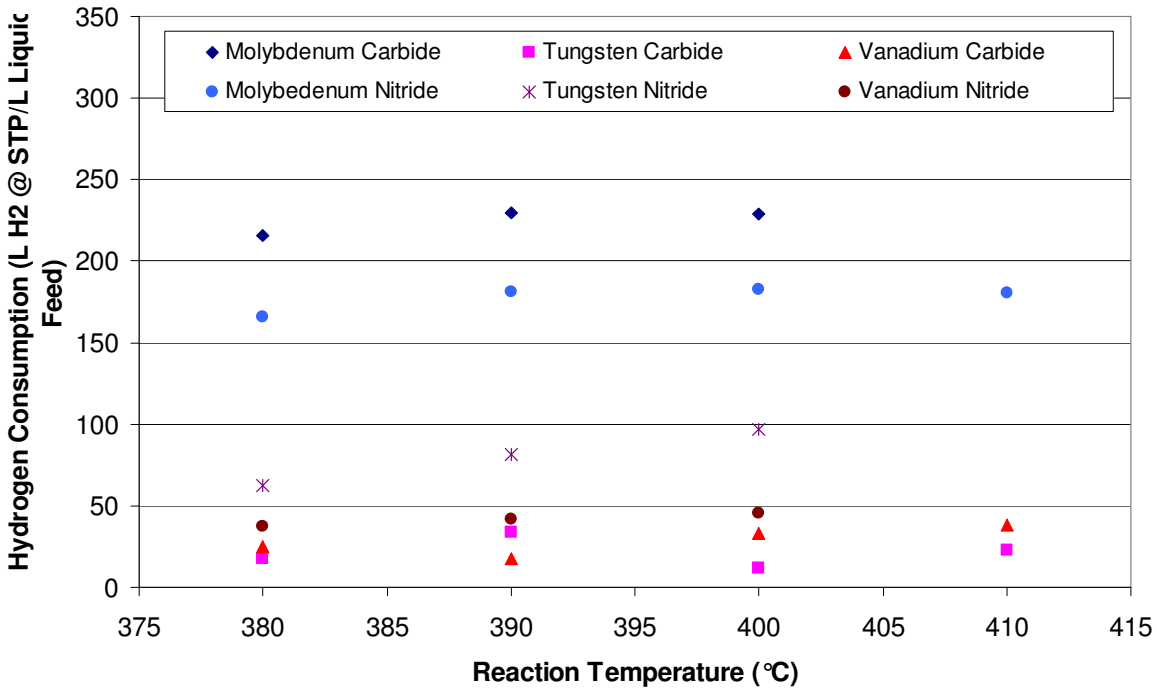

Figure 4.5: Hydrogen Consumption – Scouting Test (T = 380°C, LHSV = 0.45hr^{-1}, P_{H2} = 7150 / 8350 kPa)

It can be seen from Figure 4.5 that there is approximately four times more hydrogen consumed when using molybdenum as the active metal, as compared to the tungsten and vanadium, for all temperatures. The plot also suggests there is much higher hydrogen consumption when selecting molybdenum as the active metal regardless of the active state of the catalyst (carbide vs. nitride).

As discussed previously, it was shown that the molybdenum catalysts outperformed the tungsten and vanadium catalysts both in conversion and selectivity. As a result, it can be concluded that the high rate of hydrogen consumption is an indication of higher catalytic activity. Recalling the discussion in Chapter 2 considering the two common reaction mechanisms for hydrogenation reactions (direct hydrogenation and decarboxylation), this result suggests that the direct hydrogenation mechanism is dominant for this reaction.

Upon further examination of the results shown in Figure 4.5, it can be seen that there is in fact a small discrepancy between the molybdenum carbide and nitride catalysts. For all temperatures, the molybdenum nitride catalyst consumed approximately 20 – 25 % less hydrogen than the molybdenum carbide catalyst. It was previously shown that both molybdenum catalysts had similar results with respect to conversion and selectivity. Recalling the optimization between hydrogen consumption and the desired end products of a hydrotreating process, one could then draw the conclusion that the molybdenum nitride catalyst has an advantage. However, this is only one key performance indicator and cannot be used solely to select the best catalyst.

4.4.6 Gas By-Product Production

The gas by-products can be used in a similar fashion as the hydrogen consumption to draw conclusions about the reaction mechanisms that are occurring in this process. The gas by-products collected in each experimental run were detected using an online GC, similar to hydrogen. Argon was again used to correct the volume of the gas leaving the reactor and the liquid volume fed to the reactor was used as the basis of comparison. Applying these constraints, similar equations to Equation 4.7 and 4.8 were derived for the gas by-product production and are shown below:

$$G_i = F_{IN}\left[y_i^{OUT} * \frac{y_{Ar}^{IN}}{y_{Ar}^{OUT}} \right] \frac{P_{gc}}{RT_{gc}} \tag{4.9}$$

$$G_i^{'} = G_i * \frac{1}{v} * \frac{RT_{ST}}{P_{ST}} \tag{4.10}$$

where G_i is the rate of production of gas by-product i in mol/min, y_i^{OUT} is the mol fraction of gas by-product i leaving the reactor and G_i' is the rate of production of gas by-product i in L of gas i at STP/ L of liquid fed.

The major gas by-products that were detected using the online GC were carbon monoxide, carbon dioxide, methane and ethane. In addition to these, higher molecular weight hydrocarbon gas by-products were also found in the case of some of the six catalysts, but in much lower volumes than the four major gas by-products. It should be noted that when this process is applied to a triglyceride feed, it is expected that there will be a significantly higher volume of propane produced. The high levels of propane are due to the backbone of the triglyceride molecule being severed from the fatty acid chains. In the case of the phase I scout tests, the propane levels were low because oleic acid was used as the feed, which is a fatty acid with a single straight chain.

The total gas produced was considered to be the entire group of outlet gases not including hydrogen and argon. A plot of the total gas production for each of the six catalysts as a function of temperature is shown below in Figure 4.6.

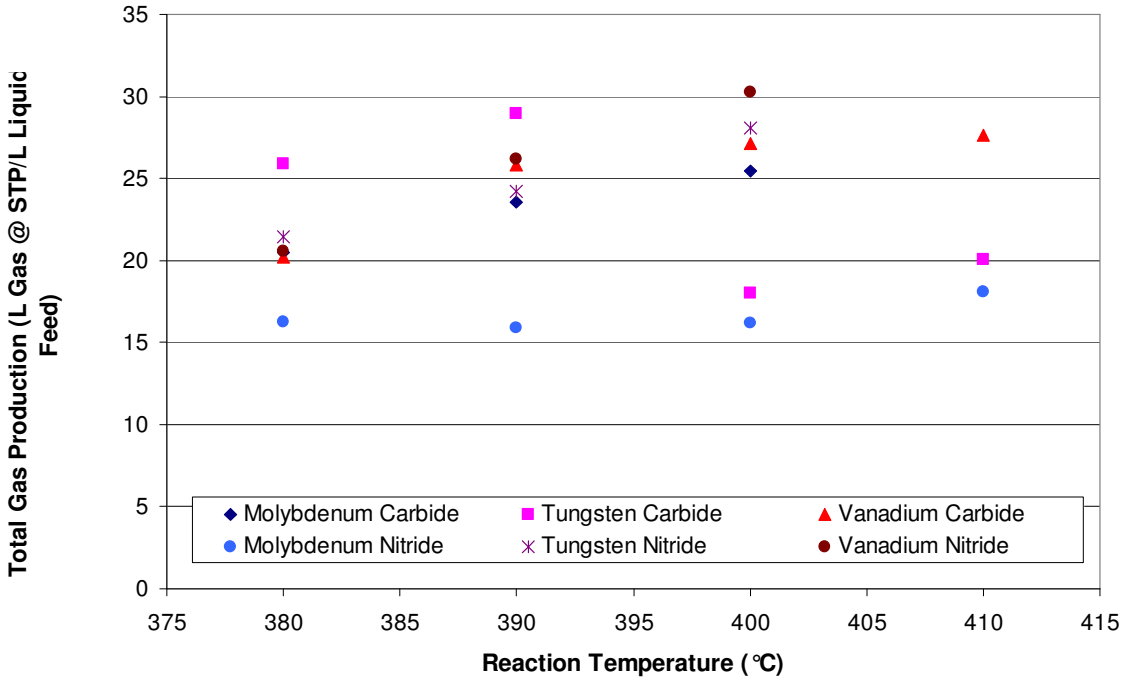

Figure 4.6: Total Gas Production – Scouting Test (T = 380°C, LHSV = 0.45hr^{-1}, P_{H2} = 7150 / 8350 kPa)

Figure 4.6 shows that the total gas produced from each of the six catalysts is comparable to one another for all temperatures. The total gas production was found to range from approximately 15 – 30 L gas @ STP / L liquid feed. It can be seen from Figure 4.6 that the molybdenum nitride catalyst consistently produced the least amount of total gases over all temperatures analyzed. It can also be seen that molybdenum carbide was on the lower end of the range of total gases produced as compared to the tungsten and vanadium catalysts. However, the total gases produced by the molybdenum carbide catalysts were significantly greater than the total gases produced by the molybdenum nitride catalysts. This may be a result of the higher hydrogenation activity of the molybdenum carbide catalyst that was reported in Section 4.4.5.

The total gas production however is not enough information to draw any conclusions about the reaction mechanisms present or which catalysts are the top performers. By taking a closer look at not only the total gas production, but also the gas

by-product distribution, evidence can be seen that is in line with the conclusions drawn from the hydrogen consumption data. The distribution of the four major gas by-products is summarized below in Table 4.11.

Table 4.11: Gas By-Product Distribution - Phase I Scouting Tests (Reaction Temperature = 390°C)

Catalyst	CO*	CO2*	Methane*	Ethane*
$Mo_2C/\gamma\text{-}Al_2O_3$	3.53	7.63	4.60	5.47
$WC/\gamma\text{-}Al_2O_3$	11.91	12.30	2.17	2.03
$VC/\gamma\text{-}Al_2O_3$	10.96	11.64	1.47	1.37
$Mo_2N/\gamma\text{-}Al_2O_3$	4.37	7.19	1.99	2.36
$WN/\gamma\text{-}Al_2O_3$	11.14	10.09	1.26	1.29
$VN/\gamma\text{-}Al_2O_3$	11.61	11.57	1.40	1.22

*Units of all values: L of Gas Produced @ STP/ L of Liquid Feed

Table 4.11 shows a large difference between the molybdenum catalysts and the tungsten and vanadium catalysts, specifically in the volumes of CO and CO_2. After reviewing the hydrogen consumption it was suspected that the decarboxylation mechanism was dominating for the tungsten and vanadium catalysts. The high levels of CO and CO_2 produced by the tungsten and vanadium catalysts support this conclusion, as CO_2 is a direct product of the decarboxylation reaction (Figure 2.4b).

The low volumes of CO and CO_2 produced by the molybdenum catalysts support the opposite conclusion; the direct hydrogenation mechanism is dominant in the case of the molybdenum catalysts. In addition to this, the volumes of methane and ethane produced by the molybdenum catalysts are higher than the other catalysts. This supports the notion the molybdenum catalysts have a higher hydrogenation capacity. It is likely that the short-chained hydrocarbons are being formed by a catalytic reaction that is

combining fragmented hydrocarbons from the C-C and C-O bond breaking and hydrogen on the catalyst surface.

Recalling that the molybdenum catalysts had a higher catalytic activity and selectivity than the tungsten and vanadium catalysts, the trends shown by the gas by-products may indicate that the molybdenum catalysts are the superior catalysts for this process due to their high hydrogenating capability. Table 4.11 also indicates that the volume of methane and ethane produced by the molybdenum nitride catalysts was less than half of that produced by the molybdenum carbide catalyst. This explains the higher hydrogen consumption in the case of the molybdenum carbide catalyst, as it appears that a larger amount of hydrogen was consumed in forming these gas by-products.

4.5 CONCLUSIONS

The objective of the phase I scouting test was to prepare six different catalysts to be examined for their potential of producing a diesel fuel cetane enhancer from canola oil. After concluding this scouting test, it can be seen that both molybdenum catalysts have significantly outperformed both the tungsten and the vanadium catalysts. Industrial hydrotreating catalysts are predominately in the form of Co(Ni)-Mo/Al_2O_3, so it is not unexpected that the Mo catalysts are the top performers in the phase I scouting test (Furimsky, 2003). However, there was not a significant differentiation between the supported molybdenum carbide and molybdenum nitride catalysts to confidently eliminate either of them. For this reason, both the molybdenum carbide and molybdenum nitride catalysts will be carried forward to the second phase of study outlined in Chapter 5.

5.0 Comparison of Supported γ-Al_2O_3 Mo_2C and γ-Al_2O_3 Mo_2N for HYD and HDO of Canola Oil

The second phase of experimental trials was designed with the primary objective of further examining the differences between the molybdenum carbide and molybdenum nitride catalysts. To do this, both catalysts were tested using more complex feed stocks, such as triolein and canola oil, with the objective of determining which catalyst can more effectively hydrotreat a real triglyceride feed stock . Section 5.1 discusses the experimental design that was implemented to study the differences between the two supported molybdenum catalysts. Section 5.2 discusses the catalyst preparation and characterization of the catalysts for this phase of the study. Finally, in Section 5.3, the results of the comparison are discussed in terms of four key performance indicators: oxygen removal from the organic phase (conversion), alkane/olefin and diesel fuel content of the organic phase (selectivity), and hydrogen consumption. In addition to this, preliminary information on the dependency of this process, with respect to conversion and selectivity, on input parameters such as temperature, residence time, and feed complexity are discussed.

5.1 EXPERIMENTAL DESIGN

The experimental design was created for the comparison of the performance of two molybdenum catalysts for HDO reactions (conversion) and alkane/olefin content (selectivity). The four key input parameters that were selected were the catalyst (molybdenum carbide and molybdenum nitride), temperature, residence time (LHSV), and feed complexity.

The objective of each experimental trial was to examine the effect of varying one of the key inputs while holding the remainder constant. To achieve this objective, a total of sixteen experiments were required to fully examine all of the input parameters. To manage this approach, a two-tiered experimental design was created to minimize the reactor down time that is required when changing either the catalyst or feed. Two nested 2^2 factorial designs were used, with a 'lower' tier 2^2 factorial design serving as one of four data points required for the 'upper' tier 2^2 factorial design.

The 'upper' tier 2^2 factorial design was made up of four unique combinations of catalyst and feed: 1. Molybdenum Carbide – Triolein; 2. Molybdenum Carbide – Canola Oil; 3. Molybdenum Nitride – Triolein; and 4. Molybdenum Nitride – Canola Oil. The choices of catalysts were supported molybdenum carbide and molybdenum nitride as these were the two catalysts selected from the phase I scouting tests. The two feed types chosen were triolein and canola oil. Recalling the phase I scouting tests, oleic acid was chosen for the feed because it was a model compound and there was a desire to maximize the overall fatty acid conversion. The results from the phase I scouting tests have shown that both of the molybdenum catalysts were capable of achieving high conversions, and so it was decided to increase the complexity of the feed. The first feed, triolein, is also a model compound, but rather than a single fatty acid chain, it is a triglyceride with oleic acid fatty acids at all three positions (see Figure 2.2). This feed was chosen as a mid point in complexity between the oleic acid, which is made up of nearly uniform free fatty acids, and canola oil, a real triglyceride feed with a wide arrangement of fatty acid chains and impurities. The second feed selected was canola oil, which is the desired feed for the final process to produce a diesel fuel cetane enhancer.

The 'lower' tier 2^2 factorial design consisted of the four unique combinations of temperature and residence time. Each of the four combinations of temperature and residence time was examined in each of the 'upper' tier cases, for a total of sixteen experimental trials. The four combinations of temperature and residence time included a high and low level for each input parameter. The temperature range was chosen to be 380-390°C, which was in the range of the phase I scouting tests that provided good conversion and moderate product selectivity. The LHSV range was chosen to be 0.64-1.28 hr^{-1}, which is higher than the value used in phase I scouting tests. The objective of increasing the LHSV was to drive the conversions to a value in the range of 20 – 80 % in order to properly evaluate the results. A visual representation of the 'lower' tier of the experimental design is shown below in Figure 5.1.

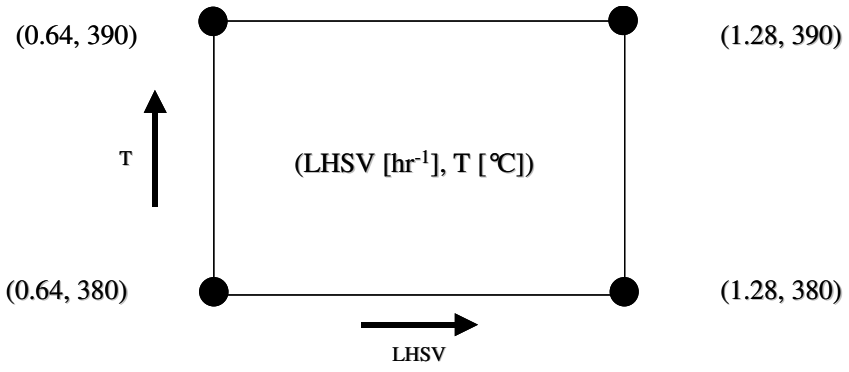

Figure 5.1: 'Lower' Tier 2^2 Factorial Experimental Design for the Evaluation of Mo_2C and Mo_2N

5.1.1 Statistical Design of Experiments

For each of the key performance indicators, the main effects of temperature and LHSV were determined, as well as the interaction between the temperature and LHSV. The main and interaction effects were calculated by looking at each of the four 'upper' tier combinations independently. The main temperature effect (E_T) for each catalyst-

feed combination was calculated by taking the difference between the average of the responses at the two temperatures:

$$E_T = \frac{\left(Y_{LHSV1}^{T2} + Y_{LHSV2}^{T2}\right)}{2} - \frac{\left(Y_{LHSV1}^{T1} + Y_{LHSV2}^{T1}\right)}{2} \tag{5.1}$$

where Y_{LHSV-y}^{T-x} is the measured response of the performance indicator being examined at temperature x (1 or 2) and LHSV y (1 or 2). The value found for the main temperature effect represents the average change in the measured response per step change in temperature, which in this case is 10°C. The LHSV main effect (E_L) for each catalyst-feed combination was calculated in a similar fashion by taking the difference between the average of the responses at the two LHSVs:

$$E_L = \frac{\left(Y_{LHSV2}^{T1} + Y_{LHSV2}^{T2}\right)}{2} - \frac{\left(Y_{LHSV1}^{T1} + Y_{LHSV1}^{T2}\right)}{2} \tag{5.2}$$

Similarly to the temperature main effect, the LHSV main effect represents the average change in the measure response per step change in LHSV, which in this case is 0.64 hr^{-1}. The final effect that was calculated was the interaction effect. This effect represents the dependency of both the temperature and LHSV on one another to affect the measured response. That is, if the interaction is low, the effect of changing the first input will be independent of the value of the second input. Conversely, if the interaction is high, the effect of changing the first input will greatly depend on the value of the second input. The interaction effect (E_I) is calculated by taking the absolute value of the difference between the average of the responses at opposing corners of the 2^2 factorial design (Figure 5.2) as follows:

$$E_I = ABS\left[\frac{\left(Y_{LHSV2}^{T2} - Y_{LHSV1}^{T2}\right) - \left(Y_{LHSV2}^{T1} - Y_{LHSV1}^{T1}\right)}{2}\right] \tag{5.3}$$

When the interaction is low, the absolute value of the interaction will be small in comparison to the value of the main effects. If the interaction is high, the value of the interaction will be similar or greater than the main effects.

The main and interaction effects are components of a non-linear regression on the data set. Therefore, these effects can be used to determine the co-efficients to a non-linear equation to predict the response over the range of parameters set out by the experiment. Prior to considering the non-linear equation, the introduction of dimensionless parameters for temperature (T') and LHSV ($LHSV'$) is necessary:

$$T' = \frac{(T - T_{mid})}{(T_2 - T_1)/2} = \frac{(T - 385)}{5} \tag{5.4}$$

$$LHSV' = \frac{(LHSV - LHSV_{mid})}{(LHSV_2 - LHSV_1)/2} = \frac{(T - 0.96)}{0.32} \tag{5.5}$$

The values of T' and $LHSV'$ have a minimum and maximum value of –1 and 1 respectively, and permit the direct use of the main and interaction effects in the non-linear equation that can be used to describe the data set. The only remaining unknown in the non-linear regression is value of the response at the origin of the data set where T' and $LHSV'$ are equal to zero. This value is taken as the average of the four responses, A. The non-linear equation to describe this data set can then be written as:

$$Y = A + \frac{E_T}{2} * T' + \frac{E_L}{2} * LHSV' + \frac{E_I}{2} * T' * LHSV' \tag{5.6}$$

In order to evaluate which of the effects has the greatest impact on the response, the contribution of each effect to the total variation from the mean can be determined. To do this, first the total variation (SST) can be determined by summing the variation from each of the effects:

$$SST = SS_T + SS_L + SS_I \tag{5.7a}$$

$$SST = 2^2 * \left(\frac{E_T}{2}\right)^2 + 2^2 * \left(\frac{E_L}{2}\right)^2 + 2^2 * \left(\frac{E_I}{2}\right)^2 \tag{5.7b}$$

where SS_T is the variation contributed by the temperature effect, SS_L is the variation contributed by the LHSV effect, and SS_I is the variation contributed by the interaction effect. The contribution of each effect to the total variation of the data set can be found by dividing each contribution by the total variation:

$$V_T = \frac{SS_T}{SST} * 100 \tag{5.8a}$$

$$V_L = \frac{SS_L}{SST} * 100 \tag{5.8b}$$

$$V_I = \frac{SS_I}{SST} * 100 \tag{5.8c}$$

where V_i (%) is the percent contribution of each effect to the total variation of the response from the mean.

The same analysis of the main and interaction effects of catalyst type and feed complexity was considered for the 'upper' tier 2^2 factorial design. To create the data set, the average response from each of the four 'lower' tier 2^2 factorial designs was used as a single data point. For example, four liquid samples (at different temperatures and LHSVs) were collected and analyzed for the catalyst-feed combination of molybdenum carbide and triolein. These four samples generated four responses for each key performance indicator that were then averaged to become one data point for each indicator. This single data point then became one of four data points required for the analysis of the 'upper' tier 2^2 factorial design. The remaining three data points were generated in the same fashion using the remaining three catalyst-feed combinations.

5.2 CATALYST PREPARATION AND CHARACTERIZATION

The catalysts that were used for evaluation of molybdenum carbide and nitride were prepared from the same stock of molybdenum oxide that was used for the phase I scouting tests. As a result, the metal loading of molybdenum on both the carbide and nitride catalysts was constant at 7.4 wt% molybdenum. Each catalyst was converted to either carbide or nitride following the catalyst preparation procedure outlined in Chapter 3. As a result, the chemical properties of the catalysts were considered the same as the phase I scouting tests.

The physical properties of the molybdenum carbide and molybdenum nitride catalysts were examined to ensure again that an unbiased comparison could be made. The surface area and pore volume were determined for both catalysts once again to ensure that there were no physical differences between the catalysts. The surface area was 189 and 192 m^2/g for the supported molybdenum carbide and nitride catalysts, respectively, where as the pore volume was 0.48 cm^3/g for the supported molybdenum carbide and 0.49 cm^3/g for the supported molybdenum nitride. The average pore diameter was found to be 10.2 nm for both the molybdenum carbide and the molybdenum nitride catalysts. It can be seen that the physical properties of the two catalysts were similar.

5.3 RESULTS AND DISCUSSION

The primary objective of evaluating the molybdenum carbide and molybdenum nitride catalysts was to determine which catalyst has the highest potential for HYD and HDO in order to produce a diesel fuel cetane enhancer from canola oil. Secondly, an

understanding of the effect of varying the aforementioned input parameters (feed, temperature, and residence time) was desired. To meet these objectives, the following key performance indicators were studied: 1. Oxygen Content in the Organic Product (Conversion); 2. Alkane/Olefin Content in the Organic Product (Selectivity); 3. Diesel Fuel Fraction in the Organic Product – Boiling point range: 155-325°C (Selectivity); and 4. Hydrogen Consumption.

These key performance indicators differ from those studied during the phase I scouting tests by the introduction of the diesel fuel fraction in the organic product. This analysis was added to increase the understanding of the organic product based on the results from the phase I scouting tests. First, the oxygen content and residual acid content indicated that the majority of oxygen had been removed in the organic product. Secondly, the alkane/olefin content of the organic product was only in the 30-35% range for the molybdenum catalysts. This indicated that there are a large number of other hydrocarbon products being formed. These other hydrocarbons may include isomers, lower molecular weight liquids (C5-C8), or cyclic compounds that may have been formed by other side reactions such as cracking or isomerization. It is likely that some of these other oxygen free hydrocarbons are in the desired diesel fuel boiling point range and can contribute to the value of the final product. Therefore, in order to characterize the entire diesel fuel fraction, as well as the entire organic product, simulated distillation was employed in order to obtain a boiling point distribution.

5.3.1 Mass Transfer Limitations

The mass transfer limitations experienced by the system during the molybdenum carbide and nitride comparison tests were addressed using the same methodology as was discussed in Section 4.4.1. The results of the evaluation of both the Weisz-Prater and Mears criteria are tabulated in Appendix E. As was the case in the phase I scouting tests, it was shown that there were no internal mass transfer limitations for either the liquid or gas phases. Similarly to the phase I scout tests, when evaluating the Weisz-Prater criterion for the liquid phase at the reactor outlet, the value of the criterion was found to be very large. Again, this was due to an extremely small residual acid concentration that was found in liquid phase exiting the reactor. This result supports the conclusion that the overall mass transfer of the liquid carrying the feed molecules was not limiting and that all of the feed was exposed to the catalyst during the experiment. The Mears criterion was used to evaluate the external mass transfer limitations versus the observed reaction rates. Again, in both the case of oleic acid and hydrogen, the Mears criterion was very small and confirmed the conclusion that there are no significant mass transfer limitations in this system.

5.3.2 Oxygen Content in the Organic Phase

The oxygen content of the organic product was used as the key performance indicator of the conversion of fatty acids fed to the reactor for the phase I scout tests. It was seen during the phase I scout tests that both molybdenum catalysts were capable of removing nearly 100% of the oxygen fed to the reactor. This was again the case during

the comparison of the molybdenum carbide and nitride catalysts as it was found all of the samples had no oxygen remaining in the organic product (Appendix A).

In the calculation of the oxygen content by difference using the C/H/N elemental analysis, a large relative error was found. This was problematic specifically for this comparison test, as all of the samples had oxygen contents approaching zero. The error in the oxygen weight percent of the organic product was calculated for each analysis and was on average 1.3 wt% oxygen. It can be seen by examining Table A.2 (Appendix A) that this error played a major role in the final value of oxygen weight percent as many of the values were calculated to be less than zero. As a result, no trends could be made from this data and it was accepted that both catalysts under all process conditions removed nearly 100% of the oxygen.

Since the oxygen content of the organic product could not be used as a measure of conversion for this phase of the experimental work, the hydrogen to carbon atomic ratio was used to obtain an indirect extent of conversion. The hydrogen to carbon atomic ratio of the organic product was examined and compared to the hydrogen to carbon atomic ratio of the feed and the desired product to gain an understanding of the extent of reaction. As oxygen is removed and the unsaturated fatty acids become saturated, the hydrogen to carbon atomic ratio will increase. The hydrogen to carbon atomic ratios for the two feeds, triolein and canola oil, were measured to be 1.81 and 1.76 respectively. The theoretical hydrogen to carbon atomic ratio for hexadecane is 2.11. A summary of the hydrogen to carbon atomic ratio of the organic phase for the sixteen experimental trials used to examine the supported molybdenum carbide and molybdenum nitride

catalysts is found in Table 5.1. Table 5.2 presents a statistical analysis of the main and interaction effects of temperature and LHSV on the final hydrogen to carbon atomic ratio.

Table 5.1: Summary of Hydrogen to Carbon Atomic Ratio in the Organic Phase

	H/C Atomic Ratio in the Organic Phase				Average Response (%)
Process Conditons (LHSV{hr-1},T{°C}):	(0.64,380)	(0.64,390)	(1.28,380)	(1.28,390)	
Mo2C/Triolein	1.96	1.97	1.95	1.95	1.96
Mo2C/Canola Oil	1.87	1.88	1.91	1.87	1.88
Mo2N/Triolein	1.92	1.85	1.91	1.95	1.91
Mo2N/Canola Oil	1.87	1.86	1.91	1.90	1.89

Table 5.2: Main and Interaction Effects of Temperature and LHSV on Hydrogen to Carbon Atomic Ratio in the Organic Phase

	Main Effects			Variation Contribution (%)		
	Temperature	LHSV	Interaction	Temperature	LHSV	Interaction
Mo2C/Triolein	0.009	-0.014	0.009	20.7	54.7	24.5
Mo2C/Canola Oil	-0.021	0.017	0.027	29.2	19.0	51.8
Mo2N/Triolein	-0.015	0.043	0.059	4.0	33.7	62.3
Mo2N/Canola Oil	-0.011	0.036	0.000	7.8	92.2	0.0

From Table 5.1 it can be seen that hydrogen to carbon atomic ratio was found to be between 1.85 and 1.96. These results show that indeed the hydrogen to carbon atomic ratio has increased. This is expected as the low oxygen levels confirm that the oxygen has been removed, which will increase the ratio. Secondly, the alkane and olefin results discussed in the previous chapter showed that there were extremely low olefin levels in the organic product for the molybdenum catalysts. This was again the case during the molybdenum nitride and carbide comparison and also leads to an increase in the hydrogen to carbon atomic ratio. However, the values reported for the hydrogen to carbon atomic ratio are still significantly less than the theoretical value of hexadecane. This is likely a result of the formation of two categories of by-products: (1) heavier molecular weight hydrocarbons and (2) cyclic hydrocarbons, both that will decrease the hydrogen to carbon atomic ratio. It will be shown in the following discussion that there

was a significant fraction of the organic product that was heavier than hexadecane and likely is the main contributor to the low hydrogen to carbon atomic ratio.

Examining the main temperature effect, it can be seen that the temperature had a notable contribution to the variation of the hydrogen to carbon atomic ratio in both cases when molybdenum carbide was used as the catalyst. This effect was not observed for the molybdenum nitride catalysts, where the temperatures contribution to the variance in the hydrogen to carbon atomic ratio was less than 10%. This is an unusual result as it is expected that both molybdenum catalyst would behave the same. This effect may be a function of the small temperature interval and may be a distortion of the results.

The main effects due to the LHSV were sizable in all cases, and specifically in the case of molybdenum nitride processing canola oil, where the effect of LHSV on the final oxygen content of the organic phase contributed over 90 % of the variance. The positive value of the LHSV effect, in all but one case, indicates that the hydrogen to carbon atomic ratio in the organic phase increased as the LHSV was increased (shorter residence time). This may be an indication that the heavier by-products that are contributing to the decrease in the hydrogen to carbon atomic ratio are being formed after longer residence times and may be controlled by the LHSV.

Next, the effects of catalyst and feed on the hydrogen to carbon atomic ratio in the organic phase were examined. Table 5.3 summarizes these results and an interaction plot of the average hydrogen to carbon atomic ratio in the organic phase is shown below in Figure 5.2.

Table 5.3: Main and Interaction Effects of Catalyst and Feed Complexity on Hydrogen to Carbon Atomic Ratio in the Organic Phase

	Main Effects			Variation Contribution (%)		
	Catalyst	Feed	Interaction	Catalyst	Feed	Interaction
H/C Atomic Ratio	-0.02	0.05	0.03	14.7	64.3	21.0

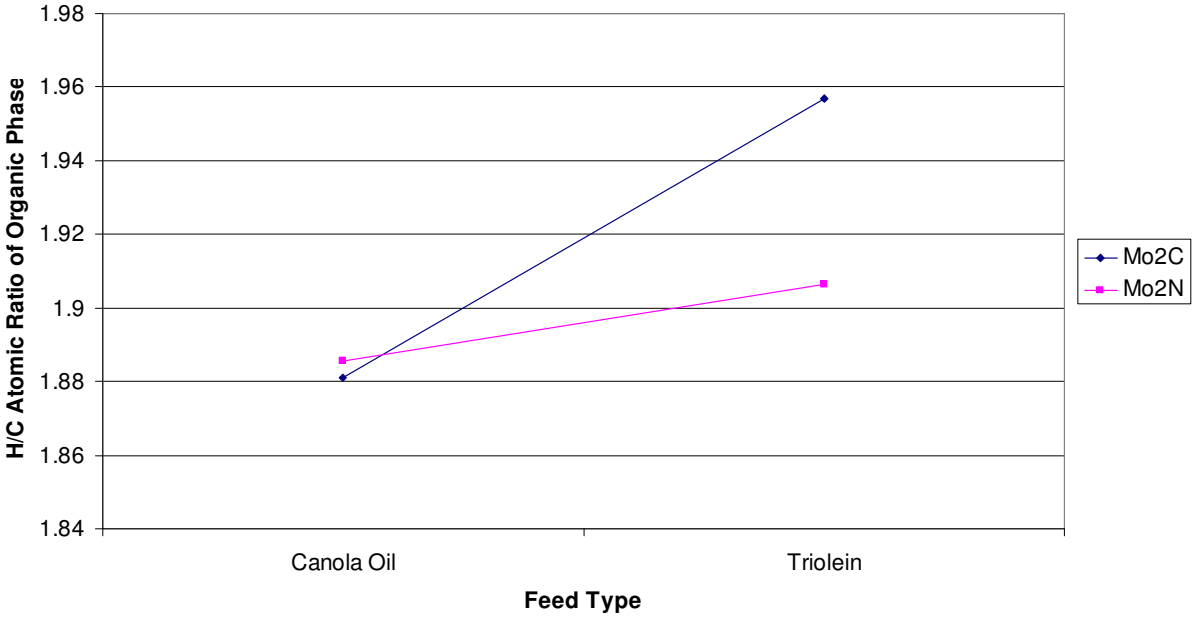

Figure 5.2: Hydrogen to Carbon Atomic Ratio in the Organic Phase – Average Response Interaction for the Molybdenum Catalyst Comparison

The results summarized in Table 5.3 show that the effect of feed on the final hydrogen to carbon atomic ratio in the organic phase is dominant, contributing nearly 65% of the variance in the final result. This result was expected when moving to more complex feeds. Considering the catalyst and interaction effects, it can be seen from the interaction plot in Figure 5.2 that the molybdenum carbide catalyst performance is significantly more impaired when moving from triolein to canola oil. From this, it can be concluded that the molybdenum nitride catalyst would be the superior catalyst with respect to hydrogen to carbon atomic ratio in the organic phase due to its robustness.

5.3.3 Alkane/Olefin Content in the Organic Phase

The liquid samples were analyzed for the alkane/olefin content of the organic phase. A summary of the alkane/olefin content in the organic phase for the sixteen experiments used to examine the molybdenum carbide and molybdenum nitride catalysts is found in Table 5.4. Table 5.5 presents a statistical analysis of the main and interaction effects of temperature and LHSV on alkane/olefin content.

Table 5.4: Summary of the Alkane/Olefin Content of the Organic Phase

	Alkane/Olefin Content in Organic Phase (wt%)				Average Response (wt%)
Process Conditons (LHSV{hr-1},T{°C}):	(0.64,380)	(0.64,390)	(1.28,380)	(1.28,390)	
Mo2C/Triolein	27.16	34.32	30.40	37.09	32.24
Mo2C/Canola Oil	18.97	24.10	17.20	19.63	19.98
Mo2N/Triolein	25.62	27.62	23.23	31.95	27.11
Mo2N/Canola Oil	24.82	24.66	19.85	24.14	23.36

Table 5.5: Main and Interaction Effects of Temperature and LHSV on the Alkane/Olefin Content fo the Organic Phase

	Main Effects			Variation Contribution (%)		
	Temperature	LHSV	Interaction	Temperature	LHSV	Interaction
Mo2C/Triolein	6.92	3.01	0.23	84.0	15.9	0.1
Mo2C/Canola Oil	3.78	-3.12	1.35	55.2	37.7	7.1
Mo2N/Triolein	5.36	0.97	3.36	70.1	2.3	27.6
Mo2N/Canola Oil	2.07	-2.75	2.23	25.5	45.0	29.6

The alkane/olefin content in all cases for this comparison ranges from approximately 17 – 37 wt% of the organic product. On average, this is lower than the results seen in the phase I scout tests, which was approximately 34 wt% of the organic product. Two of the key input parameters, feed complexity and LHSV, were changed from the phase I scouting tests and may account for the lower selectivity. The most probable explanation is that the lower selectivity was a result of the increased feed

complexity. By introducing triolein and canola oil as feeds, new elements such as triglycerides and impurities were added to the process that may have affected the reaction mechanism.

A second possibility is that while reducing the residence time (increase in LHSV) in an effort to reduce the conversion for comparison purposes, the selectivity of alkanes and olefins was also reduced. This trend is often the case when dealing with catalytic reactions that involve multiple reactions. However, by examining the main effect due to LHSV, it can be seen that it is only in the case of canola oil that a negative effect on selectivity was seen when reducing the residence time. In fact, the selectivity for alkanes and olefins increased with a lower residence time for both catalysts when treating triolein. This further concludes that the general trend of lower selectivity is due to the increase in feed complexity.

Furthermore concerning the main effect of LHSV on the alkane/olefin selectivity when processing canola oil, the results from this comparison suggest that there may be secondary reactions occurring in this process. The secondary reactions may be further processing the straight chained alkanes/olefins and yielding other hydrocarbon by-products, such as branched paraffins, which were not detected by the FAME-GC analysis. This is further supported by the results presented in Section 5.3.4, where the diesel fuel fraction of the organic product (determined by simulated distillation) was much higher than the alkane/olefin content of the organic product. Therefore, it can be concluded from these results that an optimum residence time exists to maximize the alkane/olefin content of the organic product

The effect of temperature on the alkane/olefin content was more prominent than the effect of LHSV as it contributed 25 – 85 % of the total variation from the mean. Also, it was more consistent as it showed an increase in selectivity with an increase in temperature in all cases. Table 5.5 shows that the main effect due to temperature was positive and in the range of 2-7 wt %/10°C.

Also found in Table 5.5 is the interaction effect between the temperature and LHSV on the alkane/olefin content of the organic product. By examining the variation contributed by the interaction effect, the results show the interaction between temperature and LHSV are significant only in the case of the molybdenum nitride catalyst. This is seen while treating both triolein and canola oil where the interaction effect contributes between 25 and 30 % of the variation in the final alkane/olefin content of the organic product. Further review of the measured responses shows that the impact of temperature on the final alkane/olefin content of the organic product greatly depends on the LHSV. In fact, when using the molybdenum nitride catalyst, a temperature increase from 380 to 390°C applied at a LHSV of 0.64 hr^{-1} had only a small impact on the final results, where as the same temperature increase at a LHSV of 1.28 hr^{-1} increased the alkane/olefin content of the final product on the order of 20 – 40 % (4 – 9 wt%).

Next, the effects of catalyst and feed on the alkane/olefin content of the organic product were examined. Table 5.6 summarizes these results and an interaction plot of the average alkane/olefin content is shown below in Figure 5.3.

Table 5.6: Main and Interaction Effects of Catalyst and Feed Complexity on the Alkane/Olefin Content of the Organic Phase

	Main Effects			Variation Contribution (%)		
	Catalyst	Feed	Interaction	Catalyst	Feed	Interaction
Alkane/Olefin Content of Organic Product	-0.87	8.00	4.26	0.9	77.2	21.9

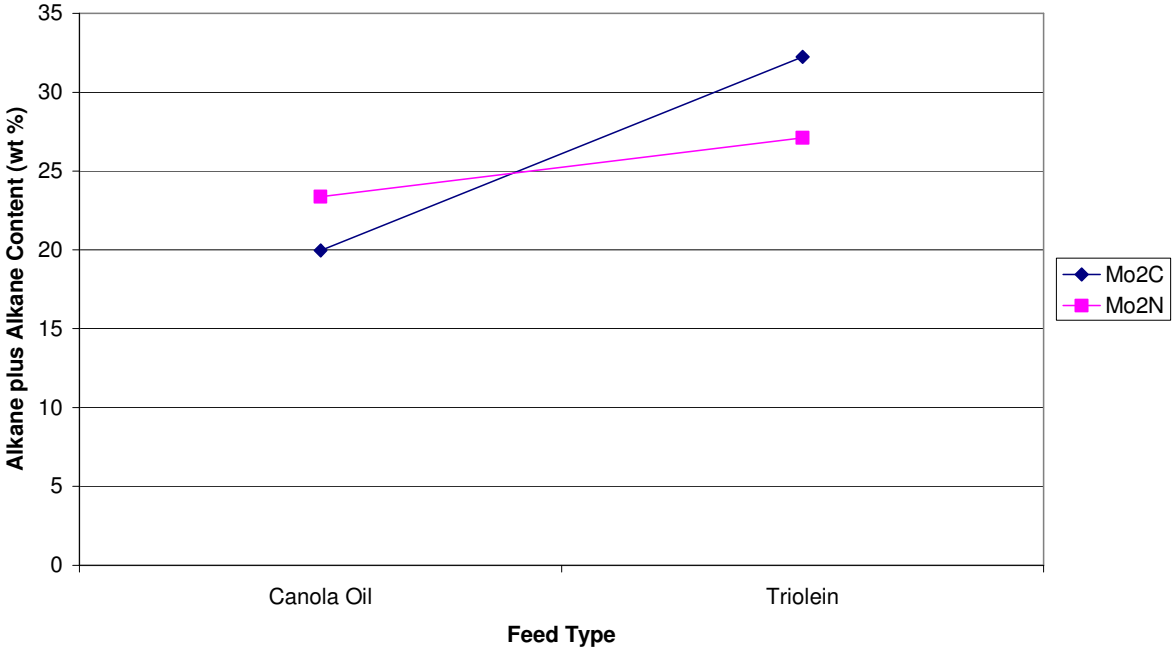

Figure 5.3: Alkane/Olefin Content in the Organic Phase – Average Response Interaction for the Molybdenum Catalyst Comparison

It can be seen from Figure 5.3 that a significant interaction exists between the catalyst and the feed type. A significant interaction can be characterized by the crossing lines, and is further supported in the fact that contribution to the total variation of the alkane/olefin content of the organic phase due to the interaction of catalyst and feed is greater than 20% (Table 5.6). Examining the main effects of catalyst and feed, it can be seen that the catalyst choice had almost zero effect on the final alkane/olefin content when considering the average responses. Contrary to this, the feed choice had a significant effect on the average responses. This confirms the previous conclusion that

higher selectivity of alkanes/olefins was obtained when processing the triolein. However, the interaction plot shows that the negative impact on the final alkane/olefin content was less significant in the case of the molybdenum nitride catalyst. This suggests that the molybdenum nitride catalyst may have more robust characteristics that are not impacted as significantly when the impurities and non-uniformity associated with the canola oil are introduced into the process. It can be concluded from this that the supported molybdenum nitride catalyst is superior catalyst for high selectivity of alkanes/olefins from canola oil.

5.3.4 Diesel Fuel Fraction in the Organic Phase

As discussed previously in this chapter, the boiling point range of the organic product was introduced to gather more information about the total product distribution, as well as characterize the entire diesel fuel fraction of the organic product. To do this, the boiling point distribution was broken down into four general groups: petroleum gases (BP: < 20°C), naphtha/gasoline (BP: 20-155°C), diesel fuel (BP: 155-325°C), and heavy oils (BP: > 325°C). The range of particular interest in this project is the diesel fuel range, however the products that are produced in the other ranges are also valuable as they could be used for different applications or further processed so that they fall in the diesel fuel range. A summary of the diesel fuel fraction in the organic phase for the sixteen experiments used to examine the molybdenum carbide and molybdenum nitride catalysts is found in Table 5.7. Table 5.8 presents a statistical analysis of the main and interaction effects of temperature and LHSV on the diesel fuel fraction.

Table 5.7: Summary of the Diesel Fuel Fraction of the Organic Phase

	Diesel Fuel Fraction of Organic Phase (wt%)				Average Response (wt%)
Process Conditons (LHSV{hr-1},T{℃}):	(0.64,380)	(0.64,390)	(1.28,380)	(1.28,390)	
Mo2C/Triolein	48.58	49.82	45.13	45.35	47.22
Mo2C/Canola Oil	41.48	45.11	39.56	40.35	41.62
Mo2N/Triolein	44.79	47.81	40.71	41.94	43.81
Mo2N/Canola Oil	46.37	44.46	38.57	41.03	42.61

Table 5.8: Main and Interaction Effects of Temperature and LHSV on the Diesel Fuel Fraction of the Organic Phase

	Main Effects			Variation Contribution (%)		
	Temperature	LHSV	Interaction	Temperature	LHSV	Interaction
Mo2C/Triolein	0.73	-3.96	0.51	3.2	95.2	1.6
Mo2C/Canola Oil	2.22	-3.34	1.42	27.1	61.7	11.1
Mo2N/Triolein	2.13	-4.97	0.90	15.1	82.3	2.7
Mo2N/Canola Oil	0.28	-5.62	2.18	0.2	86.7	13.1

It can be seen in Table 5.7 that the total organic product was found to contain approximately 40-50 wt% products in the diesel fuel boiling range. The other boiling point ranges were found to be of 35-50 wt % heavy oils, 8-18 wt % naphtha/gasoline, and negligible amounts of petroleum gases (evolved from the organic liquid). It can be noted that the high level of heavy oils, which could be further processed into the diesel fuel boiling range, may make the overall yield of diesel fuel products as high as 80 wt% with further processing.

Examining the temperature effect of the diesel fuel content of the organic product, it can be seen that the diesel fuel fraction increases as the temperature is increased for all cases. However, this effect is small contributing between 0 – 30% of the total variation from the mean for this data set. It is interesting to note that the temperature effect on the

alkane/olefin content of the organic phase was 25 – 85% of the total variation, which is much greater than the effect on diesel fuel fraction. This suggests that there are additional reactions taking place, such as isomerization reactions, that rearranges the molecules but does not crack them into smaller molecular weight products. This is especially the case for lower temperatures, specifically 380°C.

The effect of LHSV on the diesel fuel fraction of the organic phase was found to be the dominant effect in all cases. The effect of LHSV was found to contribute 60 – 95% of the total variation from the mean. In all cases, the effect of increasing the LHSV was negative, that is the diesel fuel fraction increased with a reduction of LHSV (increase in residence time). This result suggests that longer contact times in the reactor will yield a higher fraction of diesel fuel products. Recalling the previous discussion of secondary reactions, it was suggested that the desired end product was an intermediate that was being further processed to unwanted by-products. Applying the same theory to the diesel fuel fraction, it can be concluded that at these residence times the diesel fuel fraction is benefiting more from the reaction (cracking) of higher molecular weight products than it is losing from further reaction (cracking) of diesel fuel products. The high levels of heavy oils (30 – 35 wt%) and low levels of naphtha/gasoline (8 – 18 wt%) remaining in the organic product also support this theory.

The effect of the interaction between temperature and LHSV on the diesel fuel fraction is generally small for all cases examined. The interaction effect is found to be approximately one magnitude higher (10 – 15% of the total variation) in the case of the canola oil versus triolein, but remains small in comparison to the LHSV effects.

Next, the effects of catalyst and feed on the diesel fuel fraction of the organic product were examined. Table 5.9 summarizes these results and an interaction plot of the diesel fuel fraction of the organic phase is shown below in Figure 5.4.

Table 5.9: Main and Interaction Effects of Catalyst and Feed Complexity on the Diesel Fuel Fraction of the Organic Phase

	Main Effects			Variation Contribution (%)		
	Catalyst	Feed	Interaction	Catalyst	Feed	Interaction
Diesel Fuel Fraction of the Organic Product	-1.21	3.40	2.20	8.2	64.8	27.0

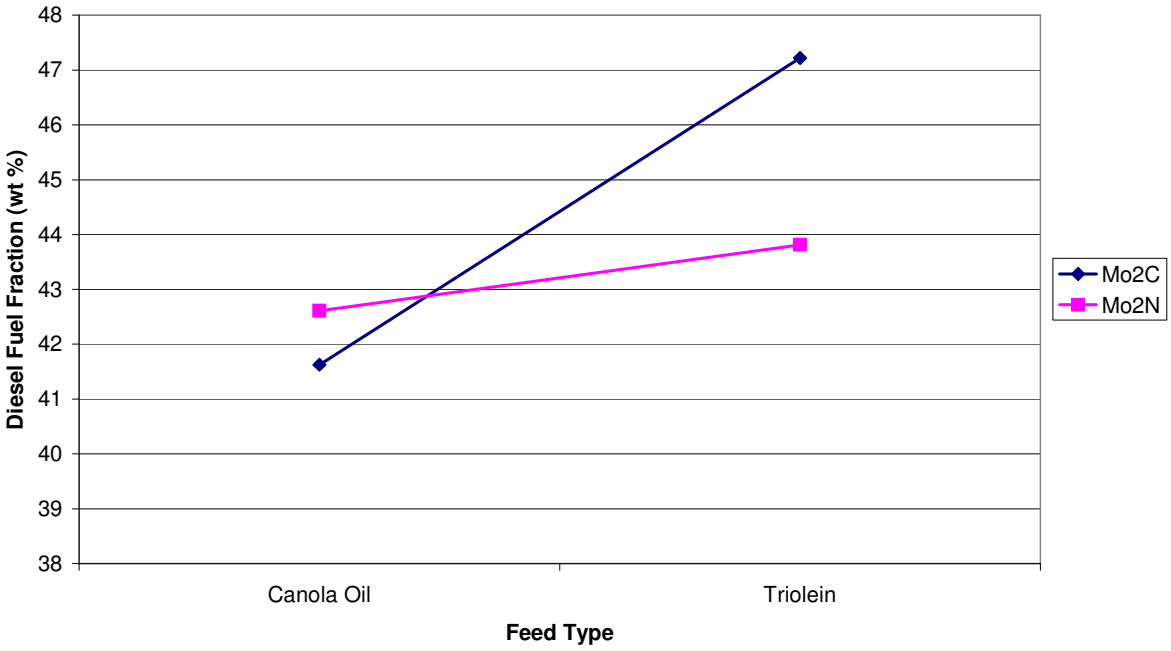

Figure 5.4: Diesel Fuel Content in the Organic Phase – Average Response Interaction for the Molybdenum Catalyst Comparison

From Table 5.9, it can be seen that again the selection of feed has the dominating effect on the diesel fuel fraction of the organic product. This same behaviour was seen when considering the alkane/olefin content of the organic product. The effect of the interaction between catalyst and feed on the diesel fuel fraction is also prominent (27% of the total variation), as was the case with the alkane/olefin selectivity. This is well

represented on the interaction plot (Figure 5.4). It can be seen that the molybdenum carbide catalyst does produce a higher diesel fraction when triolein is used as the feed. However, a larger drop off in the diesel fuel fraction is seen when the feed is changed to canola oil. From this, as was in the case of the alkane/olefin selectivity; the molybdenum nitride is shown to deliver higher selectivity when processing canola oil.

5.3.5 Hydrogen Consumption

As was done during the phase I scouting tests, the hydrogen consumption of the system was measured by an online gas chromatograph during each experimental trial after steady state had been reached. A summary of the hydrogen consumption for the sixteen experimental trials used to examine the molybdenum carbide and molybdenum nitride catalysts is found in Table 5.10. Table 5.11 presents a statistical analysis of the main and interaction effects of temperature and LHSV on hydrogen consumption.

Table 5.10: Summary of Hydrogen Consumption

	Hydrogen Consumption (L H2 @STP/L Liquid)				Average Response (L H2 @ STP/L Liquid)
Process Conditons (LHSV{hr-1},T{°C}):	(0.64,380)	(0.64,390)	(1.28,380)	(1.28,390)	
Mo2C/Triolein	235.0	248.2	264.7	218.0	241.5
Mo2C/Canola Oil	227.5	211.4	194.9	207.8	210.4
Mo2N/Triolein	203.9	254.5	242.8	271.7	243.2
Mo2N/Canola Oil	194.2	210.9	209.8	237.6	213.1

Table 5.11: Main and Interaction Effects of Temperature and LHSV on Hydrogen Consumption

	Main Effects			Variation Contribution (%)		
	Temperature	LHSV	Interaction	Temperature	LHSV	Interaction
Mo2C/Triolein	-16.80	-0.23	29.96	23.9	0.0	76.1
Mo2C/Canola Oil	-1.64	-18.09	14.47	0.5	60.7	38.8
Mo2N/Triolein	39.76	28.01	10.83	63.7	31.6	4.7
Mo2N/Canola Oil	22.20	21.11	5.57	50.8	46.0	3.2

The results from Table 5.10 show that the hydrogen consumption for the molybdenum carbide and nitride catalysts ranged from approximately 195-272 L H_2 @ STP/L liquid. These values of hydrogen consumption are on average slightly higher than the results for the molybdenum catalysts in the phase I scouting tests (160-240 L H_2 @ STP/L liquid). It would be expected that the hydrogen consumption would be less during these tests as the oxygen removal (conversion) and alkane/olefin content (selectivity) were less. However, the introduction of triglycerides into the feed with triolein and canola oil likely increased the number of reactions required to arrive at the final product. The additional reactions are likely breaking of the fatty acids from the triglycerides and hydrogenating the triglyceride backbone to propane, both that require additional hydrogen and would lead to higher levels of hydrogen consumption.

The main effects for both temperature and LHSV with respect to hydrogen consumption were difficult to interpret. In the case of the temperature effect, in all but two scenarios (constant catalyst-feed-LHSV), an increase in temperature resulted in an increase in hydrogen consumption. It was only in the case of Mo_2C-Triolein-1.28 hr^{-1} and Mo_2C-Canola Oil-0.64 hr^{-1} that the hydrogen consumption dropped with an increase in temperature. Recalling the argument that the conversion and selectivity of the molybdenum catalysts is linked to the direct hydrogenation mechanism, due to the

positive temperature effects seen in previous sections on both conversion and selectivity, the positive temperature effect for hydrogen consumption is more likely to be the correct trend.

Considering the main effect of LHSV, the hydrogen consumption dropped with an increase in LHSV in the case of the molybdenum carbide and increased with an increase in LHSV in the case of the molybdenum nitride. This behaviour is different that what was seen in the previous sections with respect to the effect of LHSV on conversion and selectivity, and as a result, no trend on hydrogen consumption can be drawn from this information.

Next, the effects of catalyst and feed on hydrogen consumption were examined. Table 5.12 summarizes these results and an interaction plot of the hydrogen consumption is shown below in Figure 5.5.

Table 5.12: Main and Interaction Effects of Catalyst and Feed Complexity on Hydrogen Consumption

	Main Effects			Variation Contribution (%)		
	Catalyst	Feed	Interaction	Catalyst	Feed	Interaction
Hydrogen Consumption	2.24	30.59	0.48	0.5	99.4	0.0

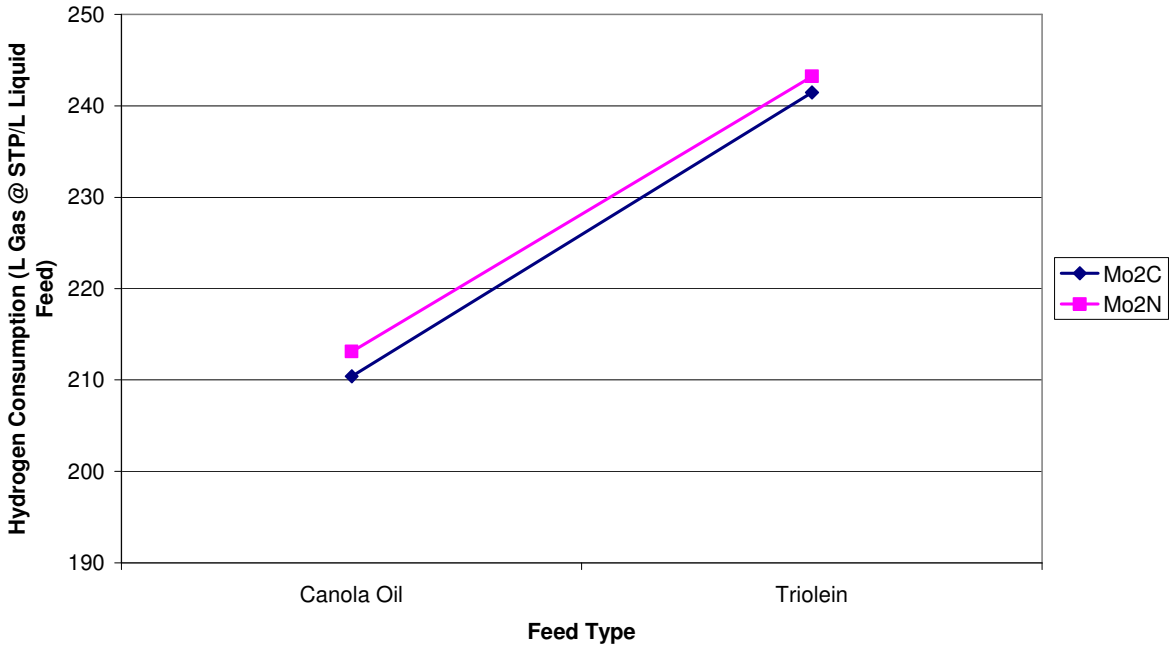

Figure 5.5: Hydrogen Consumption – Average Response Interaction for the Molybdenum Catalyst Comparison

The results shown in Table 5.12 show that the effect of the feed had the most dominant impact on the total variance of hydrogen consumption at nearly 100%. This is seen visually when examining the catalyst-feed interaction plot in Figure 5.5. This result shows that on average the hydrogen consumption drops when going from triolein to canola oil. The effect of the feed selection on hydrogen consumption can be correlated very well with conversion, as discussed previously. It can be concluded that the drop in hydrogen consumption is due to the drop in overall conversion. This supports the previous suggestion that the level of hydrogen consumption is directly related to the extent of the reaction and, by means of the hydrodeoxygenation mechanism, plays an important role in this process. Finally, it can also be seen from Figure 5.5 that there is no interaction between the catalyst and the feed and that the molybdenum nitride consumes slightly higher levels of hydrogen.

5.4 CONCLUSIONS

It was found that the molybdenum nitride was the best choice for this process. It was shown that the molybdenum nitride catalyst had higher overall conversions and higher product selectivity with respect to alkane/olefin content and diesel fuel content when canola oil was being processed. This result is supported by the literature review presented by Furimsky (2003), which reports that Mo_2N catalysts have been the most successful metallic carbide or nitride catalyst for hydrotreating processes. Based on these findings, supported molybdenum nitride has been chosen as the best catalyst amongst the six catalysts studied and will be further examined in Chapter 6 to begin optimizing the catalyst and process conditions.

6.0 Preliminary Process Optimization for HYD and HDO of Canola Oil Using Supported γ-Al_2O_3 Mo_2N

The final phase of study in this project set out with the objective to optimize the catalyst and the process conditions for the HYD and HDO of canola oil using a supported molybdenum nitride catalyst. Since this catalyst has shown throughout Chapters 4 and 5 that it has a high affinity for oxygen removal (conversion), Chapter 6 focuses on the optimization of product selectivity, both alkane/olefin and diesel fuel yield. Section 6.1 describes the two experimental designs that were implemented to study first the catalyst optimization and then the process optimization. Section 6.2 discusses the catalyst preparation and characterization of the catalysts used in both optimizations. Finally, Section 6.3 examines the results of the two optimizations and discusses the maximum product selectivity for alkane/olefin and diesel fuel yield.

6.1 EXPERIMENTAL DESIGN

6.1.1 Catalyst Optimization – Metal Loading

Prior to the catalyst optimization, only one metal loading of molybdenum nitride (7.4 wt%) had been studied. In this study, the target loadings of 10 and 20 wt% were chosen to provide two levels of metal loading. The loading target of 10% was considered to be on the lower end of the acceptable range of metal loadings for this catalyst. The choice for the second target metal loading was one that was larger than the first and within the normal range of metal loadings for supported catalysts. The second metal loading target was set at 20%, double the original target metal loading. As will be discussed in Section 6.2, the actual low and high metal loadings were measured and found to be 7.4 and 22.7 wt%, respectively.

Four sets of process conditions were selected to be tested at both the low and high metal loadings. The results from these four experimental trials were then compared to determine the effect of increasing the metal loading of the catalyst. A summary of the experiments used to evaluate the effect of metal loading on the molybdenum nitride catalyst is found in Table 6.1.

Table 6.1: Summary of the Process Conditions for the Metal Loading Comparison

Process Conditons Set #	Metal Loading	Temperature (°C)	LHSV (hr-1)	H2 Partial Pressure (kPa)	Liquid Flowrate (ml/hr)*	Gas Flowrate (ml/min)*	H2/Ar
1	7.4	400	0.9	8309	2.29	34.4	90/10
	22.7	400	0.9	8303	2.56	38.4	90/10
2	7.4	410	0.9	8327	2.29	34.4	90/10
	22.7	410	0.9	8327	2.56	38.4	90/10
3	7.4	390	0.9	8334	2.29	34.4	90/10
	22.7	390	0.9	8334	2.56	38.4	90/10
4	7.4	400	1.2	8346	3.06	45.9	90/10
	22.7	400	1.2	8309	3.42	51.3	90/10

* Small differences of the amount of catalyst charged to the reactor resulted in differences in the actual flowrates between the low and high metal loadings.

6.1.2 Process Optimization

The process inputs of interest in the process optimization were reaction temperature, residence time (LHSV), and hydrogen partial pressure. In order to effectively study these three parameters and their effect on the selectivity of the molybdenum nitride catalyst, a 3-parameter central composite experimental design (3-CCD) was employed. Similar to the previous phases of study, the key performance indicators that were studied were the diesel fuel fraction of the organic phase, the

alkane/olefin content of the organic phase, hydrogen consumption, and to a lesser extent, the oxygen removal from the organic phase.

The purpose of using the 3-CCD was to gain the maximum amount of information about the effect of the three input parameters on the final product characteristics, while minimizing the number of experiments required. The 3-CCD contains fifteen unique sets of process conditions, which contain five levels of each of the three input parameters. In addition to this, a number of repeat tests of the center point are used to determine the error in the data due to the nature of the experiment. In this case, it was decided to carry out three repeat tests resulting in a total number of experiments equal to 18. A visual representation of the 3-CCD is shown below in Figure 6.1.

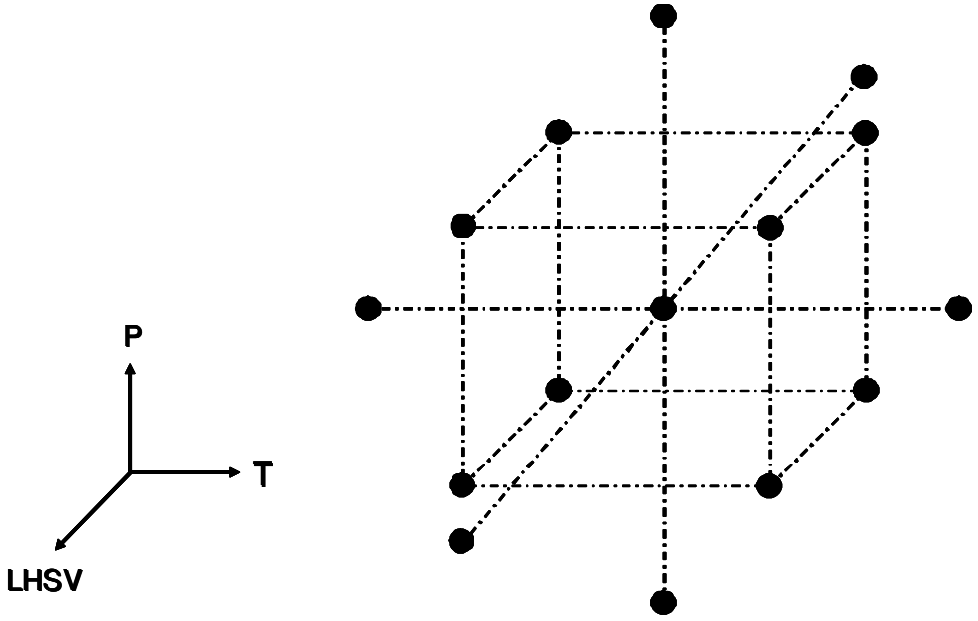

Figure 6.1: Visual Representation of the 3-Parameter Central Composite Design

The ranges of the parameters were selected based on the information that was gathered in previous phases of experimental work. The temperature range was selected to be 390-410°C. This range is slightly higher than the range used in the previous phase and was chosen because product selectivity was shown to be increasing with temperature.

The LHSV range was chosen to be 0.6-1.2 hr^{-1}. This is the same range that was studied during the molybdenum nitride and carbide comparison study and was chosen primarily due to system limitations (external mass transfer of hydrogen, pump rates). However, the fact that both positive and negative responses were seen from changing the LHSV in the previous studies, there was uncertainty in making a significant change to the range of residence times. Finally, the system pressure was varied from 8620-10,000 kPa (~7760-9000 kPa partial hydrogen pressure). This range of hydrogen partial pressures is higher than those used in the previous studies. A summary of the process conditions of the eighteen experiments is found below in Table 6.2.

Table 6.2: Summary of the Process Conditions for the 3-Parameter Central Composite Design

Experiment #	Temperature (°C)	LHSV (hr-1)	H2 Partial Pressure (kPa)	Liquid Flowrate (ml/hr)	Gas Flowrate (ml/min)	H2/Ar
1	400	0.90	8315	2.56	38.4	90/10
2	400	0.90	8303	2.56	38.4	90/10
3	410	0.90	8327	2.56	38.4	90/10
4	390	0.90	8334	2.56	38.4	90/10
5	400	1.20	8309	3.42	51.3	90/10
6	400	0.60	8346	1.71	25.6	90/10
7	400	0.90	8340	2.56	38.4	90/10
8	400	0.90	8936	2.56	38.4	90/10
9	400	0.90	7843	2.56	38.4	90/10
10	395	0.75	8098	2.14	32.0	90/10
11	395	1.05	8067	2.99	44.9	90/10
12	405	1.05	8054	2.99	44.9	90/10
13	405	0.75	8085	2.14	32.0	90/10
14	405	0.75	8718	2.14	32.0	90/10
15	405	1.05	8694	2.99	44.9	90/10
16	395	1.05	8681	2.99	44.9	90/10
17	395	0.75	8731	2.14	32.0	90/10
18	400	0.90	8321	2.56	38.5	90/10

6.2 CATALYST PREPARATION AND CHARACTERIZATION

The high metal loading catalyst was prepared by the impregnation method as outlined in Chapter 3. The target metal loading was 20 wt% molybdenum, which is twice the amount of active metal that was targeted in the preparation of the original molybdenum catalysts. The molybdenum oxide precursor was characterized by BET to determine the surface area, pore volume, and pore diameter. A summary of the BET

analysis is found in Table 6.3, along with the BET results of the low metal loading that was used.

Table 6.3: BET Results for the Catalyst/Process Optimization

Molybdenum Oxide Loading	BET Surface Area (m^2/g)	Pore Volume (cm^3/g)	Average Pore Diameter (Å)
Low	192	0.490	102
High	176	0.488	111

It can be seen from Table 6.3 that the catalysts are physically similar. However, the high metal loading catalyst did show a reduction in surface area (~8%) and an increase in average pore diameter (~9%). XRF analysis was also carried out on the molybdenum oxide precursor to determine the actual metal loading of the catalyst. The results of the XRF analysis are summarized in Table 6.4.

Table 6.4: Chemical Compositions of the Phase III Metal Loading Study (Oxide Precursor)

Catalyst Precursor	Al_2O_3 (wt%)	MoO_3 (wt%)	SiO_2 (wt%)	P_2O_5 (wt%)	Cl (wt%)	Fe_2O_3 (wt%)
Mo – Low	88.5	11.1	0.1	0.2	0.1	trace
Mo - High	65.3	34.1	0.1	0.4	0.2	0.1

It can be seen from Table 6.4 that the high metal loading catalyst did indeed obtain a higher level of active metal (molybdenum). The result of 34.1 wt% MoO_3 for the high case corresponds to a molybdenum loading of approximately 22.7 wt%. This is greater than three times the metal loading of the low case, which was approximately 7.4 wt% Mo.

6.3 RESULTS AND DISCUSSION

6.3.1 Catalyst Optimization – Metal Loading

As discussed in Section 6.1.1, a total of four process conditions (Table 6.1) were used to evaluate the effect of increasing the metal loading of the molybdenum nitride catalyst. The primary objective was to determine the impact on product selectivity for alkane/olefin content and diesel fuel fraction in the organic phase, using canola oil as the feed stock, as very high conversions of fatty acids had already been obtained with the lower metal loading catalyst. The diesel fuel yield was determined for each of the conditions summarized in Table 6.1 and the results are shown below in Figure 6.2.

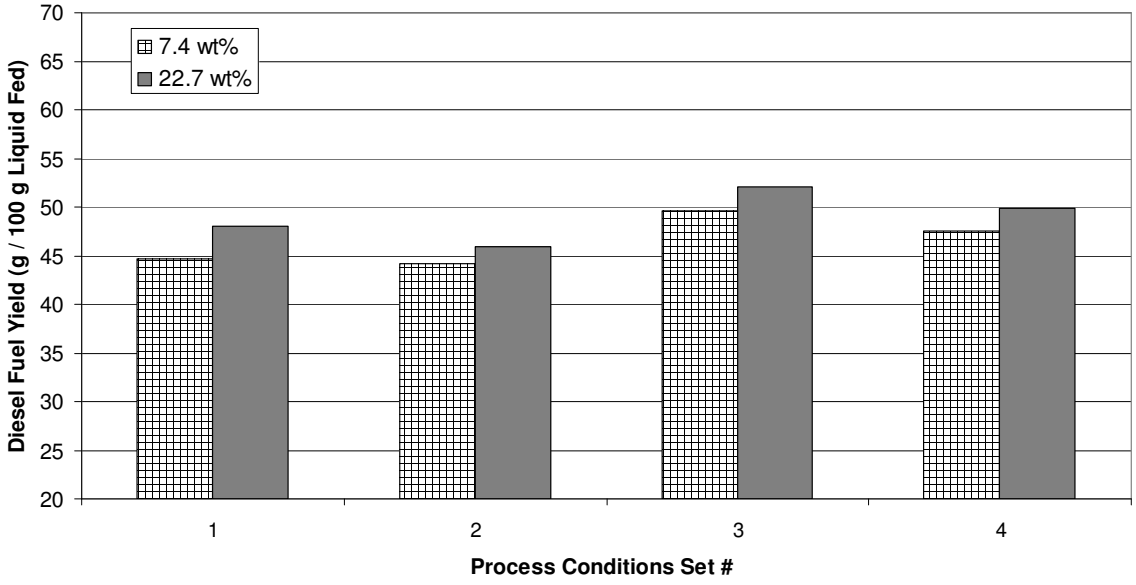

Figure 6.2: Metal Loading Comparisons – Diesel Fuel Yield

It can be seen from Figure 6.2 that the high metal loading produced a higher yield of diesel fuel products for all of the process conditions examined. It can also be seen that both catalysts responded in a similar fashion when the process conditions were changed. By averaging the increase in diesel fuel yield for each of the four process conditions

compared, it can be seen that the increase in metal loading provided an increase in the final diesel fuel yield of approximately 5.3%.

The second key performance indicator with respect to product selectivity is the alkane/olefin content of the organic phase. The effect of increasing the metal loading on the alkane/olefin yield is shown below in Figure 6.3.

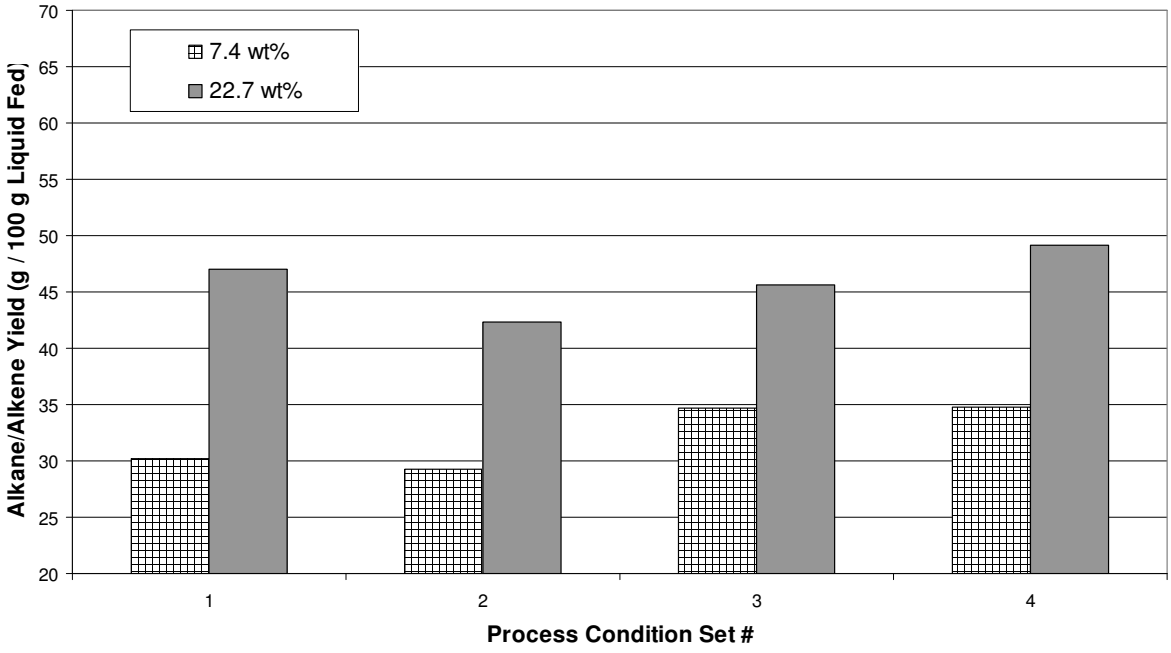

Figure 6.3: Metal Loading Comparison – Alkane/Olefin Yield

Figure 6.3 shows that an increase in the alkane/olefin yield was seen when increasing the metal loading of the catalyst. In addition to this, the behaviour of the catalyst has not changed due the increase in metal loading, as both catalysts responded to the change in conditions in the same way. By taking the average difference of the alkane/olefin yield for each of the four process conditions, it was found that an average increase of approximately 43.2% was experienced when moving to a higher metal loading.

A final note on the optimization of the catalyst loading is that only two metal loadings were studied. Therefore, it can only be concluded that by increasing the metal loading by three times to approximately 23 wt% molybdenum the product selectivity is increased, specifically in the case of alkane/olefin content of the organic product. However, the effect of further increasing the metal loading of the catalyst is unknown. It is recommended that a study of higher metal loadings be carried out with the molybdenum nitride catalyst as the absolute values of the diesel fuel and alkene/olefin yields of the organic product continue to remain less than 50-55g/100g liquid fed.

6.3.2 Process Optimization

A total of eighteen experimental trials were needed to examine the three input process parameters that were selected for study: reaction temperature, residence time (LHSV), and hydrogen partial pressure. The eighteen experimental trials were arranged in a 3-CCD experimental design (Table 6.2) and were interpreted with the aid of Design Expert 6. At the conclusion of the optimization, the optimum operating conditions, within the range of the studied parameters, were selected using the Design Expert 6 software.

6.3.2.1 Oxygen Removal from the Organic Phase

Information regarding the removal of oxygen from the organic phase with the supported molybdenum nitride catalyst was gathered from the 3-CCD experiment. It was found that nearly all of the canola oil (triglycerides) and fatty acids had been converted from their original state (>99%). However, as was the case in the molybdenum carbide

and nitride catalyst comparison, all of the calculated values of oxygen weight percent in the organic product were found to be not statistically different than zero (Appendix A). As a result, the hydrogen to carbon atomic ratio was used to gather an indirect extent of conversion.

The hydrogen to carbon atomic ratios that were calculated for the preliminary process optimization were found to be between 1.96 and 2.04 (Appendix A). Recalling that the theoretical hydrogen to carbon atomic ratio for hexadecane is 2.11, the values found during this phase of the experimental work continued to be lower than the target. However, these values are higher than those found in during the molybdenum carbide and nitride comparison test. This is likely due to the higher metal loading of the catalysts and is in agreement with the higher alkane selectivity that was found during the process optimization (Section 6.3.2.3). In addition to this, it is likely that the continuing presence of heavier molecular weight by-products in the organic product is preventing the hydrogen to carbon atomic ratio from reaching higher levels.

As shown in Table 6.2, the eighteen experimental trials included three repeat tests of the centre point of the design. This results in a total of four data points at the process conditions of the centre point of the design. In addition to being used as an indication of error, by plotting these four points as a function of time an indication of catalyst deactivation can obtained. A plot of the four centre points for hydrogen to carbon atomic ratio over time is shown below in Figure 6.4.

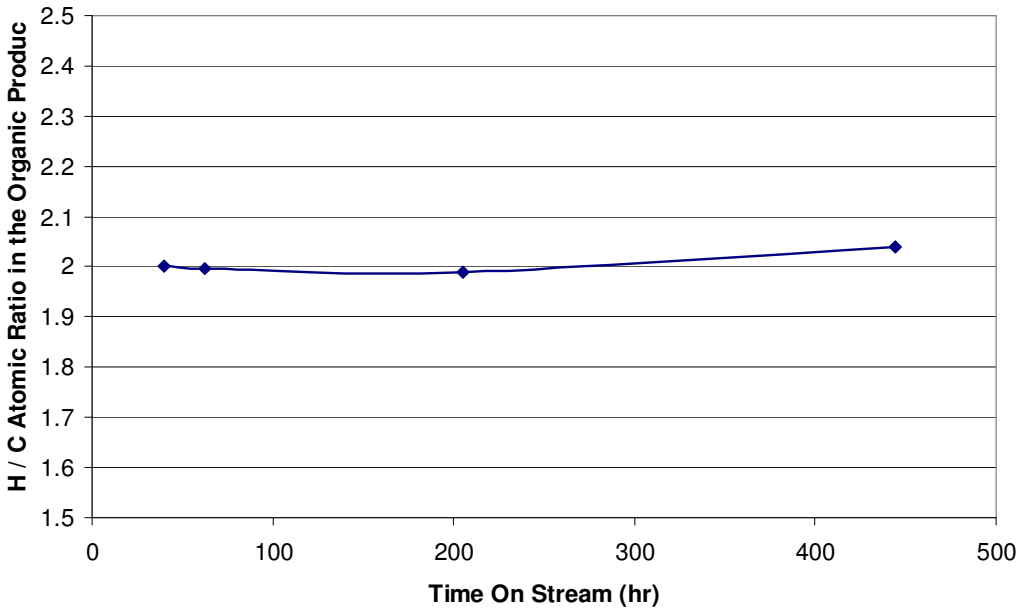

Figure 6.4: Catalyst Deactivation – Hydrogen to Carbon Atomic Ratio in the Organic Phase

It can be seen in Figure 6.4 that the catalyst performance nearly constant for up to 500 hours. In fact, the plot begins to trend upwards suggesting that the activity of the catalyst may be improving over time and allowing more hydrogen to be taken up by the organic product. This shows that the catalyst is robust and the activity of the molybdenum nitride catalyst does not decrease from irreversible damage to the catalyst surface. This result also shows that the catalyst performance did not change over time and it gave added confidence to the results that have been gathered from the 3-CCD process optimization.

6.3.2.2 Diesel Fuel Fraction in the Organic Phase

The primary objective of the process optimization was to maximize the product selectivity of the molybdenum nitride catalyst. One of the key performance indicators of

product selectivity for this process was the diesel fuel fraction of the organic product. Therefore, the effect of reaction temperature, residence time, and hydrogen partial pressure on the diesel fuel fraction of the organic product was examined. First, the effects of temperature and residence time were studied by analyzing the surface plot shown below in Figure 6.5.

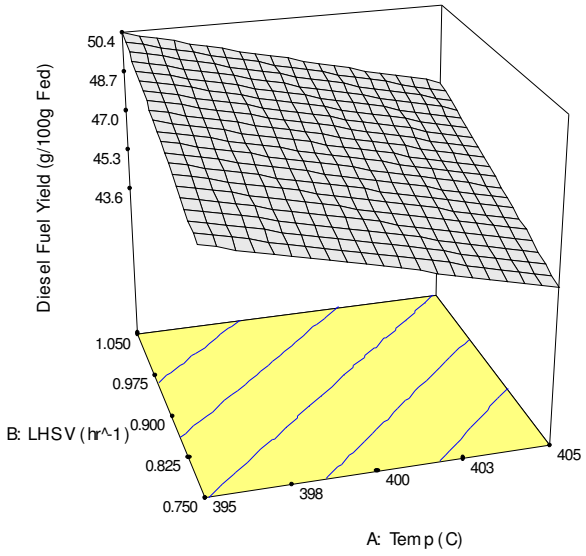

Figure 6.5: Surface Plot – Diesel Fuel Yield (P_{H2} = 8330 kPa)

Figure 6.5 shows the diesel fuel yield of the process as a function of reaction temperature and residence time at a constant hydrogen partial pressure of 8330 kPa. It can be seen from Figure 6.5 that the effect of both temperature and LHSV on the diesel fuel appears to be linear over the range of conditions studied. The linear relationship was confirmed with the statistical analysis carried out by the Design Expert 6 software. When varying hydrogen partial pressure, the linear relationship of both temperature and residence time hold.

Taking a closer look at Figure 6.5, it can be seen that as the reaction temperature is increased, the diesel fuel yield decreased. This effect is opposite of what was seen in the comparison of the molybdenum carbide and nitride catalysts as the diesel fuel yield increased as the temperature was raised from 380 to 390°C. During the process optimization, the temperature was ranged from 390 to 410°C and the diesel fuel yield decreased by approximately 10%. This suggests that there may be additional reactions taking place at higher temperatures, such as catalytic hydrocracking, that are responsible for low total yield of diesel fuel products. It can be concluded that the optimal temperature for diesel fuel yield from the molybdenum nitride catalyst is at approximately 395°C.

Examining the residence time, it can be seen from Figure 6.5 that the diesel fuel yield increased as the residence time is decreased (increase in LHSV). This result is opposite of what was experienced when comparing the molybdenum carbide and nitride catalysts. It is likely that this is a result of the higher reaction temperatures and the probability of new reactions being introduced at the higher temperatures (hydrocracking). Therefore, the increased reaction time is allowing these undesirable reactions more time to proceed. It was found that by increasing the LHSV from 0.6 to 1.2 hr^{-1}, the diesel fuel yield increased by approximately 10%. From these results, it can be concluded that the optimal residence time will be a function of the reaction temperature and the subsequent side reactions that are occurring. In the case of the process optimization considered here, the optimal LHSV for high diesel fuel yield, within the limits of the design, was found to be 1.05 hr^{-1}.

Figure 6.6 shows the dependence of the diesel fuel yield on pressure at a constant temperature of 400°C and LHSV of 0.9 hr^{-1}.

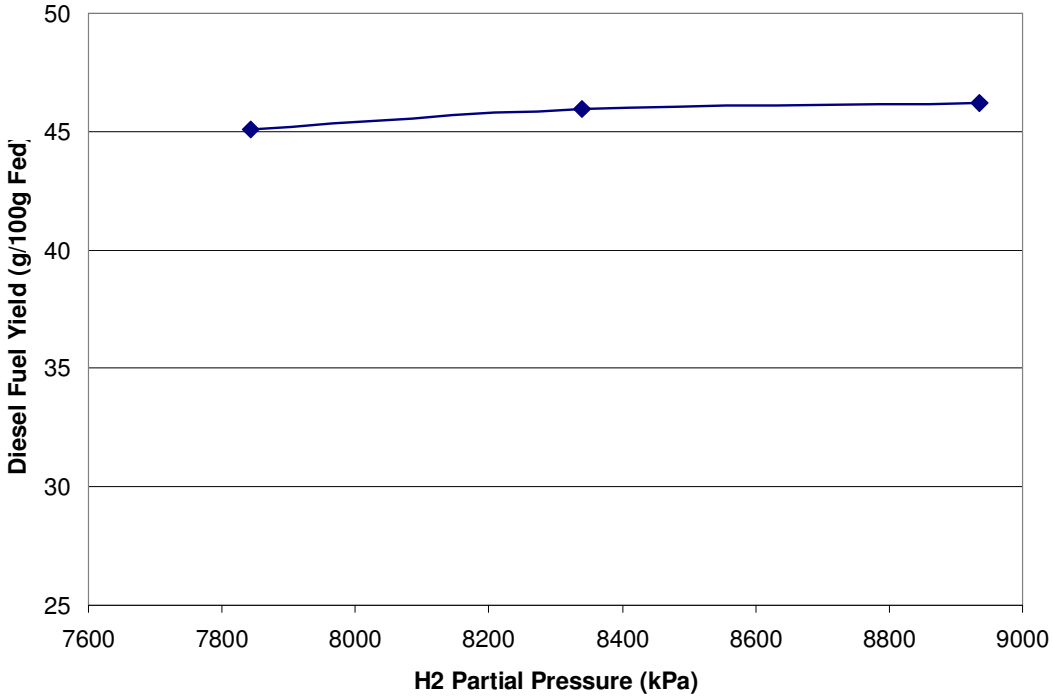

Figure 6.6: Pressure Effect on Diesel Fuel Yield (T = 400°C, LHSV = 0.9 hr^{-1})

It can be seen from Figure 6.6 that the pressure effect on the diesel fuel yield was minimal as the yield varied less then 2% over the range of hydrogen partial pressures examined (7800 – 8900 kPa). However, the general trend did show that an increase in pressure delivered a small increase in the diesel fuel yield.

6.3.2.3 Alkane/Olefin Content in the Organic Phase

The alkane/olefin content of the organic product was examined similarly to the diesel fuel yield. Figure 6.7 shows the surface plot of the alkane/olefin yield as a function of reaction temperature and residence time.

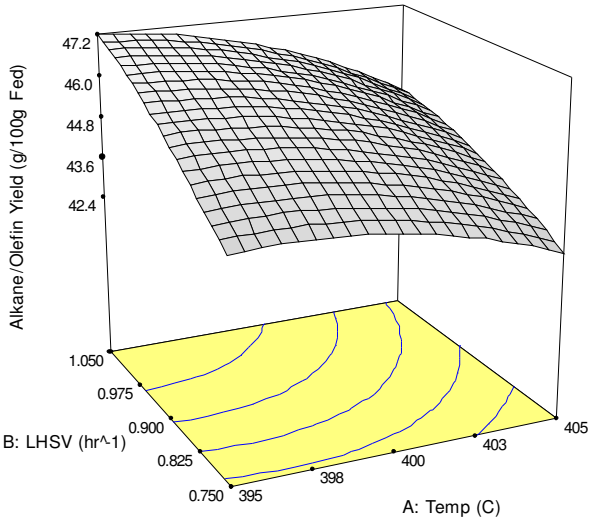

Figure 6.7: Surface Plot – Alkane/Olefin Yield (P_{H2} = 8330 kPa)

Figure 6.7 shows the effect of temperature and residence time on the alkane/olefin yield at a constant hydrogen partial pressure of 8330 kPa. It can be seen from Figure 6.7 that the alkane/olefin yield appears to fit a quadratic model and this result was supported by the Design Expert 6 software.

As was the case when considering the diesel fuel yield, the alkane/olefin yield increased with a decrease in residence time (increased LHSV). Comparing this result to those generated during the comparison of the molybdenum carbide and nitride catalysts, it can be seen that this result is again opposite of what was found when using the molybdenum nitride to process canola oil. It can be suggested that this change in

behaviour is again a result of the increased reaction temperature and the introduction of additional side reactions (hydrocracking) that are taking away from the final alkane/olefin yield. It was found that by increasing the LHSV from 0.6 to 1.2 hr^{-1}, the alkane/olefin yield increased by greater than 15%. It can be concluded that the optimum LHSV for alkane/olefin yield, within the limits of the design, is 1.05 hr^{-1}.

Examining the effect of the reaction temperature on the alkane/olefin yield, it can be seen from Figure 6.7 that the final alkane/olefin yield decreases with an increase in reaction temperature. Again, this result is opposite of what was seen in the previous studies when the reaction temperatures were limited to 380 – 390°C. This is likely due again to the introduction of additional side reactions (hydrocracking) at the elevated temperatures that caused the alkane/olefin products to further react. The effect of varying the reaction temperature from 390 – 410°C was small on the alkane/olefin yield than the LHSV, as a variation of less than 10% was found between the maximum and minimum alkane/olefin yields. It can be concluded that the optimal temperature within the given operating envelope for the molybdenum nitride catalyst to produce a high alkane/olefin yield is 395°C.

Figure 6.8 shows the effect of varying the hydrogen partial pressure on the alkane/olefin yield at a constant temperature of 400°C and LHSV of 0.9 hr^{-1}.

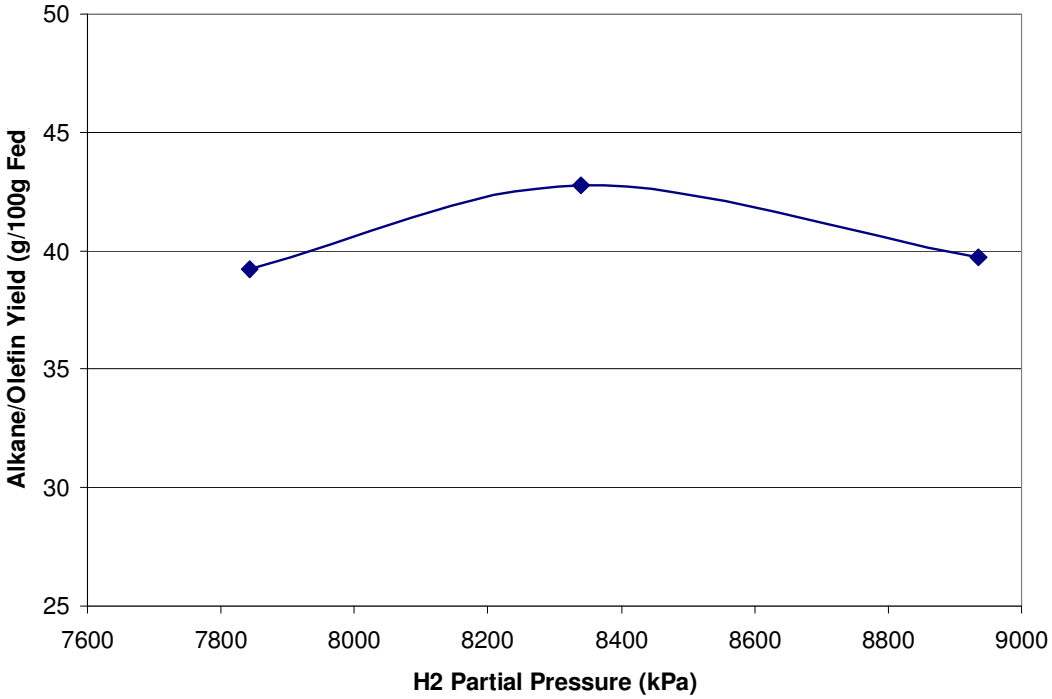

Figure 6.8: Pressure Effect on Alkane/Olefin Yield (T = 400°C, LHSV = 0.9 hr^{-1})

It can be seen from the Figure 6.8 that the hydrogen partial pressure dependency of the alkane/olefin yield shows the most prominent quadratic effect of the three input parameters studied. However, it should be noted that the overall variation of the alkane/olefin yield was only approximately 8% and this effect may be due to experimental error. Nevertheless, the optimum hydrogen partial pressure for the molybdenum nitride catalysts with respect to alkane/olefin yield appears to be approximately 8350 kPa.

6.3.2.4 Hydrogen Consumption

The hydrogen consumption was again studied during these experimental trials for information to support the conclusions made regarding the product conversion and selectivity. In the case of the process optimization, it was found that the hydrogen

consumption was consistently in the range of 200 – 300 L H_2 (STP) / L liquid fed to the reactor. No significant trends were observed when studying the effect of temperature, residence time, or pressure on the final value of hydrogen consumption. However, it was found that the hydrogen consumption increased with time on stream throughout the experiment (Figure 6.9). This is an interesting result as the conversion and selectivity of the catalyst did not appear to change as a function of time where as the hydrogen consumption steadily increased, even after 500 hours on stream. Further study on the robustness of the catalyst is required to determine if this increase in hydrogen consumption will stop changing over time or will lead to performance changes in the catalyst conversion and selectivity.

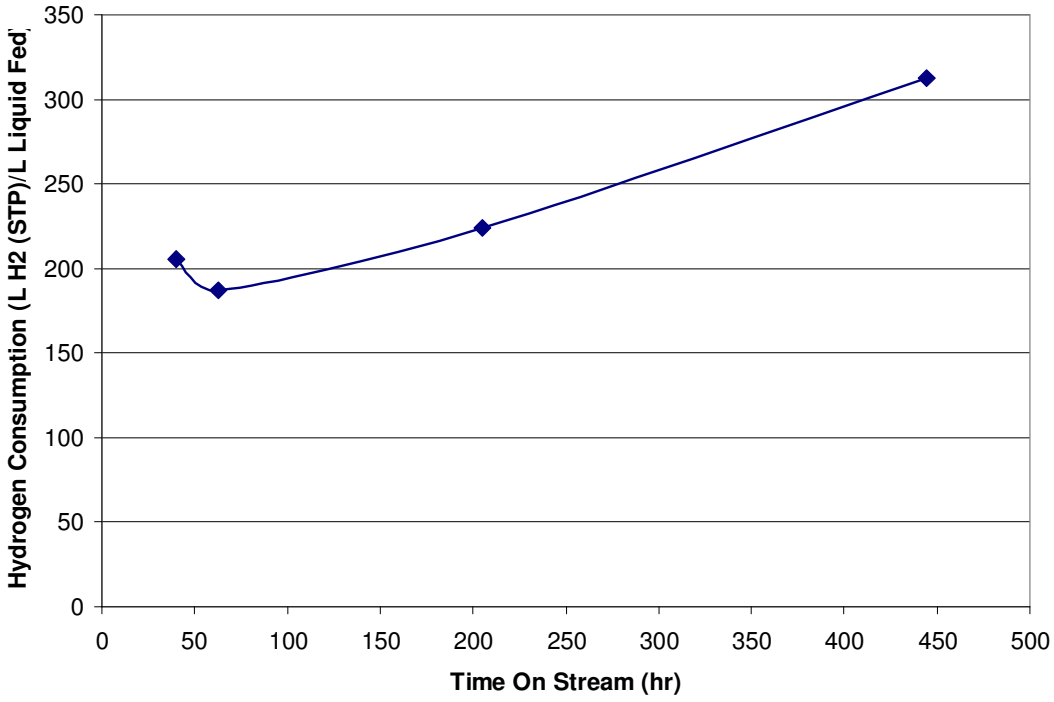

Figure 6.9 Effect of Time On Stream on Hydrogen Consumption (T = 400°C, LHSV = 0.9 hr^{-1}, P_{H2} = 8330 kPa)

6.3.2.5 Validation of Optimized Data from Experiments

The Design Expert 6 software was used to predict the optimum operating conditions within the operating envelopes that had been defined for the 3-CCD experiment. Again, the operating envelopes were 395 – 405°C for reaction temperature, 0.75 – 1.05 hr^{-1} for LHSV, and 8,000 – 8,650 kPa for hydrogen partial pressure. The optimization was set up to find the maximum product selectivity within these operating envelopes. Equal weighting was placed on maximizing both diesel fuel yield and alkane/olefin yield of the organic product. The results from the optimization showed that the selectivity would be optimized at 395°C, 1.05 hr^{-1}, and 8267 kPa. The Design Expert 6 software was then used to predict the process outputs at these operating conditions. The results from the Design Expert 6 simulation are found below in Table 6.5

Table 6.5: Design Expert 6 Simulation Results

	Optimum Operating Conditons (DE 6)	Experimental Results (RUN 11)
Temperature (°C)	395	395
LHSV (hr^{-1})	1.05	1.05
Pressure (kPa)	8267	8067
Diesel Fuel Yield (g/100g)	50.5 ± 1.4	50.7
Alkane/Olefin Yield (g/100g)	47.3 ± 4.0	44.5
H20 Production (g/100g)	9.3 ± 1.0	8.9
Hydrogen Consumption (g/100g)	2.7 ± 0.4	2.9
CO + CO2 Yield (g/100g)	2.3 ± 0.1	2.2
Methane Yield (g/100g)	0.4 ± 0.04	0.4
Ethane Yield (g/100g)	0.2 ± 0.02	0.2
Propane Yield (g/100g)	1.7 ± 0.2	2.0

The predicted results shown in Table 6.5 are reported with error bands to a confidence level of 95%. It can be seen that the predicted optimum selectivity for the supported molybdenum nitride catalyst within the bounds of these operating conditions is a diesel fuel yield of 50.5 g/100g liquid fed and an alkane/olefin yield of 47.3 g/100g liquid fed. It should be noted that the error reported for the alkane/olefin yield is much higher than the error reported for the diesel fuel yield. This increase in error is due to a slight decrease in alkane/olefin yield over the course of the experiment.

Also shown in Table 6.5 are the actual results from experiment #11. This experimental point was included as it was the trial with operating conditions closest to the optimum operating conditions. It can be seen that that the values for diesel fuel yield and alkane/olefin yield found in experiment #11 are close to the values predicted by Design Expert 6, suggesting that the optimum results predicted are realistic.

Since it has been shown that experiment #11 is the best representation of the optimum operating conditions, a few more observations can be made concerning the results from this trial. Figure 6.10 below shows the boiling point distribution from experiment #11 that was generated from the simulated distillation results.

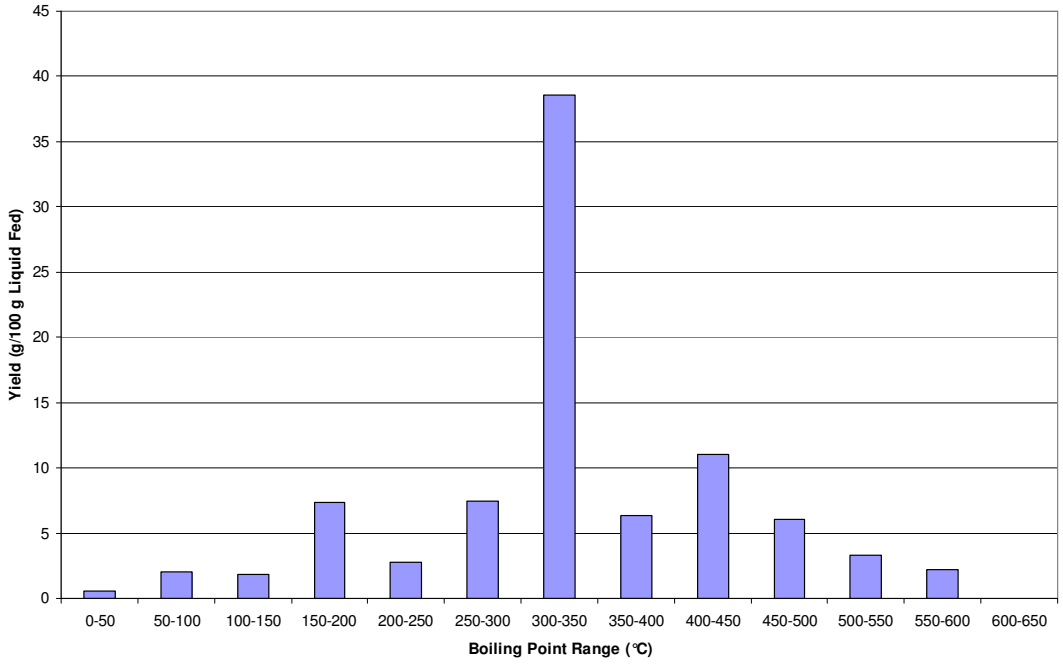

Figure 6.10a): Boiling Point Distribution – Experiment #11 (T = 395°C, LHSV = 1.05hr^{-1}, P_{H2} = 8067 kPa)

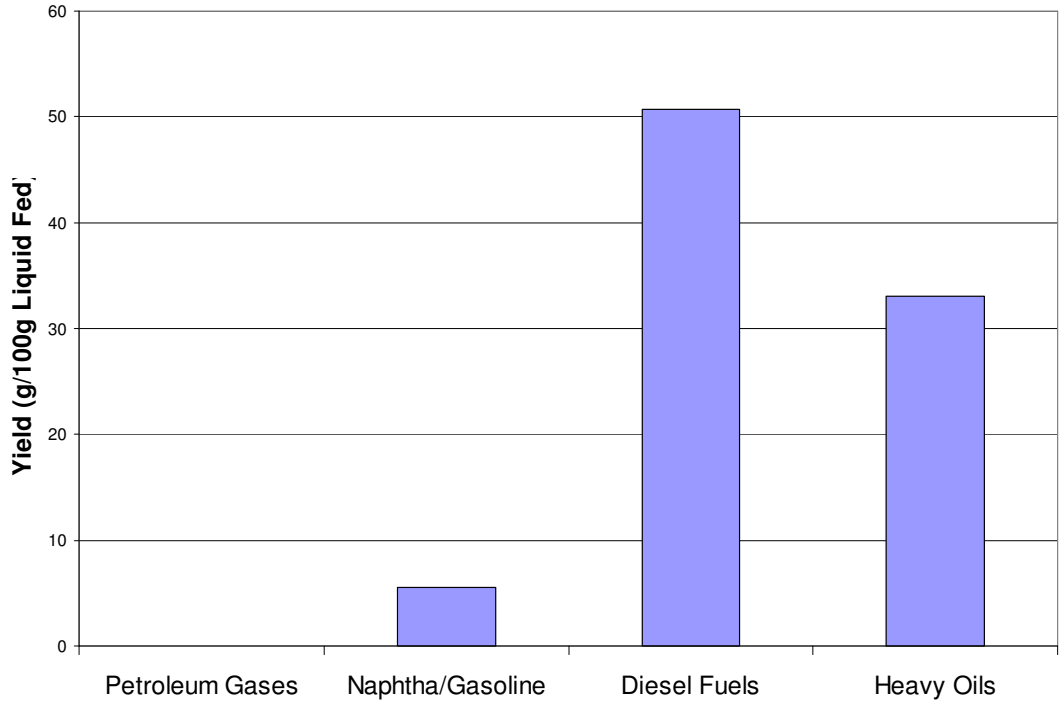

Figure 6.10b): Organic Product Fractions – Experiment #11 (T = 395°C, LHSV = 1.05hr^{-1}, P_{H2} = 8067 kPa)

From Figure 6.10(a) it can be seen that the majority of the organic product lies in the boiling point range of 300 - 350°C. This is characteristic of a diesel fuel product and corresponds to high levels of octadecane (C18, bp = 317°C). This suggests that if the organic product found in this boiling point range was separated out, it would be highly suitable for use as a diesel fuel cetane enhancer. As shown in both Figures 6.10(a) and 6.10(b), there remains a large amount of heavy oils in the organic product (>35 g/100g Liquid Fed). Although this result is not desirable at this point, it does indicate that with further design of the molybdenum nitride catalyst or further processing, these products could also be added to the diesel fuel boiling point range. If the diesel fuel products and heavy oil yields were to be combined, the total yield of the process would exceed 80 g/100g liquid fed.

6.4 CONCLUSIONS

The final phase of study set out to optimize both the catalyst and the process conditions for final product selectivity, specifically high diesel fuel and alkane/olefin yields. The catalyst optimization was carried out by examining the metal loading of the molybdenum nitride catalyst. Results were compared between a low metal loading (7.4 wt% molybdenum) and a high metal loading (22.7 wt% molybdenum). The results from this comparison showed that higher product selectivity was achieved with the high metal loading for both diesel fuel (5.3%) and alkane/olefin (43.2%) yield.

The preliminary process optimization was carried out by performing a 3-parameter central composite experimental design that set out to gather information concerning reaction temperature, residence time (LHSV), and hydrogen partial pressure.

Using Design Expert 6, the preliminary optimum operating conditions, within the design limits, were found to be a reaction temperature of 395°C, a LHSV of 1.05 hr^{-1}, and a hydrogen partial pressure of 8267 kPa. Using the models generated from the experiment, it was predicted that under these operating conditions the molybdenum nitride catalyst will yield 50.5 g of diesel fuel and 47.3 g of alkane/olefin products per 100 g of canola oil. It was also shown that at these conditions, between 30-40 g per 100 g of canola oil are hydrocarbon products classified as heavy oils (BP = 325°C+). With further catalyst design or processing, if these heavy oils are converted into diesel fuel products, the yield of this process may become greater than 80 g per 100 g of canola oil.

7.0 Conclusions and Recommendations

7.1 CONCLUSIONS

It has been shown in this thesis that the supported molybdenum nitride catalyst demonstrated superior performance when converting canola oil into a diesel fuel cetane enhancer as compared to five other supported metallic carbide and nitride catalysts (molybdenum-carbide, tungsten-carbide, tungsten-nitride, vanadium-carbide, and vanadium-nitride). The project was divided into three distinct experimental phases, of which each generated the following conclusions:

Scouting Tests

- Internal mass transfer effects, with respect to both the organic liquid phase and hydrogen, within the catalyst pellet were found to be negligible using the Weisz-Prater Criterion to evaluate the observed reaction rate against the effective internal diffusion.
- External mass transfer effects, with respect to both the organic liquid phase and hydrogen, were found to be negligible using the Mears Criterion to evaluate the observed reaction rate against the overall external mass transfer co-efficient.
- The supported molybdenum catalysts, both carbide and nitride, were found to outperform the other four catalysts in all of the five key performance indicators. The supported molybdenum catalysts showed:
  - Higher oxygen removal from the organic phase.
  - Lower fatty acid concentrations in the organic phase.

- Higher alkane/olefin selectivity in the organic phase.
- Higher hydrogen consumption, lower CO/CO_2 production, and higher methane/ethane production indicating a higher affinity for the direct hydrodeoxygenation mechanism.

Comparison of Supported γ-Al_2O_3 Mo_2C and γ-Al_2O_3 Mo_2N for HYD and HDO of Canola Oil

- The supported molybdenum nitride catalyst outperformed the supported molybdenum carbide catalyst with respect to the HYD and HDO of canola oil in three of the four key performance indicators. The supported molybdenum nitride catalyst showed:
  - Higher hydrogen to carbon atomic ratio in the organic phase.
  - Higher alkane/olefin selectivity in the organic phase.
  - Higher diesel fuel fraction in the organic phase.
  - Slightly higher hydrogen consumption.
- Preliminary information was gathered on the effect on reaction temperature and residence time on the four key performance indicators. It was concluded that:
  - Further study is required to determine the effects of temperature and residence time on oxygen removal from the organic phase and hydrogen consumption.
  - An increase in both reaction temperature (in the range of 380 – 390°C) and residence time (LHSV in the range of 0.6 – 1.2 hr^{-1}) yielded higher

alkane/olefin selectivity and a higher diesel fuel fraction in the organic phase.

Preliminary Process Optimization for HYD and HDO of Canola Oil Using Supported γ-Al_2O_3 Mo_2N

- An increase in the metal loading of the supported molybdenum nitride catalyst was found to deliver an increase in both alkane/olefin and diesel fuel yield. It was found that by increasing the molybdenum loading of the catalyst from 7.4 wt% to 22.7 wt%, the alkane/olefin yield increased by 43.2 % and the diesel fuel yield increased by 5.3%. In addition, no increase in hydrogen consumption was linked to the increase in product selectivity.
- Over the temperature range of 390 – 410°C, the LHSV range of 0.6 – 1.2 hr^{-1}, and the hydrogen partial pressure range of 7800 – 8900 kPa, it was found that the effect of reaction temperature, residence time, and hydrogen partial pressure all had a very small effect on the total removal of oxygen from the organic phase. This was due to very high conversions ranging from 85 – 95 % removal of oxygen from the organic phase.
- Over the temperature range of 390 – 410°C and the LHSV range of 0.6 – 1.2 hr^{-1} it was found that both the alkane/olefin and diesel fuel yields increased with a reduction in reaction temperature and residence time.
- Over the hydrogen partial pressure range of 7800 – 8900 kPa it was found that there was no effect of hydrogen partial pressure on the diesel fuel

yield. A minimal effect of hydrogen partial pressure on alkane/olefin yield was observed with a maximum occurring at 8350 kPa.

- The preliminary optimum operating conditions for the supported molybdenum catalyst (22.7 wt% Mo) within the range of inputs studied was found to be a reaction temperature of 395°C, a LHSV of 1.05 hr^{-1}, and a hydrogen partial pressure of 8267 kPa. At these conditions, it is predicted that the final diesel fuel yield will be 50.5g/ 100g of canola oil and the final alkane/olefin yield will be 47.3g/ 100g of canola oil.
- The simulated distillation results show that at these conditions that the yield of heavy oils (BP > 325°C) will be between 30 – 40g / 100g of canola oil. This suggests that with further processing the heavy oils could be converted to a diesel fuel product to deliver a total yield for this process of greater than 80g / 100g canola oil.

7.2 RECOMMENDATIONS

Recommendations for further study on the production of a diesel fuel cetane enhancer from canola oil using a supported molybdenum nitride catalyst are as follows:

- The metal loading of molybdenum should be further examined to determine the optimum value for maximizing alkane/olefin and diesel fuel yield.
- The boundary of the process optimization should be widened (lower temperature and higher LHSV) to determine the true optimum operating condition for this process.
- A kinetic study should be carried out to determine the reaction mechanism taking place on the surface of the supported molybdenum nitride catalyst.
- A more detailed study of the organic product, specifically of the heavy oil constituents.
- Following the kinetic study, the catalyst/process design should be revisited and tested in an effort to maximize the alkane/olefin and diesel fuel yields. Specifically, this effort should focus on preventing the formation of heavy oils that currently make up 30 – 40% of the organic product yield.
- Promotion of the supported molybdenum nitride catalyst with another metal should be examined for its effect on the alkane/olefin and diesel fuel yield.

8.0 List of References

Afonso, J.C., M. Schmal and J. N. Cardoso, "Acidic Oxygen Compounds in the Irati Shale Oil," *Industrial and Engineering Chemistry Research*, v. 31, 1992, p. 1045-1050.

Andersson, K., M. Hell, L. Lowendahl, and N. H. Schoon, "Diffusivities of Hydrogen and Glyceryl Trioleate in Cottonseed Oil at Elevated Temperature," *Journal of the American Oil Chemists' Society*, v. 51, 1974, p. 171-173.

ASTM D 613-05, "Standard Test method for Cetane Number of Diesel Fuel Oil", *ASTM International*, Designation: 41/2000.

Dymtryshyn, S.L., A. K. Dalai, S.T. Chaudhari, H.K. Mishra and M.J. Reaney, "Synthesis and characterization of vegetable oil derived esters: evaluation for their diesel additive properties," *Bioresource Technology*, v. 92, 2004, p. 55-64.

Ferdous, D., A. K. Dalai and J. Adjaye, "A series of NiMo/γ-Al_2O_3 catalysts containing boron and phosphorous Part 1. Synthesis and characterization," *Applied Catalysis A*, v. 260, 2004, p. 137-151.

Fogler, H. S., Elements of Chemical Reactions Engineering Third Edition, Prentice Hall PTR, 1999.

Furimsky, E., "Review: Metal carbides and nitrides as potential catalysts for hydroprocessing," *Applied Catalysis A*, v. 204, 2003, p. 1-28.

Furimsky, E., "Review: Catalytic hydrodeoxygenation," *Applied Catalysis A*, v. 199, 2000, p. 147-190.

Goto, S., J. Levec, and J.M. Smith, "Mass Transfer in Packed Beds with Two-Phase Flow," *Industrial and Engineering Chemistry Process Design and Development,* v. 14, n. 4, 1975, p. 473-478.

Gusmao, J., D. Brodzki, G. Djega-Mariadassou and R. Frety, "Utilization of vegetable oils as an alternative source for diesel-type fuel: hydrogracing on reduced Ni/SiO_2 and sulphided NiMo/γ-Al_2O_3," *Catalysis Today*, v. 5, 1989, p. 533-544.

Larachi, F., L. Belfares, I. Iliuta, and B. P. A. Grandjean, "Heat and Mass Transfer in Cocurrent Gas-Liquid Packed Beds. Analysis, Recommendations, and New Correlations," *Industrial and Engineering Chemistry Research*, v. 42, 2003, p. 222-242.

Laurent, E. and B. Delmon, "Study of the hydrodeoxygenation of carbonyl, carboxylic and guaiacyl groups over sulfided CoMo/γ-Al_2O_3 and NiMo/γ-Al_2O_3 catalysts. I. Catalytic reaction schemes," *Applied Catalysis A*, v. 109, 1994, p. 77-96.

Monnier, J., G. Tourigny, D.W. Soveran, A. Wong, E. N. Hogan and M. Stumborg, "Conversion of Bimass Feedstock," US Patent No. 5,705,722. Jan 5, 1998.

Monnier, J., G. Tourigny and D.W. Soveran, "Conversion of Depitched Tall Oil to Diesel Fuel Additive," Canadian Patent No. 2,149,685. Sept. 14, 1999.

Ramanathan, S. and S. T. Oyama, "New Catalysts for Hydroprocessing: Transition Metal Carbides and Nitrides," *Journal of Physical Chemistry*, v. 99, 1995, p. 16365-16372.

Ramirez, E., M. A. Larrayoz, and F. Recasens, "Intraparticle Diffusion Mechanisms in SC Sunflower Oil Hydrogenation on Pd," *American Institute of Chemical Engineers Journal*, v. 52, n. 4, p. 1539-1553.

Saada, M. Y., "Assessment of Interfacial Area in Co-current Two-Phase Flow in Packed Beds," *Chimie et Insustrie – Genie Chimique*, v. 105, n. 20, 1972, p. 1415-1422.

Satterfield, C. N., Heterogeneous Catalysis in Practice, McGraw-Hill, 1980.

Satterfield, C. N., Heterogeneous Catalysis in Industrial Practice, McGraw-Hill, 1991.

Sirvastava, A., and R. Prasad, "Triglycerides-based diesel fuels," *Renewable and Sustainable Energy Reviews*, v. 4, 2000, p. 111-133.

Velksink, J. W., M. J. Bouma, N. H. Schoon, and A. A. C. M. Beenackers, "Heterogeneous Hydrogenation of Vegetable Oils: A Literature Review," *Catalysis Reviews, Science and Engineering*, v. 39, 1997, p. 253-318.

Wisniak, Jamie, L.F. Albright, "Hydrogenating Cottenseed Oil at Relatively High Pressure", *Industrial and Engineering Chemistry*, v. 53, n. 5, 1961, p. 375-380.

Zhang, Y.J., Q. Xin, I. Rodrigues-Ramos and A. Guerrero-Ruiz, "Simultaneous hydrodesulfurization of thiophene and hydrogenation of cyclohexene over dimolybdenum nitride catalysts," *Applied Catalysis A*, v. 180, 1999, p. 237-245.

Websites:

1. "The CETC SuperCetane Technology." 2003. Natural Resources Canada. Date Accessed: September, 2008, http://www.canren.gc.ca/tech_appl/index.asp?CaId=2&PgId=1083

2. "Definitions." Biodiesel Education. Becon. Date Accessed: September, 2008, http://www3.me.iastate.edu/biodiesel/Pages/biodiesel3.html

3. "2004 Saskatchewan Crop District Crop Production." 2005. Crops – StatFact. Saskatchewan Agriculture, Food and Rural Revitalization. Date Accessed: April, 2005, http://www.agr.gov.sk.ca/docs/statistics/crops/production/SkCrpDistrict04.pdf

4. "Oleic Acid Physical Properties." Date Accessed: September, 2008. http://www.sjlipids.com/c181.htm

Appendix A: Product C/H/N Analytical Results

Table A.1: C/H/N Analytical Results – Scouting Test

Catalyst (Experimental Trial)	Carbon (wt%)	Hydrogen (wt%)	Nitrogen (wt%)	Oxygen* (wt%)	H / C Atomic Ratio
Oleic Acid (Feed)	77.2	12.1	0.0	10.7	1.87
$Mo_2C/\gamma\text{-}Al_2O_3$	86.2	14.5	0.0	-0.7	2.00
$WC/\gamma\text{-}Al_2O_3$	85.1	13.4	0.0	1.5	1.88
$VC/\gamma\text{-}Al_2O_3$	83.6	13.1	0.0	3.3	1.86
$Mo_2N/\gamma\text{-}Al_2O_3$	87.2	14.8	0.0	-2.1	2.03
$WN/\gamma\text{-}Al_2O_3$	86.4	13.3	0.2	0.0	1.84
$VN/\gamma\text{-}Al_2O_3$	83.7	13.0	0.2	3.0	1.86

*Values for oxygen are calculated by difference. Due to experimental error, oxygen values of less than zero were taken to be equal to zero.

Table A.2: C/H/N Analytical Results – Comparison of Supported γ-Al_2O_3 Mo_2C and γ-Al_2O_3 Mo_2N for HYD and HDO of Canola Oil

Experimental Trial ID	Catalyst / Feed	Carbon (wt%)	Hydrogen (wt%)	Nitrogen (wt%)	Oxygen* (wt%)	H / C Atomic Ratio
	Triolein (Feed)	78.4	11.9	0.0	9.7	1.81
	Canola Oil (Feed)	78.1	11.6	0.0	10.3	1.77
SC07R02	Mo_2C / Triolein	87.2	14.3	0.0	-1.5	1.95
SC07R03	Mo_2C / Triolein	87.6	14.3	0.0	-2.0	1.95
SC07R04	Mo_2C / Triolein	87.3	14.5	0.0	-1.8	1.97
SC07R05	Mo_2C / Triolein	87.3	14.3	0.0	-1.6	1.96
SC07R08	Mo_2C / Canola Oil	86.0	13.6	0.0	0.5	1.88
SC07R09	Mo_2C / Canola Oil	85.9	13.8	0.0	0.3	1.91
SC07R10	Mo_2C / Canola Oil	88.0	13.8	0.0	-1.7	1.87
SC07R11	Mo_2C / Canola Oil	87.8	13.8	0.0	-1.6	1.88
SC08R01	Mo_2N / Canola Oil	87.8	13.8	0.0	-1.6	1.87
SC08R03	Mo_2N / Canola Oil	86.6	13.9	0.0	-0.5	1.91
SC08R04	Mo_2N / Canola Oil	86.9	13.8	0.0	-0.7	1.90
SC08R05	Mo_2N / Canola Oil	88.1	13.8	0.0	-1.8	1.86
SC08R06	Mo_2N / Triolein	87.8	14.2	0.0	-2.0	1.92
SC08R07	Mo_2N / Triolein	87.5	14.0	0.0	-1.4	1.91
SC08R08	Mo_2N / Triolein	88.0	13.7	0.0	-1.7	1.85

*Values for oxygen are calculated by difference. Due to experimental error, oxygen values of less than zero were taken to be equal to zero.

Table A.3: C/H/N Analytical Results – Process Optimization for HYD and HDO of Canola Oil Using Supported γ-Al_2O_3 Mo_2N

Experimental Trial ID	Carbon (wt%)	Hydrogen (wt%)	Nitrogen (wt%)	Oxygen* (wt%)	H / C Atomic Ratio
Canola Oil (Feed)	78.1	11.6	0.0	10.3	1.76
SC12R01	86.3	14.5	0.0	-0.8	2.00
SC12R02	86.8	14.5	0.0	-1.4	2.00
SC12R03	86.8	14.5	0.0	-1.2	1.98
SC12R04	86.9	14.6	0.0	-1.5	2.00
SC12R05	86.7	14.6	0.0	-1.3	2.00
SC12R06	86.8	14.3	0.0	-1.1	1.96
SC12R07	86.6	14.5	0.0	-1.0	1.99
SC12R08	86.5	14.4	0.0	-0.8	1.98
SC12R09	86.8	14.5	0.0	-1.3	1.99
SC12R10	86.8	14.5	0.0	-1.2	1.99
SC12R11	86.0	14.5	0.0	-0.5	2.02
SC12R12	86.7	14.7	0.0	-1.4	2.02
SC12R13	86.4	14.7	0.0	-1.1	2.02
SC12R14	86.0	14.6	0.0	-0.6	2.03
SC12R15	86.1	14.7	0.0	-0.8	2.03
SC12R16	86.4	14.8	0.0	-1.2	2.04
SC12R17	86.1	14.8	0.0	-0.8	2.04
SC12R18	86.4	14.8	0.0	-1.2	2.04

*Values for oxygen are calculated by difference. Due to experimental error, oxygen values of less than zero were taken to be equal to zero.

Appendix B: Liquid Product FAME GC/MS, GC/MS, and Simulated Distillation Analytical Results

Table B.1: FAME GC/MS / GC/MS / Simulated Distillation Analytical Results – Scouting Test

	FAME GC/MS Results	GC/MS Results
Catalyst (Experimental Trial)	**Residual Acid Content (wt%)**	**Alkane/Olefin Content (wt%)**
Oleic Acid (Feed)	100.0	0.0
$Mo_2C/\gamma\text{-}Al_2O_3$	1.81	34.8
$WC/\gamma\text{-}Al_2O_3$	4.43	10.6
$VC/\gamma\text{-}Al_2O_3$	0.16	14.0
$Mo_2N/\gamma\text{-}Al_2O_3$	0.03	33.6
$WN/\gamma\text{-}Al_2O_3$	3.47	13.0
$VN/\gamma\text{-}Al_2O_3$	3.56	10.0

Table B.2: FAME GC/MS / GC/MS / Simulated Distillation Analytical Results – Comparison of Supported $\gamma\text{-}Al_2O_3$ Mo_2C and $\gamma\text{-}Al_2O_3$ Mo_2N for HYD and HDO of Canola Oil

		FAME GC/MS Results	GC/MS Results	Simulated Distillation Results			
Experimental Trial ID	**Catalyst / Feed**	**Residual Acid Content (wt%)**	**Alkane/Olefin Content (wt%)**	**Petroleum Gases BP < 20°C (wt%)**	**Naphtha/Gasoline BP: 20 - 155° (wt%)**	**Diesel Fuel BP: 155 - 325°C (wt%)**	**Heavy Oils BP > 325°C (wt%)**
	Triolein (Feed)	100.0	0.0				
	Canola Oil (Feed)	100.0	0.0				
SC07R02	Mo_2C / Triolein	2.6E-02	30.4	0.0	10.2	45.1	44.7
SC07R03	Mo_2C / Triolein	1.9E-02	37.1	0.0	11.0	45.3	43.6
SC07R04	Mo_2C / Triolein	1.8E-02	34.3	0.0	13.3	49.8	36.9
SC07R05	Mo_2C / Triolein	2.1E-02	27.2	0.0	12.2	48.6	39.2
SC07R08	Mo_2C / Canola Oil	1.2E-01	19.0	0.0	14.0	41.5	44.5
SC07R09	Mo_2C / Canola Oil	1.5E-01	17.2	0.0	11.4	39.6	49.0
SC07R10	Mo_2C / Canola Oil	5.1E-02	19.6	0.0	13.0	40.4	46.6
SC07R11	Mo_2C / Canola Oil	8.5E-02	24.1	0.0	16.8	45.1	38.1
SC08R01	Mo_2N / Canola Oil	2.6E-02	24.8	0.0	16.4	46.4	37.2
SC08R03	Mo_2N / Canola Oil	6.3E-02	19.8	0.0	11.2	38.6	50.2
SC08R04	Mo_2N / Canola Oil	5.0E-02	24.1	0.0	13.3	41.0	45.7
SC08R05	Mo_2N / Canola Oil	7.1E-03	24.7	0.0	16.6	44.5	38.9
SC08R06	Mo_2N / Triolein	5.2E-02	25.6	0.0	13.3	44.8	42.0
SC08R07	Mo_2N / Triolein	1.1E-01	23.2	0.0	9.8	40.7	49.5
SC08R08	Mo_2N / Triolein	6.0E-02	27.6	0.0	8.2	47.8	44.0

Table B.3: FAME GC/MS / GC/MS / Simulated Distillation Analytical Results – Process Optimization for HYD and HDO of Canola Oil Using Supported γ-Al_2O_3 Mo_2N

	FAME GC/MS Results	GC/MS Results	Simulated Distillation Results			
Experimental Trial ID	Residual Acid Content (wt%)	Alkane/Olefin Content (wt%)	Petroleum Gases BP < 20°C (wt%)	Naphtha/Gasoline BP: 20 - 155° (wt%)	Diesel Fuel BP: 155 - 325°C (wt%)	Heavy Oils BP > 325°C (wt%)
Canola Oil (Feed)	100.0	0.0				
SC11R01	4.8E-02	34.1	0.0	8.8	50.3	40.9
SC11R02	5.2E-02	33.2	0.0	11.2	50.2	38.6
SC11R03	2.3E-02	38.9	0.0	6.2	55.5	38.3
SC11R04	4.7E-02	39.4	0.5	7.6	53.9	37.9
SC12R01	6.2E-02	57.9	0.0	8.3	53.7	38.0
SC12R02	3.5E-02	53.8	0.0	8.0	55.0	37.0
SC12R03	3.6E-02	47.9	0.0	10.2	52.1	37.7
SC12R04	6.0E-02	51.7	0.4	5.8	58.9	34.9
SC12R05	2.7E-02	56.0	0.4	6.8	56.9	35.9
SC12R06	1.1E-01	47.8	0.0	9.0	51.4	39.6
SC12R07	3.0E-02	49.6	0.6	7.6	53.3	38.5
SC12R08	4.6E-02	46.2	0.0	7.8	53.7	38.5
SC12R09	7.0E-02	46.2	0.6	7.6	53.1	38.8
SC12R10	7.4E-02	45.8	0.0	7.2	53.8	38.9
SC12R11	7.4E-02	49.8	0.0	6.2	56.8	37.0
SC12R12	6.9E-02	45.0	0.0	8.2	52.1	39.6
SC12R13	7.0E-02	41.8	0.0	8.5	50.0	41.6
SC12R14	6.6E-02	46.0	0.0	13.7	45.5	40.8
SC12R15	1.3E-01	45.3	0.0	8.3	51.9	39.8
SC12R16	5.2E-02	46.6	0.0	6.2	56.8	37.0
SC12R17	6.5E-02	49.2	0.4	6.8	51.9	40.9
SC12R18	9.0E-02	49.6	0.8	7.4	52.9	38.9

Appendix C: Gas Product GC/MS Analytical Results

Table C.1: Gas Product GC/MS Analytical Results – Scouting Test

Catalyst (Experimental Trial)	H2 (vol%)		Ar (vol%)		N2 (vol%)		CO (vol%)	CO2 (vol%)	CH4 (vol%)	C2H6 (vol%)	C2H4 (vol%)	C3H8 (vol%)	C3H6 (vol%)	C4+ (vol%)
	In	Out	In	Out	In	Out								
$Mo_2C/\gamma\text{-}Al_2O_3$	90.75	85.03	9.25	11.73	0.00	0.15	0.46	1.00	0.60	0.72	0.31	0.00	N.A.	N.A.
$WC/\gamma\text{-}Al_2O_3$	90.18	87.06	9.78	9.83	0.03	0.06	1.26	1.30	0.23	0.21	0.06	0.00	N.A.	N.A.
$VC/\gamma\text{-}Al_2O_3$	90.18	87.52	9.78	9.70	0.03	0.05	1.16	1.23	0.16	0.15	0.04	0.00	N.A.	N.A.
$Mo_2N/\gamma\text{-}Al_2O_3$	90.18	85.77	9.78	11.96	0.03	0.11	0.59	0.97	0.27	0.32	0.00	0.00	N.A.	N.A.
$WN/\gamma\text{-}Al_2O_3$	90.18	86.58	9.78	10.45	0.03	0.06	1.34	1.21	0.15	0.16	0.05	0.00	N.A.	N.A.
$VN/\gamma\text{-}Al_2O_3$	90.18	87.09	9.78	9.94	0.03	0.09	1.28	1.27	0.15	0.13	0.04	0.00	N.A.	N.A.

N.A. = Not Analyzed

Table C.2: Gas Product GC/MS Analytical Results – Comparison of Supported $\gamma\text{-}Al_2O_3$ Mo_2C and $\gamma\text{-}Al_2O_3$ Mo_2N for HYD and HDO of Canola Oil

Experimental Trial ID	Catalyst / Feed	H2 (vol%)		Ar (vol%)		N2 (vol%)		CO (vol%)	CO2 (vol%)	CH4 (vol%)	C2H6 (vol%)	C2H4 (vol%)	C3H8 (vol%)	C3H6 (vol%)	C4+ (vol%)
		In	Out	In	Out	In	Out								
SC07R02	Mo_2C / Triolein	90.18	83.58	9.78	13.21	0.03	0.03	0.91	1.43	0.53	0.31	0.00	0.00	N.A.	N.A.
SC07R03	Mo_2C / Triolein	90.18	84.54	9.78	12.36	0.03	0.04	0.83	1.24	0.67	0.31	0.00	0.00	N.A.	N.A.
SC07R04	Mo_2C / Triolein	90.18	83.63	9.78	12.86	0.03	0.04	0.74	1.19	1.06	0.47	0.00	0.00	N.A.	N.A.
SC07R05	Mo_2C / Triolein	90.18	84.20	9.78	12.71	0.03	0.04	0.68	1.12	0.82	0.42	0.00	0.00	N.A.	N.A.
SC07R08	Mo_2C / Canola Oil	90.18	83.57	9.78	12.48	0.03	0.04	1.18	1.38	0.45	0.63	0.02	0.25	N.A.	N.A.
SC07R09	Mo_2C / Canola Oil	90.18	84.82	9.78	12.00	0.03	0.04	1.32	1.02	0.19	0.38	0.05	0.17	N.A.	N.A.
SC07R10	Mo_2C / Canola Oil	90.18	84.17	9.78	12.15	0.03	0.04	1.36	1.28	0.28	0.49	0.03	0.19	N.A.	N.A.
SC07R11	Mo_2C / Canola Oil	90.18	83.65	9.78	12.17	0.03	0.04	1.13	1.35	0.68	0.71	0.01	0.27	N.A.	N.A.
SC08R01	Mo_2N / Canola Oil	90.18	84.22	9.78	11.84	0.03	0.04	1.07	1.18	0.77	0.63	0.02	0.24	N.A.	N.A.
SC08R03	Mo_2N / Canola Oil	90.18	84.10	9.78	12.18	0.03	0.04	1.57	1.28	0.18	0.40	0.06	0.19	N.A.	N.A.
SC08R04	Mo_2N / Canola Oil	90.18	83.19	9.78	12.60	0.03	0.04	1.56	1.55	0.26	0.51	0.04	0.25	N.A.	N.A.
SC08R05	Mo_2N / Canola Oil	90.18	83.70	9.78	12.14	0.03	0.04	1.12	1.37	0.64	0.73	0.01	0.24	N.A.	N.A.
SC08R06	Mo_2N / Triolein	90.18	84.64	9.78	12.14	0.03	0.04	0.90	1.19	0.39	0.52	0.01	0.18	N.A.	N.A.
SC08R07	Mo_2N / Triolein	90.18	83.56	9.78	12.72	0.03	0.04	1.55	1.32	0.19	0.35	0.04	0.22	N.A.	N.A.
SC08R08	Mo_2N / Triolein	90.18	82.54	9.78	12.82	0.03	0.04	1.11	1.76	0.75	0.74	0.00	0.23	N.A.	N.A.

Table C.3: Gas Product GC/MS Analytical Results – Process Optimization for HYD and HDO of Canola Oil Using Supported γ-Al_2O_3 Mo_2N

Experimental Trial ID	H2 (vol%)		Ar (vol%)		N2 (vol%)		CO (vol%)	CO2 (vol%)	CH4 (vol%)	C2H6 (vol%)	C2H4 (vol%)	C3H8 (vol%)	C3H6 (vol%)	C4+ (vol%)
	In	Out	In	Out	In	Out								
SC11R01	89.80	83.22	10.14	12.78	0.06	0.07	0.74	1.38	0.91	0.28	0.00	0.55	0.00	0.06
SC11R02	89.80	83.14	10.14	12.73	0.06	0.07	0.75	1.31	1.06	0.39	0.00	0.48	0.00	0.07
SC11R03	89.80	83.26	10.14	13.19	0.06	0.07	0.65	1.41	0.52	0.22	0.00	0.63	0.00	0.04
SC11R04	89.80	82.77	10.14	13.31	0.06	0.07	0.77	1.62	0.50	0.26	0.00	0.65	0.00	0.05
SC12R01	89.80	83.96	10.14	12.38	0.06	0.07	0.46	1.21	0.88	0.27	0.00	0.71	0.00	0.05
SC12R02	89.80	83.96	10.14	12.38	0.06	0.07	0.46	1.21	0.88	0.27	0.00	0.71	0.00	0.05
SC12R03	89.80	81.80	10.14	13.65	0.06	0.07	0.63	1.42	1.27	0.38	0.00	0.71	0.00	0.07
SC12R04	89.80	82.82	10.14	13.73	0.06	0.08	0.47	1.17	0.68	0.20	0.00	0.80	0.00	0.04
SC12R05	89.80	82.95	10.14	13.46	0.06	0.07	0.55	1.21	0.73	0.23	0.00	0.75	0.00	0.05
SC12R06	90.28	82.49	9.66	13.33	0.06	0.08	0.43	1.06	1.10	0.32	0.00	1.13	0.00	0.06
SC12R07	90.28	82.53	9.66	13.29	0.06	0.08	0.50	1.20	0.86	0.27	0.00	1.21	0.00	0.05
SC12R08	90.28	81.50	9.66	14.09	0.06	0.09	0.48	1.26	0.97	0.29	0.00	1.26	0.00	0.05
SC12R09	90.28	82.73	9.66	13.23	0.06	0.08	0.50	1.15	0.82	0.26	0.00	1.18	0.00	0.05
SC12R10	90.28	82.66	9.66	13.34	0.06	0.07	0.43	1.10	0.82	0.25	0.00	1.26	0.01	0.05
SC12R11	90.28	82.98	9.66	13.21	0.06	0.07	0.45	1.10	0.63	0.21	0.00	1.30	0.01	0.04
SC12R12	90.28	82.58	9.66	13.24	0.06	0.07	0.53	1.12	0.90	0.29	0.00	1.20	0.01	0.06
SC12R13	90.28	82.68	9.66	13.14	0.06	0.07	0.48	1.02	1.15	0.34	0.00	1.05	0.01	0.06
SC12R14	90.28	82.56	9.66	13.28	0.06	0.07	0.45	1.05	1.18	0.36	0.00	0.99	0.01	0.06
SC12R15	90.28	82.45	9.66	13.36	0.06	0.07	0.51	1.08	0.95	0.31	0.00	1.19	0.02	0.06
SC12R16	90.28	82.77	9.66	13.45	0.06	0.07	0.46	1.04	0.64	0.22	0.00	1.29	0.01	0.04
SC12R17	90.28	82.36	9.66	13.71	0.06	0.08	0.42	1.06	0.83	0.25	0.00	1.24	0.01	0.05
SC12R18	90.28	82.82	9.66	13.47	0.06	0.07	0.43	0.97	0.83	0.26	0.00	1.09	0.00	0.04

Appendix D: Conversion and Yield Sample Calculation

Hydrogen Consumption

Hydrogen consumption for each experiment was calculated using the method shown below. The sample calculation and results for experiment SC12R01 are as follows:

$$HC = F_{IN}\left[y_{H2}^{IN} - y_{H2}^{OUT} * \frac{y_{Ar}^{IN}}{y_{Ar}^{OUT}} \right] \frac{P}{RT} \qquad \text{(D.1)}$$

Where,

F_{IN} = Volumetric flow rate entering the reactor = 42.7 ml/min

y_{H2}^{IN} = Volumetric fraction of hydrogen entering the reactor = 0.898

y_{H2}^{OUT} = Volumetric fraction of hydrogen leaving the reactor = 0.840

y_{Ar}^{IN} = Volumetric fraction of argon entering the reactor = 0.101

y_{Ar}^{OUT} = Volumetric fraction of argon leaving the reactor = 0.124

P = Pressure at analysis (GC) = 101325 Pa

R = Ideal gas constant = 8.3145 J/mol*K

T = Temperature at analysis (GC) = 298.65 K

Substituting into Equation D.1, the hydrogen consumption was found to be:

HC = 3.66 x 10^{-4} mol/min

The hydrogen consumption can then be normalized on the basis of one liter of liquid fed to the reactor and standard conditions using the following equation:

$$HC' = HC * \frac{1}{v} * \frac{RT}{P} \qquad \text{(D.2)}$$

Where,

v = Liquid flow rate entering the reactor = 0.04 ml/min

T = Temperature at standard conditions = 273.15 K

P = Pressure at standard conditions = 101325 Pa

Substituting into Equation D.2, the hydrogen consumption was found to be:

HC' = 206 L (STP) / L (Liquid)

Gas By-Product Production

Gas by-product production for each experiment was calculated using a similar method to the hydrogen consumption and is outlined below. The sample calculation and results for the methane production for experiment SC12R01 are as follows:

$$G_i = F_{IN}\left[y_i^{OUT} * \frac{y_{Ar}^{IN}}{y_{Ar}^{OUT}} \right] \frac{P}{RT} \qquad \text{(D.3)}$$

Where,

F_{IN} = Volumetric flow rate entering the reactor = 42.7 ml/min

y_{CH4}^{OUT} = Volumetric fraction of methane leaving the reactor = 0.0088

y_{Ar}^{IN} = Volumetric fraction of argon entering the reactor = 0.101

y_{Ar}^{OUT} = Volumetric fraction of argon leaving the reactor = 0.124

P = Pressure at analysis (GC) = 101325 Pa

R = Ideal gas constant = 8.3145 J/mol*K

T = Temperature at analysis (GC) = 298.65 K

Substituting into Equation D.3, the hydrogen consumption was found to be:

G_{CH4} = 1.26 x 10^{-5} mol/min

The methane production can then be normalized on the basis of one liter of liquid fed to the reactor and standard conditions using the following equation:

$$G_i^{'} = G_i * \frac{1}{v} * \frac{RT}{P} \quad \text{(D.4)}$$

Where,

v = Liquid flow rate entering the reactor = 0.04 ml/min

T = Temperature at standard conditions = 273.15 K

P = Pressure at standard conditions = 101325 Pa

Substituting into Equation D.4, the hydrogen consumption was found to be:

G'_{CH4} = 7.1 L (STP) / L (Liquid)

Oxygen Removal (Conversion)

The extent of oxygen removal was calculated for each experiment to determine the conversion of the liquid feed. A sample calculation and results for experiment SC12R01 are as follows:

$$\%HDO = \frac{\left(x_0^{IN} - x_O^{OUT-ADJ}\right)}{x_O^{IN}} * 100 \quad \text{(D.5)}$$

Where,

x_O^{IN} = Weight percent of oxygen in the liquid entering the reactor = 9.72 wt%

$x_O^{OUT-ADJ}$ = Adjusted weight percent of oxygen in the liquid exiting the reactor = 1.13 wt%

Substituting into Equation D.5, the oxygen removal from the liquid phase was found to be:

% HDO = 88.4 %

Alkane/Olefin Yield / Diesel Fuel Yield (Selectivity)

The product selectivity was described in terms of liquid yield during the process optimization. A sample calculation and results from SC12R01 are as follows, beginning by calculating the normalized organic liquid yield (OLY_N {g/100g}):

$$OLY_N = OLY * \frac{M^{OUT}}{M^{IN}} * 100 \quad \text{(D.6)}$$

Where,

OLY = Organic liquid yield = 0.873 g produced / g fed

M^{OUT} = Total mass exiting the reactor = 70.17 g

M^{IN} = Total mass entering the reactor = 70.16 g

Substituting into Equation D.6, the normalized organic liquid yield was found to be:

OLY_N = 87.3 g produced / 100 g fed

Next, the organic liquid yield was separated into the desired selectivity parameters using the liquid weight percents:

$$AOY = OLY_N * \frac{w_{AO}^{OUT}}{100} \quad \text{(D.7)}$$

$$DFY = OLY_N * \frac{w_{DF}^{OUT}}{100} \quad \text{(D.8)}$$

Substituting into Equations D.6, the alkane/olefin yield and diesel fuel yield were found to be:

AOY = 50.6 g alkanes/olefins / 100 g fed

DFY = 46.9 g diesel fuel / 100 g fed

Appendix E: Internal and External Mass Transfer Sample Calculation

External Mass Transfer Limitations

Prior to evaluating the overall external mass transfer for both hydrogen and oleic acid, each component of the external resistance was considered individually. In the case of hydrogen mass transfer, there were four components identified for external mass transfer resistance:

1. Transport from the bulk gas phase to the gas-liquid interface.
2. Equilibrium at the gas-liquid interface.
3. Transport from the gas-liquid interface to bulk liquid.
4. Transport from the bulk liquid to the external catalyst surface.

Component 1 was assumed to be negligible due to the high partial pressure of hydrogen (see Section 4.4.1).

The equilibrium constant for hydrogen at the gas-liquid interface (component 2) was estimated using a correlation for hydrogen solubility in cottonseed oil at high pressures given by Wisniak et al (1961). Wisniak et al. determined an empirical relationship relating the hydrogen solubility in cottonseed oil to both temperature and pressure. For eqperiment SC03R01, the temperature and hydrogen partial pressure were 390°C and 7,142 kPa, respectively. Under these conditions, the solubility of hydrogen in oleic acid is estimated from the correlation by Wisniak et al. to be:

$$\mathbf{S_{H2} = C_{H2,i} = 233\ mol/m^3}$$

The resistance to hydrogen mass transfer for components 3 and 4 for experiment SC03R01 are found below. The resistance to hydrogen mass transfer from the gas-liquid interface to the bulk liquid is:

$$R_{G-L} = \frac{(1-\varepsilon_b)\rho_c}{k_L a_i} \tag{E.1}$$

Where,

ε_b = Catalyst bed porosity = 0.483

ρ_c = Apparent catalyst pellet density = 1.33×10^6 g/m^3

$k_L a_i$ = Mass transfer coefficient = (see below) s^{-1}

To determine the resistance to mass transfer through the gas-liquid interface, the mass transfer coefficient was estimated using a correlation proposed by Saada et al. (1972) relating the Sherwood number to the mass transfer coefficient:

$$Sh_M = \frac{k_L a_i * d_p^2}{D_{H2}} \tag{E.2}$$

Where,

d_p = Catalyst particle diameter = 6.38×10^{-4} m

D_{H2} = Bulk diffusivity of hydrogen in oleic acid = (see below) m^2/s

The bulk diffusivity of hydrogen in oleic acid was estimated based on the findings of Andersson et al. (1974) that suggested that the bulk diffusivity of hydrogen in oleic acid is approximately 100 times greater than the bulk diffusivity of oleic acid. The bulk diffusivity of oleic acid was estimated based on a linear relationship between the diffusivity of cottonseed oil and T/μ as reported by Andersson et. al (1974). In order to use this relationship, the viscosity of oleic acid had to be estimated at elevated temperatures. To do this, the Arrhenius Model, along with reported values of the viscosity of oleic acid at different temperatures (Website 4), was used to estimate the viscosity of oleic acid at the desired reaction temperature.

$$\mu_{OA}(T) = \mu_O \exp\left(\frac{E}{RT}\right) \quad \text{(E.3)}$$

The parameters μ_O and E were evaluated using reported values for the viscosity of oleic acid and were found to be:

$\mu_O = 1.40\text{x}10^{-3}$ mPa*s

E = 24600 J/mol

The viscosity of oleic acid at the reaction temperature of 663.15 K (390°C) was found by substituting these values back into Equation E.3, and was found to be:

$\mu_{OA}(T)$ **= 0.122 mPa*s**

This value was then passed back to the relationship proposed by Andersson et. al (1974). For a value of T/μ_{OA} equal to 5444 K/cP, the bulk diffusivity of oleic acid is estimated to be:

$D_{OA} = 1.01\text{x}10^{-8}$ m^2/s

Using the bulk diffusivity of oleic acid and multiplying by 100 (Andersson et al.) the bulk diffusivity of hydrogen was estimated to be:

$D_{H2} = 1.01\text{x}10^{-6}$ m^2/s

Saada et al. (1972) proposed the following empirical relationship to estimate the Sherwood number:

$$Sh_M = 10.72(\text{Re}_L)^{0.32}(\text{Re}_G)^{0.22}\left(\frac{d_p}{d_t}\right)^{0.33} \quad \text{(E.4)}$$

Where,

Re_L = Liquid Reynolds number = 0.131

Re_G = Gas Reynolds number = 4.50

d_p = Catalyst particle diameter = $6.38\text{x}10^{-4}$ m

d_t = Reactor effective inside diameter = 5.75×10^{-3} m

Substituting into Equation E.4, the Sherwood number was found to be:

Sh_M = 3.77

Substituting the Sherwood number into Equation E.2, the hydrogen mass transfer coefficient was estimated to be:

$k_L a_i$ = 9.36 s^{-1}

Next, substituting the hydrogen mass transfer coefficient into Equation E.1, the resistance to the mass transfer of hydrogen from the gas to the liquid phase was estimated to be:

$R_{G\text{-}L,\ H2}$ = 73 kg*s/m^3

The resistance to hydrogen mass transfer from the liquid to the solid is:

$$R_{L-S} = \frac{1}{k_S a_C} \tag{E.5}$$

Where,

k_S = Mass transfer coefficient = (see below) m/s

a_C = External catalyst surface area per gram of catalyst = 3.66 m^2/kg

To hydrogen mass transfer coefficient for the liquid-solid interface was estimated using a correlation for liquid filled beds proposed by Goto et al (1975). This correlation was used as a conservative estimate to the upflow configuration of the experimental reactor used. Goto et al. (1975) proposed the following relationship between a mass transfer factor (J_D) and the mass transfer coefficient:

$$J_D = k_S a_C \left(\frac{1}{u_L}\right)\left(\frac{\mu_L}{\rho_L D_{H2}}\right)^{2/3} \tag{E.6}$$

Where,

u_L = Superficial liquid velocity = 2.95×10^{-5} m/s

μ_L = Liquid viscosity = 1.22×10^{-4} kg/m*s

ρ_L = Liquid density = 850 kg/m^3

D_{H2} = Bulk diffusivity of hydrogen in oleic acid = 1.01×10^{-6} m^2/s

Goto et al. (1975) proposed the following empirical relationship to predict the mass transfer factor:

$$J_D = 1.31(\mathrm{Re}_L)^{-0.436} \quad \text{(E.7)}$$

Where,

Re_L = Liquid Reynolds number = 0.131

Substituting into Equation E.7, the mass transfer factor for hydrogen is found to be:

J_D = 3.18

Substituting into Equation E,6, the hydrogen liquid-solid mass transfer coefficient is estimated to be:

$k_{S,H2} = 3.43 \times 10^{-4}$ m/s

Next, substituting into Equation E.8, the resistance to mass transfer of hydrogen through the liquid-solid interface was found to be:

$R_{L\text{-}S,\,H2} = 795$ kg*s/m^3

In the case of the external mass transfer of oleic acid, only the resistance between the bulk liquid and the surface of the catalyst was considered. The mass transfer coefficient and resistance to oleic acid were calculated similarly to hydrogen using the relationship of Goto et al. (1975), instead using the bulk diffusivity of oleic acid equal to 1.01×10^{-8} m^2/s. The results for the external mass transfer resistance to oleic acid are summarized below:

$k_{S,OA} = 1.60 \times 10^{-5}$ m/s

$R_{L\text{-}S,\,OA}$ = 17137 kg*s/m^3

Next, the Mears criterion was used to evaluate the impact of these external mass transfer resistances (Fogler, 1999). Shown below are a sample calculation and results from experiment SC01R03 for both hydrogen and oleic acid at the entrance of the reactor. The Mears criterion applied to hydrogen is given as follows:

$$\frac{-r'_{H2}(obs)n}{k_{H2}A_{cat}C_{H2,i}} = \frac{-r'_{H2}(obs)n}{C_{H2,i}/R_{H2}} < 0.15 \qquad \text{(E.7)}$$

Where,

$-r'_{H2}(obs)$ = Observed rate of reaction of hydrogen = (see below) mol/s*kg

n = Reaction order = 1

k_{H2} = Overall hydrogen external mass transfer coefficient = m/s

R_{H2} = Overall hydrogen external mass transfer resistance = (see below) kg*s/m^3

A_{cat} = Mass transfer area per mass of catalyst = m^2/kg

$C_{H2,i}$ = Concentration of hydrogen at the gas/liquid interface at the entrance of the reactor = 233 mol/m^3

The observed rate of reaction was found by using differential reactor design equation for a plug flow reactor and assuming that the reaction rate is first order and constant over the length of the bed.

$$-r'_{H2} = \frac{N^{IN}_{H2}X_{H2}}{W} * \frac{1}{3600} \qquad \text{(E.8)}$$

Where,

N^{IN}_{H2} = Molar flow of hydrogen into the reactor = 8.70x10^{-4} mol/hr

X_{H2} = Final conversion of hydrogen = 0.262

W = Weight of catalyst charged to the reactor = 2.0 g

Substituting into Equation E.8, the observed reaction rate of hydrogen was found to be:

$-r'_{H2}$ **= 1.90x10^{-6} mol/s*g**

The overall hydrogen mass transfer resistance is found next by adding the individual gas-liquid and liquid-solid mass transfer resistances.

$$R_{H2} = R_{G-L,H2} + R_{L-S,H2} \tag{E.9}$$

R_{H2} = 869x10^{3} g*s/m^{3}

Substituting these values into Equation E.7, it can be found that the left hand side of the equation becomes:

LHS = 0.00708

Equation E.11 can also be applied to the oleic acid entering the reactor by considering the values for observed reaction rate, mass transfer coefficient, and surface concentration of oleic acid.

$$\frac{-r'_{OA}(obs)n}{k_{OA}A_{cat}C_{OA,b}} = \frac{-r'_{OA}(obs)n}{C_{OA,b}/R_{OA}} < 0.15 \tag{E.10}$$

$-r'_{OA}(obs)$ = Observed rate of reaction of oleic acid (Equation E.8) = 5.75x10^{-7} mol/s*g

k_{OA} = Overall oleic acid external mass transfer coefficient = m/s

R_{OA} = Overall oleic acid external mass transfer resistance = R_{L-S} = 17137 kg*s/m^{3}

$C_{OA,S}$ = Concentration of oleic acid in the bulk liquid at the enterance of the reactor = 3.16x10^{3} mol/m^{3}

Substituting these values into Equation E.11, it can be found that the left hand side of the equation becomes:

LHS = 0.0031

A summary of the Mears criterion calculated for the molybdenum carbide and nitride comparison study are tabulated below in Table E.1:

Table E.1: Summary of External Mass Transfer Estimations for the Molybdenum Carbide and Nitride Comparison Study

Experimental Trial ID	Oleic Acid			Hydrogen			
	R_{L-S}	Mears Criteria		R_{G-L}	R_{L-S}	Mears Criteria	
	kg*s/m3	Inlet	Outlet	kg*s/m3	kg*s/m3	Inlet	Outlet
SC07R02	10068	0.005	20.924	48	467	0.015	0.015
SC07R03	9374	0.005	27.436	43	435	0.011	0.011
SC07R04	13858	0.004	19.901	63	643	0.009	0.009
SC07R05	14884	0.004	21.918	69	691	0.010	0.010
SC07R08	21843	0.006	24.025	100	1014	0.011	0.011
SC07R09	14767	0.008	4.930	69	685	0.016	0.016
SC07R10	13749	0.007	16.003	62	638	0.016	0.016
SC07R11	20336	0.005	7.094	91	944	0.012	0.012
SC08R01	21288	0.006	29.785	99	988	0.011	0.011
SC08R03	14395	0.007	8.592	68	668	0.017	0.017
SC08R04	13402	0.007	8.482	62	622	0.017	0.017
SC08R05	19820	0.005	76.335	90	920	0.011	0.011
SC08R06	21288	0.006	10.845	100	988	0.012	0.012
SC08R07	14395	0.007	7.228	68	668	0.019	0.019
SC08R08	19820	0.005	9.691	90	920	0.014	0.014

Internal Mass Transfer Limitations

The Weisz-Prater criterion (C_{WP}) was used to evaluate the effect of the internal mass transfer resistances (Fogler, 1999). Shown below are a sample calculation and the results of experiment SC01R03 for oleic acid entering the reactor:

$$C_{WP} = \frac{-r'_{OA}(obs)\rho_C R^2}{D_{eff,OA} C_{OA,S}} \qquad \text{(E.11)}$$

Where,

$-r'_{OA}(obs)$ = Observed rate of reaction of oleic acid (Equation E.8) = 5.75×10^{-7} mol/s*g

ρ_c = Catalyst pellet density = 1.33×10^6 g/m^3

R = Catalyst pellet radius = 3.19×10^{-4} m

$D_{eff,OA}$ = Effective diffusivity of oleic acid = (see below) m^2/s

$C_{OA,S}$ = Concentration of oleic acid at the surface of the catalyst pellet at the enterance of the reactor = (see below) mol/m^3

Using a relationship proposed by Veldsink et. al. (1997), the effective diffusivity of oleic acid can be estimated from the bulk diffusivity as follows:

$$D_{eff,OA} = \frac{\varepsilon}{\tau}(D_{OA}) x 10^{-2 d_{mol} / d_{pore}} \quad \text{(E.12)}$$

Where,

ε = Catalyst pellet porosity = 0.636

τ = Tortuosity factor = 4 (Satterfield, 1980)

D_{OA} = Bulk diffusivity of oleic acid = 1.01×10^8 m^2/s

d_{mol} = Average molecule diameter = 4×10^{-10} m

d_{pore} = Average pore diameter = 1×10^{-8} m

Substituting into Equation E.4, the effective diffusivity of oleic acid was estimated to be:

$D_{eff,OA} = 1.33 \times 10^{-9}$ m^2/s

The concentration of the oleic acid at the surface of the catalyst can be calculated using the external mass transfer resistances calculated previously:

$$C_{OA,S} = C_{OA,b} - (-r'_{OA} * R_{OA}) \quad \text{(E.13)}$$

$C_{OA,S} = 3.15 \times 10^3$ mol/m^3

Substituting into Equation E.11, the Weisz-Prater criterion for oleic acid entering the reactor can be calculated, and was found to be:

$C_{WP} = 0.019$

The Wiesz-Prater criterion can be calculated for hydrogen by modifying Equation E.11

$$C_{WP} = \frac{-r'_{H2}(obs)\rho_C R^2}{D_{eff,H2} C_{H2,S}} \quad \text{(E.14)}$$

Where,

$-r'_{H2}(obs)$ = Observed rate of reaction of oleic acid (Equation E.8) = 1.90×10^{-6} mol/s*g

$D_{eff,H2}$ = Effective diffusivity of hydrogen = (see below) m^2/s

$C_{H2,S}$ = Concentration of hydrogen at the surface of the catalyst pellet at the entrance of the reactor = (see below) mol/m^3

Ramirez et al. (2006) suggest that the effective diffusivity of hydrogen in oleic acid can be estimated as 70 times as large as the effective diffusivity of oleic acid. Following this approximation:

$D_{eff,H2} = 9.33 \times 10^{-8}$ m^2/s

The concentration of hydrogen at the surface of the catalyst pellet at the entrance of the reactor can be approximated by modifying Equation E.13:

$$C_{H2,S} = C_{H2,i} - (-r'_{H2} * R_{H2}) \quad \text{(E.15)}$$

$C_{H2,S} = 35.4$ mol/m^3

Substituting into Equation E.14, the Weisz-Prater criterion for hydrogen entering the reactor can be calculated, and was found to be:

$C_{WP} = 0.078$

A summary of the Wiesz-Prater criterion calculated for the molybdenum carbide and nitride comparison study are tabulated below in Table E.2:

Table E.2: Summary of Internal Mass Transfer Estimations for the Molybdenum Carbide and Nitride Comparison Study

Experimental Trial ID	Weisz - Prater Criterion			
	Oleic Acid		Hydrogen	
	Inlet	Outlet	Inlet	Outlet
SC07R02	0.075	N/A	0.364	0.396
SC07R03	0.069	N/A	0.270	0.289
SC07R04	0.034	N/A	0.152	0.165
SC07R05	0.037	N/A	0.158	0.170
SC07R08	0.037	N/A	0.129	0.137
SC07R09	0.075	N/A	0.273	0.292
SC07R10	0.069	N/A	0.267	0.288
SC07R11	0.034	N/A	0.133	0.144
SC08R01	0.037	N/A	0.130	0.140
SC08R03	0.074	N/A	0.290	0.313
SC08R04	0.068	N/A	0.303	0.332
SC08R05	0.034	N/A	0.130	0.140
SC08R06	0.037	N/A	0.136	0.146
SC08R07	0.074	N/A	0.338	0.368
SC08R08	0.034	N/A	0.157	0.173

Appendix F: Analysis Procedures for FAME GC/MS and n-alkane/α-oleifn GC/MS (Caravaggio, 2008)

Sample preparation for fatty acid methyl ester (FAME), n-alkane and alpha olefin analysis:

An aliquot of the sample was weighed (~50mg) in a test tube (11 mm ID X 105 length) and BF_3/MeOH (1ml, 14% W/W), toluene, and methanol (1ml) were added. The solution was spiked with deuterated hexadecanoic acid (50 ul X~2.5 mg/ml in hexane, used as a derivatization surrogate) and deuterated hexacosane ((100ulX10mg/ml, used for the *n*-alkanes and alpha olefin recovery surrogate). The tube was flushed with ultra high purity nitrogen (to reduce the risk of oxidizing the unsaturated fatty acids), was capped tightly with a Teflon cap and put into a heating block (preheated to 100°C) for 1 hour. The mixture was shaken every 10 minutes to ensure complete mixing. The tube was left to cool to room temperature. Deionized water (5ml) and hexane (1ml) were added to the solution and the tube was capped and shaken for ~ 1 minute. The hexane portion was transferred using a Pasteur pipette into another test tube containing ~ 1 g of Sodium Sulphate to remove the water. The dried hexane was transferred into a 10 ml volumetric flask. More hexane (~2 ml) was added to the initial mixture and the same procedure was repeated until the volumetric flask was filled. The solution was diluted 20 times for *n*-alkane and alpha olefin analysis, and analysed as is for the FAME analysis.

GC/MS parameters

FAME analysis

GC/MS analyses were done using an Agilent 6890 GC equipped with an autosampler and a 5972A quadrupole mass selective detector operated in electron impact mode (electron

energy 70 eV, ion source temperature 250°C) and a Programmable Temperature Vaporizing Injector (PTV). The chromatography was done with a supelco SP-2380 column (0.20 µm film, 0.25 mm ID, 30 m) using the following conditions: column flow: 1.5 ml min-1, oven temperature program: initial temperature: 50°C, final temperature: 250°C with a ramp of 3°C/min. The PTV conditions were: initial temperature 70°C, final temperature 275°C with a ramp of 720 °C/min. The analyses were carried out either in selective ion mode for quantitative analysis (mz^{-1}: 74 and 87 for unsaturated and mono unsaturated FAMEs, 81 and 95 for double and 79 and 95 for triple unsaturated FAMEs with a dwell time of 15 or 20 msec per ion) or in scan mode (total ion count, mass range 40 to 550) for identification of compounds. FAMEs were identified either by comparison with retention times of reference compounds and/or with the help of their MS fragmentation patterns using the National Institute of Standards and Technology NIST02 library database software. MS data and chromatograms were recorded using Chemstation software.

<u>*N*-alkane and alpha olefin analysis</u>

GC/MS analyses was performed with an Agilent 6890 GC equipped with an autosampler and a 5973 quadrupole mass selective detector operated in electron impact mode (electron energy 70 eV, ion source temperature 250°C) and split/splitless injector operated in splitless mode at 275°C. The chromatography was done with a DB-5MS column (0.25 µm film, 0.25 mm ID, 30 m) using the following conditions: column flow: 1.5 ml min-1, oven temperature program: initial temperature: 50°C, temperature #1: 280°C with a ramp of 4°C/min, final temperature: 320°C with a ramp rate of 6°C/min .

The analyses were carried out either in selective ion mode for quantitative analysis (mz^{-1}: 85,71 for *n*-alkanes, 83 for alpha olefins and 66 for deuterated hexacosane with a dwell time of 40 or 45 msec per ion) or in scan mode (total ion count, mass range 40 to 550) for identification of compounds. The *n*-alkanes and alpha olefins were identified using the same approach as the FAMES as described above.